Sequestration of infected red blood cells and reduced venous efflux precede excessive inflammatory responses in experimental cerebral malaria

Thesis
for the degree of
doctor rerum naturalium
(Dr. rer. nat.)

approved by the Faculty of Natural Sciences of Otto von Guericke University Magdeburg
by **M.Sc. Rituparna Bhattacharjee**
born on 13.03.1992 in Kolkata, India

Examiner: apl. Prof. Dr. Eike Budinger

Prof. Dr. Bernd Lepenies

Submitted on: 25.06.2021

Defended on: 23.02.2022

TABLE OF CONTENTS

TABLE OF CONTENTS II
ABBREVIATIONS IV
1. SUMMARY 1
2. INTRODUCTION 2
2.1 PARASITIC DISEASES 2
2.2 MALARIA 2
2.2.1 HISTORY 2
2.2.2 INFECTION 3
2.2.3 DIAGNOSIS 9
2.2.4 TREATMENT 11
2.3 CEREBRAL MALARIA 15
2.3.1 CLINICAL FEATURES 15
2.3.2 EXPERIMENTAL CEREBRAL MALARIA 17
2.3.3 PATHOGENESIS 19
2.3.4 TWO MAJOR HYPOTHESES OF CM PATHOGENESIS 28
2.3.5 DIAGNOSIS 29
2.3.6 TREATMENT 30
2.4 *In vivo* NEURO-IMAGING 31
2.4.1 MAGNETIC RESONANCE IMAGING 32
2.4.2 SINGLE PHOTON EMISSION COMPUTED TOMOGRAPHY 34
3. AIMS OF THIS STUDY 37
4. MATERIALS AND METHODS 38
4.1 MATERIALS 38
4.1.1 ANIMALS 38
4.1.2 PARASITES 38
4.1.3 ANIMAL INFECTION AND EXPERIMENTS 38
4.1.4 IMMUNOHISTOCHEMISTRY 39
4.1.5 MOLECULAR BIOLOGY 41
4.1.6 NEURO-IMAGING 41
4.1.7 LABORATORY EQUIPMENT 42
4.1.8 SOFTWARE 43

4.2 METHODS 44
4.2.1 MALARIA INFECTION 44
4.2.2 ANTI-MALARIAL TREATMENT 45
4.2.3 PARASITEMIA 45
4.2.4 EVANS BLUE STAINING 46
4.2.5 IMMUNOHISTOCHEMISTRY 46
4.2.6 QUANTITATIVE REVERSE TRANSCRIPTION-PCR (qRT-PCR) 51
4.2.7 SPECT/CT IMAGING 53
4.2.8 MR IMAGING 56
5. RESULTS 59
5.1 Severe neurological symptoms of ECM develop around day 7 p.i. 59
5.2 Intracerebral iRBC sequestration is an early event in ECM development 60
5.3 Severe reduction in venous efflux and edema formation progresses with ECM development 61
5.4 Cerebral hypo-perfusion precedes the development of ECM neurological symptoms 64
5.5 Anti-malarial treatment in the early stages prevents the spread of ECM 66
5.6 Progression of ECM results in the disruption of the rostral migratory stream from an early stage of the disease 70
5.7 Acute inflammation develops throughout the brain in the later stages of ECM pathology 73
5.8 Increased expression of cytokines and chemokines in the later stages of ECM further augments the inflammation 77
5.9 Supplementary figures 80
6. DISCUSSION 85
6.1 Sequestration of iRBCs and cerebral blood flow 85
6.2 Brain pathology and inflammation 88
BIBLIOGRAPHY VII
DECLARATION OF HONOUR XVII

ABBREVIATIONS

A

ACT: Artemisinin-based Combination Therapy
AIDS: Acquired Immunodeficiency Syndrome
Ang-1/2: Angiopoietin-1/2
ANKA: Antwerpen-Kasapa
APC: Activated Protein C

B

BBB: Blood Brain Barrier
BrdU: Bromodeoxyuridine
BSA: Bovine Serum Albumin

C

Casp3: cleaved Caspase 3
CBF: Cerebral Blood Flow
CBV: Cerebral Blood Volume
CCL2/20: C-C motif Ligand 2/20 chemokine
CD8/31/36: Cytoplasmic Domain 8/31/36
CDC: Centres for Disease Control and Prevention
cDNA: complementary DNA
CelTOS: Cell Traversal protein for Ookinetes and Sporozoites
CM: Cerebral Malaria
CNS: Central Nervous System
CSA: Chondroitin Sulphate A
CSF: Cerebrospinal Fluid
CSP: Circumsporozoite Protein
CT: Computed Tomography
CXCL1/2/3/6/8/9/10/11: C-X-C motif Ligand 1/2/3/6/8/9/10/11 chemokine
CXCR3: C-X-C motif chemokine Receptor-3

D

d0/5/7: day 0/5/7
DAB: Diaminobenzidine
DCX: Doublecortin
DICOM: Digital Imaging and Communications in Medicine
DMSO: Dimethyl Sulfoxide
DNA: Deoxyribonucleic Acid
dNTP: Deoxyribonucleotide Triphosphate
DPBS: Dulbecco's Phosphate Buffered Saline
dT: Deoxythymine
DTT: Dithiothreitol

E

EBL: Erythrocyte Binding-Like protein
EC: Endothelial Cell
EEF: Exoerythrocytic Form
EPCR: Endothelial Protein C Receptor
ECM: Experimental Cerebral Malaria

G

GTS: Global Technical Strategy for malaria
GFAP: Glial Fibrillary Acidic Protein

H

HBsAg: Hepatitis B surface Antigen
H&E: Haematoxylin and Eosin
HGF: Hepatocyte Growth Factor
HMPAO: Hexamethylpropylene-Amine Oxime
H_2O_2: Hydrogen peroxide
HPRT: Hypoxanthine Phosphoribosyl-transferase
HRP2: Histidine Rich Protein-2
HSPG: Heparan Sulphate Proteoglycan

I

Iba1: Ionized calcium-binding adapter molecule-1
ICAM-1: Intercellular Adhesion Molecule-1
IFN-γ: Interferon-γ
IgG: Immunoglobulin G
IHC: Immunohistochemistry
IL-1α/1β/10: Interleukin-1α/1β/10
iNOS: inducible Nitric Oxide Synthase
i.p.: intraperitoneally
iRBCs: infected Red Blood Cells
i.v.: intravenously

K

KC: Kupffer Cell

L

LTα/β: Lymphotoxin-α/β

M

MATLAB: Matrix Laboratory
MHC-I: Major Histocompatibility Complex-I
MIP: Maximum Intensity Projection
MPI: Multi-Purpose Imaging
ms: millisecond
MSP1: Merozoite Surface Protein-1
MRA: Magnetic Resonance Angiography
MRI: Magnetic Resonance Imaging
mRNA: messenger RNA
MTT: Mean Transit Time

N

NaCl: Sodium Chloride
NaI: Sodium Iodide
NCAM: Neural Cell Adhesion Molecule
ND: Nanodrop
NK cell: Natural Killer cell
NKT cell: Natural Killer T cell
NMR: Nuclear Magnetic Resonance
NO: Nitric Oxide
NTD: Neglected Tropical Disease

O

OB: Olfactory Bulb

P

***Pb*A**: *Plasmodium berghei* ANKA
PBS: Phosphate Buffered Saline
PCR: Polymerase Chain Reaction
PECAM-1: Platelet Endothelial Cell Adhesion Molecule-1
PET: Positron Emission Tomography
PFA: Paraformaldehyde
***Pf*EMP1**: *Plasmodium falciparum* Erythrocyte Membrane Protein-1
***Pf*HRP2**: *Plasmodium falciparum* specific Histidine Rich Protein-2
***Pf*-pLDH**: *Plasmodium falciparum* specific Lactate Dehydrogenase
***Pf*Rhs**: *Plasmodium falciparum* Reticulocyte-binding protein homologs
p.i.: post infection
PL: Phospholipase
PMap: Probability Map
PPLP1: *Plasmodium* Perforin-Like Protein-1
PVM: Parasitophorous Vacuole Membrane
***Pv*-pLDH**: *Plasmodium vivax* specific Lactate Dehydrogenase

Q

qRT-PCR: quantitative Reverse Transcription-PCR

R

RBC: Red Blood Cell
rCBF: regional Cerebral Blood Flow
RCT: Randomized Controlled Trial
RDT: Rapid Diagnostic Test
RF: Radio Frequency
RGB: Red Green Blue
RMCBS: Rapid Murine Coma and Behaviour Scale
RMS: Rostral Migratory Stream
RNA: Ribonucleic Acid
RPMI 1640 medium: Roswell Park Memorial Institute 1640 medium
RTS, S vaccine: R for central repeat region of *P. falciparum* CSP; T for T-cell epitopes of the CSP; S for HBsAg; free S protein

S

$SnCl_2$: Tin (II) Chloride
SPECT-1/2: Sporozoite Microneme Protein Essential for Cell Traversal-1/2
SPECT: Single Photon Emission Computed Tomography
SSS: Superior Sagittal Sinus
SUV: Standard Uptake Value
SVZ: Sub-Ventricular Zone

T

^{99m}Tc: ^{99m}Technetium
TCR: T Cell Receptor
TNF-α: Tumor Necrosis Factor-α
TOF: Time of Flight
TRAP: Thrombospondin Related Anonymous Protein
TRIS: Tris(hydroxymethyl) aminomethane

V

VCAM-1: Vascular Cell Adhesion Molecule-1
VOI: Volume Of Interest
VWF: Von Willebrand Factor

W

WHO: World Health Organization

Z

ZO-1: Zona Occludens-1

1. SUMMARY

Cerebral malaria (CM) is a complex neurological complication of severe malaria caused by *Plasmodium falciparum*. Sequestration of infected red blood cells to the brain vasculature and excessive inflammatory responses in the brain are the key features of CM pathogenesis. Recent imaging studies have established edema development with rise in intracranial pressure as an indicator of fatal CM outcome. However, the link between sequestration of infected red blood cells, excessive inflammation and edema development remains elusive till date. In the present study, in vivo neuroimaging techniques, SPECT/CT and MRI, followed by immunohistochemistry stainings and quantitative reverse transcription-PCR measurements were performed on the mouse model of experimental cerebral malaria (ECM) investigating the rapid progression of the disease starting from an early stage. Sequestration of infected red blood cells, especially in the regions of large draining veins, was observed as the primary event of ECM pathogenesis, present already at a neurologically asymptomatic stage. Reduction of cerebral venous efflux and impaired perfusion in the territories of large draining veins and sinuses ensued, also from the early stage, which worsened with disease progression. In comparison, activation of astrocytes, microglia, endothelial cells and accumulation of leukocytes like $CD8^+$ T cells were observed mostly at a later stage in the neurologically sick mice. Simultaneously, a pro-inflammatory storm of cytokines and chemokines could be detected at this late phase of ECM. Also, a disturbance in rostral migratory stream was observed, from an early stage, which could lead to an impairment in neurogenesis. Severe bilateral edema developed in the white matter tracts of the fatally sick mice. Collectively, the present study suggests direct effect of infected RBC sequestration on the spatiotemporal patterns of edema development by venous efflux reduction while excessive inflammation appears at a later stage

2. INTRODUCTION

2.1 PARASITIC DISEASES

Parasites belong to a diverse spectrum of complex eukaryotic organisms that live on or inside the body of a host deriving its nutrition for survival and replication. They have a complex life cycle alternating between different host species, infection routes, tissue specificity and cause major global health problems (Benns *et al*., 2019). Parasitic diseases affect millions of people worldwide every year; yet they fall under the most neglected tropical diseases (NTDs) since they are prevalent in the economically poor countries of the world. Drugs available in the market to treat such diseases are mostly old and have several limitations like poor efficacy, severe side effects and drug resistance with evolving parasites (Renslo and McKerrow, 2006).

The Centres for Disease Control and Prevention (CDC), USA, segregate human infecting parasites into three main classes: protozoa, helminths and ectoparasites, out of which protozoa are responsible for severe diseases. Malaria, Leishmaniasis, Trypanosomiasis, Schistosomiasis and Giardiasis are the top five NTDs caused by parasites, with malaria being the most fatal one (Renslo and McKerrow, 2006) (Rodrigues *et al*., 2015).

2.2 MALARIA

2.2.1 HISTORY

Malaria is an ancient disease which is thought to have originated in our primate ancestors in Africa and spread to the new world with human migration. The earliest documents with reports of malaria could be traced back to 2700 BC and it was considered a disease associated with marshes and swamps (Simpson *et al*., 2002). The term `malaria´ was coined from the Italian word *mala* meaning bad and *aria* meaning air in 1827 (Manson-Bahr, 1938). Scientific

understanding of the disease began much later with the discovery of the protozoa in blood in 1880 by Charles Louis Alphonse Laveran and with the identification of mosquitoes as the vector of the disease by Ronald Ross in 1897. It took almost another century for the scientists to determine the complete, complex life cycle of the parasite in mosquitoes and in human hosts (Simpson *et al*., 2002) (Cox, 2010).

2.2.2 INFECTION

Malaria is one of the four most life-threatening infectious diseases in the world along with tuberculosis, AIDS and hepatitis (Pham *et al*., 2018). According to the World Malaria Report 2020 by the World Health Organization (WHO), there were 229 million cases of malaria worldwide, including 87 endemic countries in 2019 with 409.000 deaths. The highest burden of the cases, 94%, were in the WHO African regions. Children below 5 years of age are at a higher risk of being affected by malaria followed closely by pregnant women (WHO, 2020).

Malaria is caused by the protozoa, *Plasmodium spp.*, which has a complex, alternating life cycle between female *Anopheles* mosquito and its vertebrate hosts. There are five known species of *Plasmodium* infecting humans: *P. falciparum*, *P. vivax*, *P. ovale*, *P. knowlesi* and *P. malariae*. It spreads by the bite of an infected female *Anopheles* mosquito on the skin where sporozoites are injected into the dermis thus, starting its life cycle in human hosts (Gomes *et al*., 2016) (Bhagavathula *et al*., 2016).

2.2.2.1 Stages of infection in humans

SKIN: In an infected mosquito, sporozoites gather in its salivary glands and are transferred onto the skin of the host when the mosquito probes for blood (Sinnis and Zavala, 2012). As low as 100-200 sporozoites deposited onto the dermis would be sufficient in evading the immune response of the host causing an infection (Gomes *et al*., 2016) (Figure 1). The primary barrier the sporozoites face is to invade the dermal blood vessel without getting drained into

the lymphatic system of the host (Sinnis and Zavala, 2012). To overcome this, the sporozoites rely on their gliding motility and cell traversal property which help them to penetrate blood vessels (Tavares *et al*., 2013). Thrombospondin-related anonymous protein (TRAP) is a surface protein found on the sporozoites which has a specific amino acid motif that confers the sporozoites the ability to bind to sulphated glycoconjugates (Müller *et al*., 1993). TRAP is necessary for the gliding motility of the sporozoites which is required for invading the bloodstream (Sultan *et al*., 1997). Mechanised special proteins are required for host cell traversal of the sporozoites: SPECT-1 (sporozoite microneme protein essential for cell traversal) (Sultan *et al*., 1997), SPECT-2 (also known as *Plasmodium* perforin-like protein-1, PPLP1) (Risco-Castillo *et al*., 2015), CelTOS (cell traversal protein for ookinetes and sporozoites) (Kariu *et al*., 2006) and PL (phospholipase) (Bhanot *et al*., 2005). Studies have shown that sporozoites deficient in these proteins are blocked in the dermis and are cleared by phagocytes. This suggests that the these proteins work simultaneously to form pores and wound host cell membrane (Hamaoka and Ghosh, 2014). After exiting the dermis, the sporozoites enter the blood circulation and reach the liver.

LIVER: In the liver, the sporozoites are arrested on the inner side of the sinusoidal vein where they traverse through the Kupffer cell (KC) and endothelial cell (EC) lining in order to infect hepatocytes (Tavares *et al*., 2013) (Figure 1). Recent studies claim that sporozoites exploit multiple ways to invade the sinusoidal barrier. One of the ways to facilitate traversal is the interaction between the circumsporozoite protein (CSP) on the surface of the parasite and the heparan sulphate proteoglycans (HSPGs) on the surface of the host cells (Gomes *et al*., 2016). Sporozoites have also been known to modulate the cytokine profiles and induce apoptosis in murine Kupffer cells (Klotz1 and Frevert, 2008).

Once they cross the sinusoidal border, the sporozoites traverse through several hepatocytes wounding them before finally settling in one of them by forming a parasitophorous vacuole membrane (PVM) (Mota *et al*., 2001). This membrane separates the parasite from the cytosol of the host thus, avoiding lysosomal degradation and autophagy (Gomes *et al*., 2016). Wounding of the hepatocytes induces the secretion of hepatocyte growth factor (HGF) which transforms the hepatocytes and makes them susceptible to infection (Carrolo *et al*., 2003). Over the next 2-10 days, sporozoites enter their exoerythrocytic form (EEF) where they undergo asexual reproduction (schizogony) to form tens of thousands of pathogenic merozoites. These merozoites are packaged into vesicles surrounded by the hepatocyte membrane called merosomes which allows them to evade killing by liver phagocytes. They bud off and enter the hepatic circulation to start the final stage of infection, that is, infecting red blood cells (Gomes *et al*., 2016) (Ménard *et al*., 2013) (Cowman *et al*., 2016).

BLOOD: In this stage of the infection, the merozoites rapidly invade red blood cells (RBCs), undergo cell division (schizogony) and maturation from ring stage to trophozoites to schizonts to finally form 6-32 daughter merozoites (Yam and Preiser, 2017) (Figure 1). The merozoites exit the host RBC by rupturing its cell membrane in a process called egress, to invade new RBCs (Garg *et al*., 2013). Merozoite surface protein-1 (MSP1) expressed on the surface of the merozoites plays an integral role in their invasion and egression from the erythrocytes (Yam and Preiser, 2017). In *P. falciparum* infections, two more ligand families are involved: the erythrocyte binding-like proteins (EBLs) and *P. falciparum* reticulocyte-binding protein homologs (*Pf*Rhs) which can bind to glycophorins and complement receptors which have become drug and vaccine targets (Cowman *et al*., 2016). During the rounds of schizogony, a part of the merozoites undergo sexual reproduction to form male and female gametes which would be transferred to the gut of the mosquito during its blood meal thus, continuing the transmission (Cox, 2010).

Rupturing of RBCs by merozoites elicit a strong immune response in the host including priming of macrophages, activation of T cells, production of cytokines like IFN-γ and TNF-α and generation of antibodies. The parasites hide inside the RBCs to evade detection by the host immune system as RBCs do not express MHC-I molecules and therefore, cannot be recognised by $CD8^+$ T cells. Alternatively, infected RBCs cluster with other infected and uninfected RBCs to form rosettes and avoid detection. In *P. falciparum* infections, the iRBCs can adhere to vascular endothelial cells with the help of a surface protein called *P. falciparum* erythrocyte membrane protein-1 (*Pf*EMP1) thus, avoiding clearance (Gomes *et al*., 2016) (Yam and Preiser, 2017). *Plasmodium spp.* have developed diverse immune evasion strategies to survive within the host without detection.

2.2.2.2 Symptoms

The liver stage of parasite replication is generally asymptomatic as it fails to elicit an immune response. The clinical symptoms start appearing with the blood stage of the infection when the merozoites burst out of the RBCs (Marks *et al*., 2014). Malaria causes acute febrile illness and it takes around 10-15 days of incubation period for the symptoms to appear after a mosquito bite. Patients have classical symptoms which lasts for 6-10 hours beginning with cold chills with shivering followed by high body temperature and fever and then profuse sweating with return to normal temperature (Randall and Seidel, 1985). Generally, these attacks are periodic, occurring every two to three days depending on the reproduction cycle of the *Plasmodium spp*. However, this periodicity is infrequent and though children develop high temperature and fever they do not show the typical periodicity. Normally, the patients with uncomplicated malaria show a combination of the following symptoms (Stanley, 1997) (White, 1996):

- Irregular fever
- Chills
- Headache and body ache

- Nausea and vomiting
- Malaise
- Dehydration
- Delirium
- Diarrhoea (not so common)

In regions with low incidence of malaria, these symptoms are frequently attributed to influenza and common cold which leads to a delay in detection. Conversely, in regions with frequent occurrence of malaria, patients treat themselves based on the clinical symptoms without seeking medical help. If left untreated or partially treated, infection can progress to severe malaria which might lead to the death of the individual.

2.2.2.3 Severe malaria

According to WHO, severe malaria is characterised by one or more of the following conditions: coma from cerebral malaria, metabolic acidosis, severe anaemia, hypoglycaemia, acute renal failure or acute pulmonary edema leading to fatality in most of the cases (World Health Organization, 2015). The clinical manifestations of severe malaria depend on age, immune status and transmission area with children being the susceptible ones. In infected pregnant woman, severe malaria could lead to stillbirths or abortion, maternal anaemia and low birth weight of the infant (Cowman *et al*., 2016).

P. falciparum is largely, but not entirely, responsible for severe, fatal malaria. The main observation in severe malaria is the sequestration of infected RBCs in the microvasculature of organs lined by endothelial cells and this might lead to obstruction of tissue blood flow. About 60 two-exon *var* genes in the haploid genome of this species are responsible for the pathogenicity of *P. falciparum*. They encode the *P. falciparum* erythrocyte membrane protein-1 (*Pf*EMP1) which modulates the surface of the infected erythrocytes to bind to endothelial cells, activated platelets and uninfected RBCs (Cowman *et al*., 2016) (Milner, 2018). These

"sticky" infected RBCs adhere and activate the endothelial cells of the capillaries and postcapillary venules of brain, lungs, kidney and other vital organs starting a cascade of immune response (Hviid and Jensen, 2015) (Figure 1). Binding to uninfected RBCs leads to formation of rosettes or clumps which block vascular blood flow (Stanley, 1997). This acts as an antigenic decoy to evade recognition by humoral immune system. On top of this, *P. falciparum* has acquired resistance to all the anti-malarial drugs used against it, making it difficult to treat with fatality to up to 1% in infected patients (Thu *et al.*, 2017). Early diagnosis and assessment of severity of the disease is vital for survival of infected individuals.

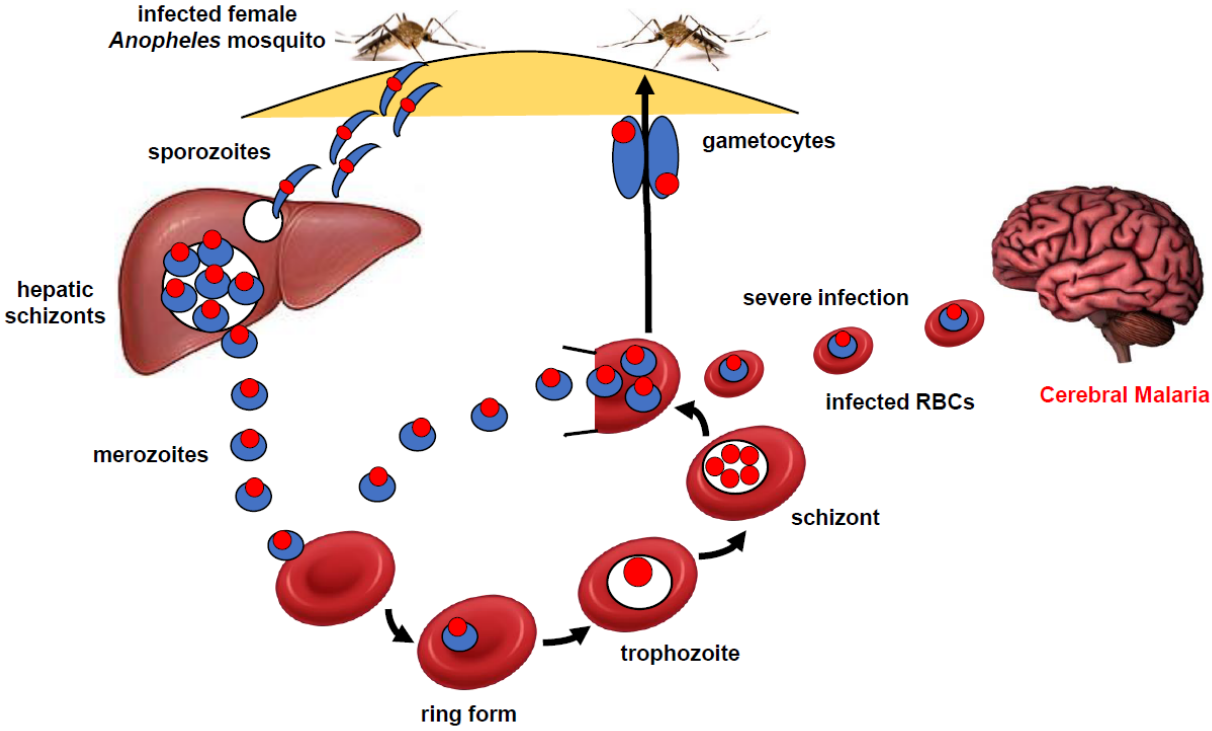

Figure 1: Life cycle of *Plasmodium spp.* in human hosts. Sporozoites are released onto the skin through the bite of an infected female *Anopheles* mosquito and they are carried in the bloodstream to the liver. They invade hepatocytes and undergo asexual reproduction (schizogony) to form merozoites. Merozoites hide in red blood cells (RBCs) to continue their replication to form large number of their clones which rupture the RBCs and spread their attack. Switch in replication signal allows merozoites to undergo gametogenesis which are then taken up during a mosquito meal. In cases of severe malaria by *P. falciparum*, infected RBCs sequester to the brain endothelium causing cerebral malaria which can prove to be fatal.

The other human infecting members of the *Plasmodium spp.* do not show prolonged sequestration of infected RBCs to the vasculature, thus, decreasing their lethality. According to WHO, *P. vivax* is the most common malaria parasite causing disease outside Africa. Though

considered to be a relatively benign species, cases of severe disease have been reported especially in children in high transmission areas. Severe anaemia and few cases of multi-organ failure have been reported though their mechanism remains unclear (Cowman *et al*., 2016). Both *P. vivax* and *P. ovale* can remain in quiescent forms in liver from months to years and can re-emerge to cause infection again. *P. malariae* causes the most benign form of malaria infection. *P. knowlesi* is the primate species which is restricted to regions in South-east Asia and can cause moderately severe to rather serious infection affecting mostly adults; however, its occurrence is low and restricted (Singh and Daneshvar, 2013) (Lee *et al*., 2009).

2.2.2.4 Naturally acquired immunity

Humans residing in endemic regions can acquire natural immunity to severe malaria to some degree. Adults and older children are protected from morbidity and death though they still remain susceptible to infection. The burden of severe infection falls mostly on children and immunocompromised persons (Marsh and Kinyanjui, 2006). Naturally acquired immunity is developed through repeated exposure to the disease where antibodies mediate protection generally against the blood stage of the infection. However, natural immunity is inefficient and it is unknown how much exposure is required to develop such immunity. Consecutively, the longevity of the antibodies is highly debatable with evidences for both short-term and long-term antibodies. Further research regarding the acquisition and development of antibodies is required to comprehend the naturally acquired immunity to malaria (Fowkes *et al*., 2016).

2.2.3 DIAGNOSIS

Prompt and accurate diagnosis is the most important aspect of malaria disease management. The clinical symptoms of severe and uncomplicated malaria are nonspecific; therefore, all patients with suspected malaria should undergo a parasitological diagnosis by microscopic examination or rapid diagnostic tests (RDTs) of the blood sample.

Microscopic examination of Giemsa-stained thick and thin blood smears, collected just by finger pricking, remains the golden standard for malaria parasite detection (Wongsrichanalai *et al*., 2007). It is inexpensive to perform, is able to differentiate between the five species of *Plasmodium* and can also quantify the parasitemia, providing an indication of severe malaria. Thick filmed smears have higher chances of accurate diagnosis while thin filmed smears allow better species determination and quantification (Payne, 1988). The different species of the parasite can be identified based on their morphological differences under the microscope (Figure 2). However, poor microscopic examinations performed by untrained professionals could lead to false positive, false negative results, error in species identification leading to mistreatment (Wongsrichanalai *et al*., 2007).

RDTs are quick, ready to use devices that are impregnated with mono- or polyclonal antibodies that detect malaria-specific antigens and enzymes through colorimetric transformation or nitrocellulose strips. They are highly efficient in identifying *P. falciparum* infections as they specifically detect *P. falciparum* specific histidine rich protein 2 (*Pf*HRP2) and *P. falciparum* specific lactate dehydrogenase (*Pf*-pLDH). Therefore, it is helpful in accurately distinguishing the lethal *P. falciparum* from the other four species of *Plasmodium* with 95% sensitivity. *P. vivax* infections can be detected with RDTs against *P. vivax* specific lactate dehydrogenase (*Pv*-pLDH). All the human infecting *Plasmodium* can be detected with pan-pLDH and pan-aldolase RDTs which are common enzymes in the species. Currently, there exists no species-specific RDTs for *P. ovale*, *P. malariae* and *P. knowlesi* (Wongsrichanalai *et al*., 2007) (Mukkala *et al*., 2018).

Nucleic acid amplification with polymerase chain reaction (PCR) could be sometimes useful in distinguishing the species for which RDTs are not available. However, PCR is largely used as a research technique and not so much in clinical diagnosis of malaria.

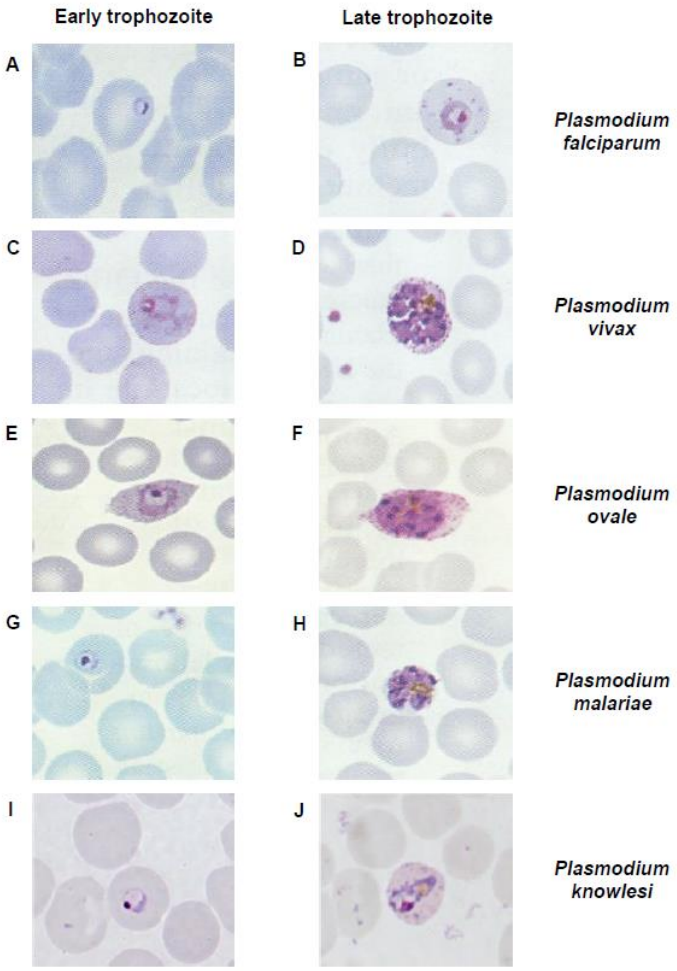

Figure 2: Morphological differences amongst the five human infecting strains of *Plasmodium spp.* Microscopic examination of Giemsa-stained blood smears collected from infected patients. (A, B, C, D, E, F, G, H adapted from (Erber, 2000) and I, J adapted from (Singh and Daneshvar, 2013)).

2.2.4 TREATMENT

Treatment of malaria depends on the severity of the disease, the infecting *Plasmodium spp.*, transmission area and the patient's pre-existing immunity. Anti-malarial drugs fall into four main categories (Stanley, 1997) (WHO, 2015) (Thu *et al.*, 2017):

- the quinoline-related compounds (quinine, quinidine, chloroquine, mefloquine, halofantrine and primaquine): fast acting compounds that generally interfere with the parasite's ability to metabolize haemoglobin thus, killing blood stage asexual parasites. Primaquine is used for long term treatment for total eradication of the parasites as it can kill the hepatic parasites and the gametocytes and prevent relapse.
- the artemisinin derivatives (artemether, artesunate and arteether): most potent antimalarials against blood stage infection. The compound has an endoperoxide ring which breaks down

when it comes in contact with the haem group in haemoglobin releasing free radicals and killing the parasites.

- the antifolates (pyrimethamine and proguanil): kill hepatic parasites and gametocytes by blocking the parasite specific actions of folic acid and prevent relapse.
- the antimicrobials (sulphonamides, dapsone, tetracyclines, clindamycin and azithromycin): slow acting drugs with different mechanism of actions, used for synergistic killing of blood stage parasites.

Since, the development of resistance to chloroquine and pyrimethamine, the multi-drug resistant *P. falciparum* infections are treated with artemisinin-based combination therapies (ACTs) (Thu *et al*., 2017). ACT is a combination of rapid acting artemisinin drugs with a slow acting partner drug. Artemisinin compounds act quickly reducing the blood parasite number in 48 hours while the slow acting partner will act longer to clear the remaining parasite and provide protection against artemisinin resistant strains. The five ACTs approved by WHO for treatment of uncomplicated *P. falciparum* malaria are (World Health Organization, 2015):

- artemether + lumefantrine
- artesunate + amodiaquine
- artesunate + mefloquine
- artesunate + sulphadoxine-pyrimethamine
- dihydroartemisinin + piperaquine

Chloroquine is the choice of drug to treat *P. vivax*, *P. ovale*, *P. malariae* and *P. knowlesi* infections. However, due to emergence of chloroquine-resistant *P. vivax* strains in some regions, patients affected there are treated with an ACT. Infected pregnant women in their first tri-semester are treated with quinine and not an ACT. To prevent relapse, all patients are advised a dose of primaquine for up to two weeks for total eradication of the parasite from the host's body (WHO, 2015) (Plewes *et al*., 2019).

However, most of the antimalarial drugs have adverse side effects. Quinine and its derivatives have narrow therapeutic ratios and could lead to hypoglycaemia due to increased insulin secretion, hypotension, cardiotoxicity in severe cases (Plewes *et al*., 2019). Pyrimethamine-sulphadoxine are not used anymore as a chemoprophylactic drug because of severe exfoliative dermatitis, erythema multiforme (Stanley, 1997). Primaquine can induce haemolytic anaemia in patients with glucose-6-phosphate deficiency (Cowman *et al*. 2016).

In cases of severe malaria, intravenous doses of ACT drugs are more effective than oral delivery (Plewes *et al*., 2019). If the species of infecting *Plasmodium* is not known, then patients should be treated for uncomplicated *P. falciparum* malaria. In the past few years, strains of *P. falciparum* have been reported to have less sensitivity to artemisinin and its derivative compounds across South East Asia (Thu *et al*., 2017). Resistance to antimalarial drugs with the ever evolving, lethal, multi-drug resistant *P. falciparum* poses the major threat to malaria eradication.

Vaccine: No licensed malaria vaccine exists at this time. After extensive research, a recombinant protein based vaccine, RTS, S, also named *Mosquirix*, completed phase III trial in sub-Saharan African countries with low efficacy after four doses, 27% in children aged 6-12 weeks and 31% in children aged 5-17 months (Bhagavathula *et al*., 2016) (Laurens, 2018). The vaccine is made up of a recombinant protein *P. falciparum* circumsporozoite protein (CSP) conjugated to hepatitis B surface antigen and acts against the pre-erythrocytic stage of the infection (Frimpong *et al*., 2018). After being approved by the European Medicines Agency and WHO, the vaccine is being administered in children aged 5-17 months in three sub-Saharan African countries with moderate to high transmission of malaria (Laurens, 2018). Currently, 20 other vaccines are undergoing clinical trials (Frimpong *et al*., 2018).

In 2015, the World Health Organization (WHO) set up the *Global technical strategy for malaria 2016-2030 (GTS)* to reduce the burden of malaria infection and mortality worldwide by 90% by the year 2030 (WHO and Global Malaria Programme, 2017). According to World Malaria Report, 2020 by WHO (WHO, 2020), incidence of malaria globally reduced between 2000 and 2015 by 27% whereas, between 2015 and 2019 it declined by less than 2% (Figure 3). However, accelerated changes for malaria prevention and eradication is urged by WHO to achieve the goals of GTS by 2030. Decreasing the risk of malaria include indoor and outdoor spraying of insecticides to destroy breeding grounds of mosquitoes and the use of mosquito net and repellents help in preventing mosquito bites. Spreading awareness in parallel with early diagnosis and development of novel drugs and vaccines could altogether be effective in the elimination of malaria.

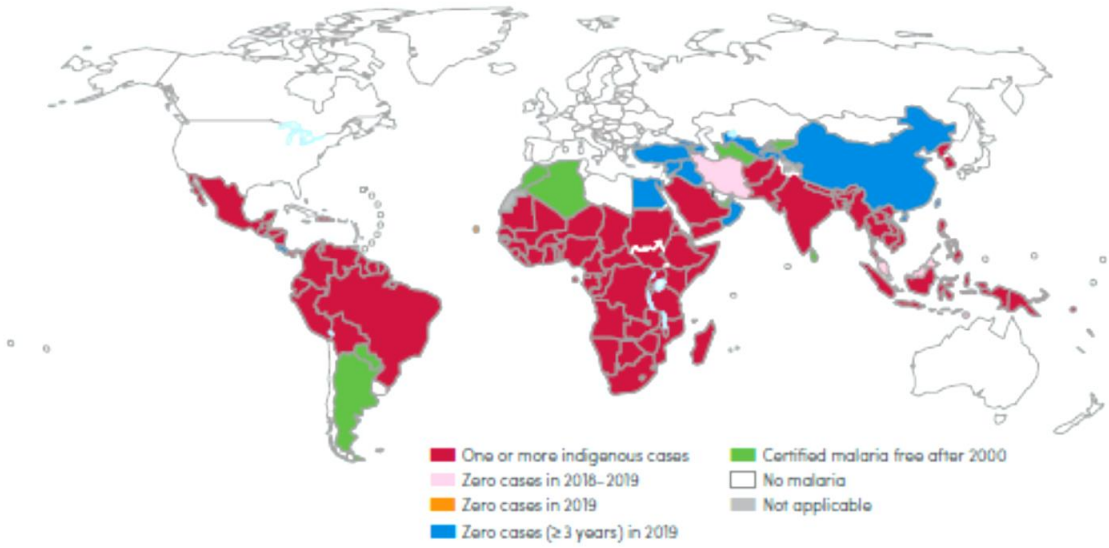

Figure 3: Countries with indigenous cases of malaria in 2000 and their status in 2019. Reduction in number of cases of malaria was seen worldwide from 2000 to 2019 with many countries reporting no cases for consecutive years. *Source: WHO database (WHO, 2020).*

2.3 CEREBRAL MALARIA

Cerebral malaria (CM), a complex neurological syndrome, is the most common form of manifestation of severe malaria which can lead to devastating consequences, including coma and death. In most of the cases, it develops during severe *P. falciparum* infection whereas, few instances of CM caused by severe *P. vivax* infection have also been reported (Manning *et al*., 2012). CM primarily affects children below 5 years of age in high transmission areas of sub-Saharan Africa where older children and adults gain partial immunity due to repeated exposure. While, in South East Asia it is also common in older children and adults where transmission is less intense (Sahu *et al*., 2015). Around 1% of the children infected with *P. falciparum* develop CM with a fatality around 15-20% and 90% of these cases are being reported in sub-Saharan Africa (Storm and Craig, 2014). In 2019, 67% of the affected children below 5 years of age died due to severe malaria, 90% of them were CM related deaths (WHO, 2020). Long-term neurological effects and cognitive deficits such as behavioural abnormality, epilepsy, and impaired motor functions are common in 10-20% of the surviving patients (Nishanth and Schlüter, 2019). Despite the reduction in global malarial burden in the past few years, the rate of mortality due to CM remains the same, especially in African children. Early diagnosis, proper care and treatment are critical for CM management and survival.

2.3.1 CLINICAL FEATURES

According to WHO, the hallmarks of CM are presence of asexual *P. falciparum* parasites in blood, inability to localize a painful stimulus, unarousable coma, multiple convulsions, exclusion of other causes of encephalopathy (Luzolo and Ngoyi, 2019). Coma in CM is assessed by verbal and motor responses and rated on either the paediatric Blantyre Coma Score (1 or 2 on a scale of 5) or Glasgow Coma Score (<11 on a scale of 15) for adults (Storm and Craig, 2014). Patients generally have all the clinical symptoms of malaria such as fever, chills,

headache, body ache and altered state of consciousness. CM is often accompanied with manifestations of severe malaria like metabolic acidosis, severe anaemia, hypoglycaemia, renal failure and respiratory distress, leading to multiple organ failure (Wah *et al*., 2016). The ultimate confirmation of CM is made through post-mortem detection of sequestered infected RBCs in the brain microvasculature (Figure 4) and presence of ring haemorrhages (Storm and Craig, 2014). A post-mortem examination of the brains of CM affected children in Malawi reported extensive myelin and axonal damage and blood brain barrier breakdown with the presence of cerebral edema (Dorovini-Zis *et al*., 2011).

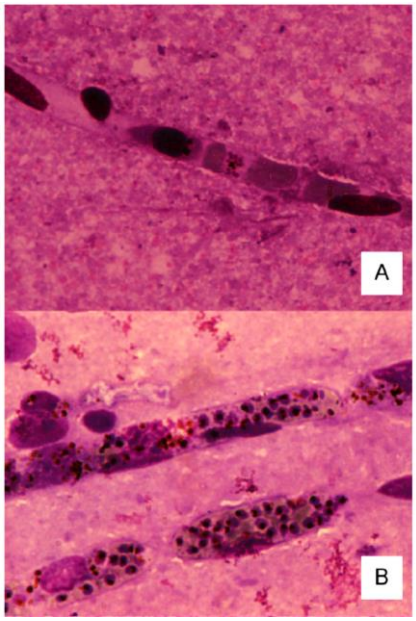

Figure 4: Post-mortem brain smears show sequestration of infected red blood cells in the microvasculature. Light microscopy of Giemsa-stained (400X magnification) brain tissues from fatal paediatric cases of cerebral malaria detected (A) occasional mature forms and (B) trophozoites and schizont forms of *Plasmodium falciparum* in the microvasculature (Manning *et al*., 2012).

In recent years, definitive diagnosis of CM is made by the presence of malignant retinopathy which is caused by sequestration of infected RBCs in the brain. Confirmation of malaria-specific retinopathy can differentiate between a malaria induced coma and a non-malarial coma in patients. Retinopathy can be observed in both children and adults affected with CM and can be characterised by four features: retinal whitening, vessel changes, retinal haemorrhages and papilledema. The inclusion of retinopathy in clinical diagnosis increases the specificity of detecting patients affected with CM (Luzolo and Ngoyi, 2019) (Seydel *et al*., 2015).

2.3.2 EXPERIMENTAL CEREBRAL MALARIA

The major setback in years of CM research has been the fact that invasive observations and analysis of the intracerebral changes during CM development could mostly be done in post-mortem studies in humans. In particular, there is an ethical and physical barrier to test the early stages of the disease in human patients, prior to neurological manifestations (Brian De Souza *et al*., 2010). Therefore, murine models of CM have been developed since mice and humans have similar genomes and immune responses, mice have short generation time and large reproductive capacity and mouse genome can be easily manipulated to investigate the role of different signalling molecules (Torre *et al*., 2018). *P. yoelii* and *P. berghei* Antwerpen-Kasapa (ANKA) are the two species of rodent specific *Plasmodium* which cause development of cerebral syndromes in mice. However, the most widely used murine model of CM is induced by *P. berghei* ANKA (*Pb*A) infection in CBA or C57BL/6 strains of mice and is known as experimental cerebral malaria (ECM) (Hunt *et al*., 2006). *Pb*A-infected mice show similar pathological and clinical features like human CM. These include sequential signs of neurological symptoms with disease development such as paralysis, ataxia, seizures and if untreated they succumb to the disease between 5 to 10 days of infection (Ghazanfari *et al*., 2018). Similarities in histopathological, immunological and behavioural alterations between ECM and CM have helped in delving deeper into CM immunopathology.

However, there is a significant debate regarding the validity of ECM in understanding human CM. The main difference is the fact that sequestration of infected RBCs is regarded as a controversial event in ECM development. While some studies have reported accumulation of infected RBCs in the murine brain during ECM, it is still unclear whether this was due to true sequestration of infected RBCs like in human CM or simply an accumulation due to an intracerebral haemorrhage (Strangward *et al*., 2017). This might be due to the reason that the

mouse infecting strain, *P. berghei* ANKA, lacks the *P. falciparum* erythrocyte membrane protein-1 (*Pf*EMP1) protein which renders *P. falciparum*-infected RBCs to adhere to endothelial cells and lead the sequestration process in human CM (Torre *et al*., 2018). Consequently, ECM might be driven by a storm of pro-inflammatory cytokine release and excessive leukocyte accumulation in the brain. The characteristic feature of ECM development is the excessive accumulation of $CD8^+$ T cells in the murine brain and $CD8^+$ T cell knock out mice do not show any neurological symptom and are protected from the disease (Howland *et al*., 2015). Granzyme B and perforin expression by murine $CD8^+$ T cells are essential for the development of ECM (Haque *et al*., 2011) (Nitcheu *et al*., 2003). Though accumulation of different leukocytes have been reported in post-mortem studies of human CM cases, the role of $CD8^+$ T cell in human CM pathogenesis is unclear and remains to be determined (Torre *et al*., 2018). Despite the unresolved issues, murine model of CM, induced by *Pb*A infection, is the best and most available experimental animal model of CM and has been used widely for scientific research purposes.

Since, the rate of disease progression, from the appearance of clinical, neurological symptoms to death, is very rapid in ECM, the best way to keep a track of the disease is to score the animals based on their deteriorating health from the day of infection. Carroll *et al*., 2010 proposed a rapid murine coma and behaviour scale (RMCBS) to assess the functional impairment of malaria infected mouse. A mouse can be scored rapidly based on 10 physical traits that are associated with clinical symptoms of ECM: gait, balance, motor performance, body position, limb strength, touch escape, pinna reflex, toe pinch, aggression and grooming. Each parameter is scored from 0-2 with 2 being normal functioning and 0 being the worst/loss of functioning. So, in total a mouse would get a score between 0-20, with 20 being a healthy mouse without any disease while a mouse with score 1-2 is a severely sick one with neurological symptoms of ECM. Some other parameters like coordination, exploratory behaviour, strength and tone,

reflexes and self-preservation, hygiene-related behaviour also alter with disease progression (Carroll *et al*., 2010). The RMCBS has since been in use to label mice according to the stage of disease progression they are in during ECM development.

2.3.3 PATHOGENESIS

Despite decades of research conducted, the cause and development of CM and the risk factors associated remain yet to be fully elucidated. The pathogenesis of CM has been attributed to several factors such as: sequestration of *P. falciparum* infected RBCs in the microvasculature of the brain, massive expression of pro-inflammatory cytokines and chemokines in the brain, microvascular thrombosis, loss of endothelial cell functioning leading to blood brain barrier (BBB) disruption, edema and increased cranial pressure (Sahu *et al*., 2015) (Luzolo and Ngoyi, 2019). The majority of the hypotheses regarding CM development state that an important event in pathogenesis is the sequestration of infected erythrocytes in the microvasculature of the brain by adhering to the endothelial cells (ECs) of the vasculature.

2.3.3.1 Sequestration of infected RBCs

More than a century ago, Italian malariologists Marchiafava and Bignami had proposed that the fundamental pathological process underlying severe *P. falciparum* malaria was microvascular obstruction (White *et al*., 2013). Post-mortem studies of brains of the fatal CM cases have reported dense sequestration of infected RBCs within the cerebral microvasculature. Infected RBC sequestration is generally quantitatively higher in brains of patients who died because of CM in comparison to individuals who succumbed to non-cerebral malarial complications (Storm and Craig, 2014). This cytoadherence is mediated by the expression of *P. falciparum* erythrocyte membrane protein-1 (*Pf*EMP1) on the surface of the *P. falciparum* infected RBCs. The expressed *Pf*EMP1 antigen is localized to small cup-like projections on the cell membrane of the infected RBCs called knobs (Nishanth and Schlüter, 2019). The

*Pf*EMP1 can specifically bind to multiple cell surface receptors like intercellular adhesion molecule-1 (ICAM-1), CD36, E-selectin, neural cell adhesion molecule (NCAM) and CD31 (PECAM-1) for endothelial cells as well as chondroitin sulphate A (CSA) for placental syncytiotrophoblasts thus, immobilizing the infected RBCs on the endothelial cells (Wassmer and Grau, 2017). The adherent, infected RBCs pack into the microcirculation reducing the luminal diameter of the capillaries and lead to disruption of the normal cerebral blood flow (Dondorp *et al*., 2000). The uninfected red blood cells can also adhere to the infected ones forming rosettes or clumps of RBCs which could further obstruct the blood flow and cause hypoxia and hypoglycemia, leading to brain cell death. Platelet-mediated clumping of *P. falciparum*-infected RBCs is associated with severe malaria and might contribute to reducing cerebral blood flow (Pain *et al*., 2001). Stiffness of infected RBCs has also been observed as the parasite grows in the erythrocyte, making it less deformable and preventing RBC destruction. The metabolically active sequestered infected RBCs compete with host tissues for substrates, for instance, glucose and oxygen and might also produce toxins that interfere with host tissue metabolism (Ohnishi, 2009). Thus, sequestration of infected RBCs to the endothelial cells is an important event in the development of CM which might lead to mechanical obstruction of cerebral blood flow, activation of endothelial cells as well as pro-inflammatory and pro-coagulant responses and cell death. However, the parasites do not directly enter or attack the brain or the nervous tissue at any point of infection (Schiess *et al*., 2020); they remain inside the RBCs and attach to the endothelial cells of the cerebral blood vessels forming rosettes and so far, RBC accumulation has been reported only in the cerebral microcirculation.

2.3.3.2 Inflammation

It has been hypothesized for several years that an imbalance between pro- and anti-inflammatory immune responses is a leading cause of pathogenesis in CM. An exacerbated immune response is elicited in the central nervous system due to the release of a storm of pro-

inflammatory cytokines and leukocyte accumulation in the brain during CM. The critical role in triggering inflammation during CM is played by a number of pro-inflammatory cytokines, such as, tumor necrosis factor-α (TNFα), interferon-γ (IFN-γ), interleukin-1α and -1β (IL-1α, IL-1β) and lymphotoxin-α (LTα) (Dunst *et al*., 2017). Activated brain endothelial cells, microglia, circulating macrophages and monocytes and accumulating leukocytes are the major producers these of pro-inflammatory cytokines. *In vitro* studies with human endothelial cells infected with *P. falciparum* and serum from infected individuals have demonstrated induction of chemokines like CCL2, CCL20, CXCL1, CXCL2, CXCL6, CXCL8, CXCL9 and CXCL10 during severe malaria (Ioannidis *et al*., 2014). Cytokine and chemokine guided movement allows leukocytes, like $CD8^+$ T cells, to migrate to the brain endothelium starting systemic inflammation.

TNFα and IFN-γ play an important role in CM development by activating endothelial cells and upregulating the expression of adhesion molecules on ECs for infected RBC sequestration. In CM affected African children, high concentrations of TNFα have been reported in their serum and are associated with hypoglycaemia, hyperparasitemia, coma and death (Ohnishi, 2009). TNFα has been hypothesized to increase local production of NO, by upregulating the inducible nitric oxide synthase (iNOS) gene in the brain endothelium. NO diffuses through the BBB, interferes with synaptic transmission and affects consciousness (Postels and Birbeck, 2013). Despite this association with disease severity in CM, *Tnf*-deficient mice were not protected from murine CM and though patients treated with anti-TNF antibodies had reduced body temperature, it did not help in their survival (Dunst *et al*., 2017). On the other hand, neutralization or deletion of IFN-γ in murine CM protected them and improved their mortality (Hunt and Grau, 2003). IFN-γ is produced by multiple cell types: natural killer (NK) cells, natural killer T (NKT) cells, γδ T cell receptor (TCR), αβ TCR, $CD4^+$ and $CD8^+$ T cells. In *Ifn*-

deficient mice with CM, reduced expression of adhesion and antigen presenting molecules were observed, thus, explaining its role in CM pathogenesis (Ghazanfari *et al*., 2018).

Deletion of LTα protected mice from murine CM and could be a key player in CM pathogenesis. Elevated levels of LTα have seen observed in malaria patients and its possible role in CM development remains to be studied. Anti-inflammatory cytokine, IL-10, expression provides some protection in murine CM by inhibiting the production of cytokines, like TNF, and chemokines; however, its host-protective mechanism either falls short or is deficient during severe CM as lower levels of plasma IL-10 was detected in CM victims in comparison to survivors in a study (Hunt and Grau, 2003).

Intracerebral trafficking of leukocytes is the result of increased pro-inflammatory response and aids in further cerebral inflammation. Post-mortem studies in humans affected with CM have shown accumulation of intracerebral leukocytes along with sequestered RBCs (Nishanth and Schlüter, 2019). The C-X-C motif chemokine receptor-3 (CXCR3) is expressed on leukocytes, especially on T cells, and is necessary for the recruitment of leukocytes in the brain in response to the increased pro-inflammatory cytokines. Majority of the mice deficient in CXCR3 did not develop murine CM and showed less accumulation of $CD8^+$ T cells in their brain, thus, establishing CXCR3 as a therapeutic target for treatment of CM (Ghazanfari *et al*., 2018).

2.3.3.3 Endothelial dysfunction

Endothelial dysregulation plays an important role in the pathogenesis of CM and can be caused due to multiple factors: adhesion of infected RBCs, excessive pro-inflammatory cytokine response and increased coagulation in the microvasculature leading to obstruction of cerebral blood flow. Activation of endothelial cells occurs as a consequence of binding of *Pf*EMP1 to number of endothelial cell surface receptors such as endothelial protein C receptor (EPCR), intercellular adhesion molecule-1 (ICAM-1), the vascular cell adhesion molecule-1 (VCAM-

1), CD36, CD31 (PECAM-1) and E-selectin (Nishanth and Schlüter, 2019) (Wassmer and Grau, 2017).

Binding of infected RBCs to EPCR prevents the activation of protein C which enhances thrombin production and results in activation of endothelial cells. Thrombin is a key mediator of localized coagulation and inflammatory processes and its increased production leads to increased angiopoietin-2 (Ang-2) / angiopoietin-1 (Ang-1) ratio, TNF and Von Willebrand Factor (VWF) production, resulting in the loss of endothelial barrier function (Luzolo and Ngoyi, 2019). Normally low levels of EPCR in the cerebral endothelium are further down-regulated in CM along with infected RBCs causing a loss of EPCR binding sites thus, interfering with the cytoprotective function of activated protein C (APC) and normal homeostasis (Wassmer and Grau, 2017).

Angiopoetin-1 stabilizes the endothelium while its antagonist angiopoetin-2 induces vascular permeability and upregulates the expression of endothelial cell receptors. Increased Ang-2/Ang-1 ratio is generally a predictor of severity in CM. Ang-1 and Ang-2 levels are regulated by nitric oxide (NO) which is produced in the endothelium from L-arginine. NO helps in vasorelaxation, down-regulation of endothelial cell adhesion molecules and decreases thrombosis. Reduction in L-arginine production is a hallmark of severe malaria resulting in decreased bioavailability of NO which leads to over-expression of endothelium receptors like ICAM-1, VCAM-1 and E-selectin thereby, immobilizing infected RBCs on the vascular endothelium (Storm and Craig, 2014) (Luzolo and Ngoyi, 2019).

In addition to this, a storm of pro-inflammatory cytokine release, like TNF-α and IFN-γ, is triggered which leads to recruitment of leukocytes to the brain endothelium, modulating the tight-junction proteins and localized leakiness of the blood brain barrier. Over-expression of endothelial microparticles have been reported in CM which causes cell activation and apoptosis

(Wah *et al*., 2016). Intense accumulation of infected RBCs in the vascular endothelium might obstruct the blood flow decreasing the oxygen and glucose supply to the brain which could aid in CM induced coma in affected patients (Luzolo and Ngoyi, 2019).

2.3.3.4 Blood-brain barrier damage

The blood brain barrier (BBB) is a protective, selectively permeable interface separating the central nervous system from the vasculature of the rest of the body. It tightly regulates the transport of essential nutrients like glucose, amino acids and small moieties from the blood into the brain and allows the release of metabolic waste products from the brain back into the blood with the help of special transport channels. The BBB also protects the brain from injury and diseases by restricting the entry of foreign substances like pathogens, toxins and immune cells of the body (Daneman, 2012). The BBB constitutes of capillaries and post capillary venules which are made up by tightly packed endothelial cells connected by tight junctions and the underlying basal lamina. A cellular layer of pericytes, extended processes of astrocytes, called end-feet and neural cells ensheathe the BBB providing support and integrity and form the neurovascular unit. Microglia and perivascular macrophages survey the BBB giving it immune protection (Combes *et al*., 2010). In post-mortem studies and examination of cerebrospinal fluid (CSF) in fatal CM cases, BBB breakdown, leakage and disruption have been consistently reported (Figure 5). The same have been confirmed in murine CM with Evans blue dye and radiological tests. Cerebral endothelial cells are the key components of the BBB and infected RBC adherence to the endothelial surface leads to disruption of BBB structure and function. Sequestration of infected RBCs leads to activation of endothelial cells and their dysfunction along with excessive inflammation with the release of a storm of pro-inflammatory cytokines,

intravascular coagulation, all of which ultimately aids in loss of BBB integrity (Nishanth and Schlüter, 2019).

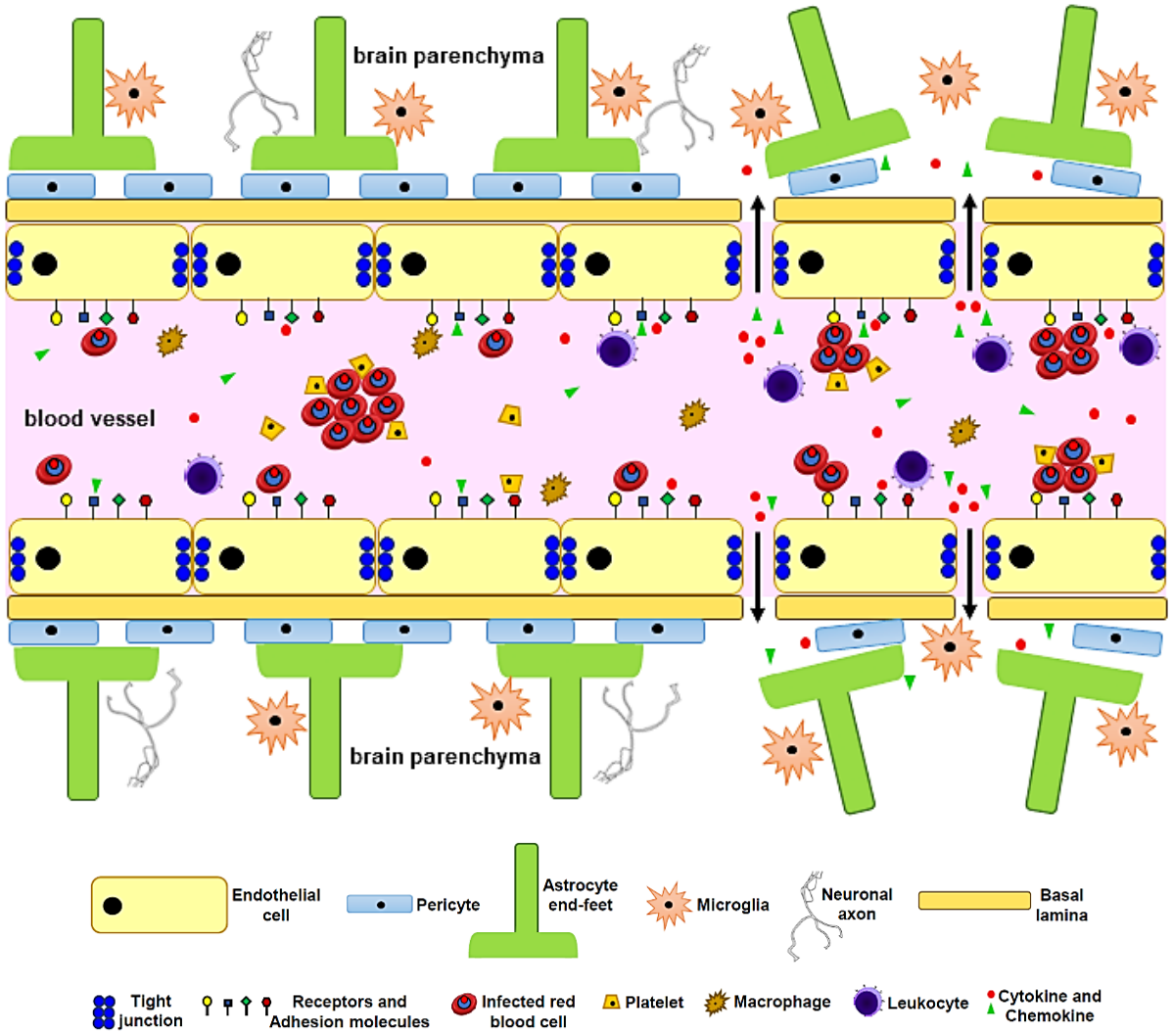

Figure 5: Blood brain barrier (BBB) disruption during cerebral malaria. An important event in cerebral malaria is the sequestration of infected red blood cells (iRBCs) to the endothelial cells of the blood brain barrier (BBB). Binding of iRBCs to the cell adhesion molecules on the endothelial cell surface activates the endothelial cells which are tightly held together by tight junction proteins. Consequently, exacerbated pro-inflammatory response results from excessive leukocyte accumulation and a storm of cytokines and chemokines being released. Furthermore, rosette formation by clumping of iRBCs, sometimes, aided by platelets, might block cerebral blood flow. Simultaneous occurrence of these events leads to endothelial dysfunction and downregulation of tight junction proteins; thus, opening the BBB. Astrocytes and pericytes lose their protective functioning and widen the damage to the BBB.

Intracellular cascades are affected leading to decreased expression of the tight junction protein, zona occludens-1 (ZO-1), of the endothelial cells which further opens up the BBB (Medana and Turner, 2007). Astrocytes have been shown to be unevenly distributed and retract their end-feet from the BBB leading to its loss of ensheathment in murine CM (Medana *et al.*, 2001).

Pericytes lose their protective function of the BBB due to increased angiopeotin-2 level during CM (Nishanth and Schlüter, 2019). Sequestration of infected RBCs, endothelial cell activation, excessive inflammation act synergistically in promoting BBB permeability (Figure 5). Disruption of the BBB results in astrocyte and microglia activation and neuroinflammation (Dunst *et al*., 2017). These are accompanied by micro-haemorrhages, lesions and cell death, specially of neurons (Combes *et al*., 2010). Increased permeability could result in increased brain volume and swelling in affected CM patients.

2.3.3.5 Intracranial pressure and edema

Cerebral edema is the trapping or excess accumulation of fluids in the brain leading to rise in intracranial pressure. Since intracranial space is limited, any increase in brain volume can lead to tissue damage, herniation and brain death. It can arise from a number of factors like, any molecular, cellular, structural or functional changes in the blood-brain barrier integrity, cerebral blood flow, cerebral homeostasis and neuroinflammation. Significant increase in brain volume, raised intracranial pressure, cerebral edema have been reported in patients affected with CM, especially in children (Ohnishi, 2009). Both non-invasive imaging techniques like computed tomography (CT) scans and magnetic resonance imaging (MRI) and post-mortem studies have confirmed the presence of brain swelling, herniation and edema in patients worldwide (Figure 6). In a study with CM affected African children, increased brain volume was evident in children who succumbed to CM whereas it was uncommon in the affected survivors. In majority of the fatal cases, increased intracranial pressure was associated with decreased pre-pontine and post-pontine cerebrospinal fluid (CSF) levels and brain-stem herniation (Seydel *et al*., 2015). Thus, raised intracranial pressure has been attributed as a critical factor in severity of CM with greater depth of coma and acts as a predictor of fatality.

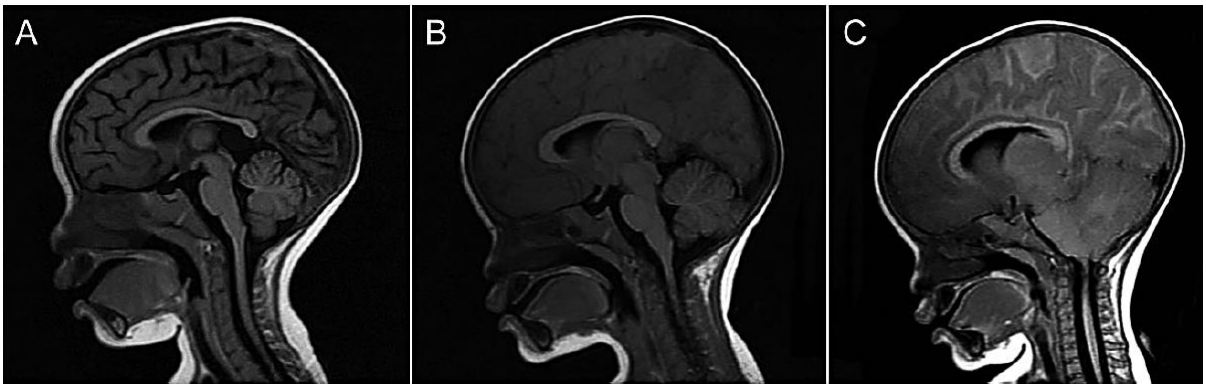

Figure 6: Increasing brain volume in a fatal case of paediatric cerebral malaria (Taylor and Molyneux, 2015)**.** MRI studies show (A) brain of a recovered patient with rounded gyri in black and cerebrospinal fluid in sulci and surrounding brain stem, (B) brain of a CM affected child and (C) brain of the same child 24 hours after image B was taken. Flattened gyri and narrow sulci can be observed in both B and C. Indication of herniation can be observed in C, just 4 hours before death by the encroachment of cerebellar tonsils in the brainstem.

The pathophysiology of cerebral edema in CM remains poorly defined. Sequestration of infected red blood cells in the cerebral microvasculature could play a crucial role in cerebral edema development during severe CM; however, a direct link with *in vivo* neuroimaging in humans has not been reported yet. Obstruction of venous blood flow could lead to diffused leakage forming lesions. Cerebral blood flow could also increase due to anaemia, fever and seizures (Ohnishi, 2009). Impaired perfusion, mechanical injuries, ischemia and cell death could result in cytotoxic edema whereas, endothelial activation, excessive pro-inflammatory response and blood brain barrier disruption could lead to inflammation and vasogenic edema (Seydel *et al*., 2015). Uncertainty regarding the role of brain swelling in CM remains with the heterogeneity of the disease, underpowered clinical trials and mis-classification of CM. Though, raised intracranial pressure is not always fatal, but it has been shown to be associated with poor prognosis of the disease. Surviving patients with increased brain volume in CM are prone to long lasting cognitive deficits. Feasibility of non-invasive imaging to determine the alterations in cerebral blood flow is low in the African countries where it is needed the most. Adjuvant therapies to treat increased intracranial blood pressure yet remains to be employed.

2.3.4 TWO MAJOR HYPOTHESES OF CM PATHOGENESIS

Uncertainty in the clinical definitions of the pathological processes in CM are still prevalent in spite of the rigorous studies for decades. Though the sequestration of infected RBCs in the brain capillaries of infected patients remain the most common observation in CM, it might not be the only cause for CM pathogenesis. Since, it has been detected solely through post-mortem studies, the degree of sequestration in CM is incompletely understood and debated. Also, it is hypothesized that the presence of infected RBCs alone would produce subtler cerebral symptoms indicating that it is not solely responsible for the clinical manifestations of CM (Clark and Rockett, 1994). To explain all the processes taking place in CM pathogenesis, two central concepts have evolved over the years: the sequestration theory and the cytokine theory.

The sequestration theory is based on the presence of large numbers of infected RBCs in the brain microvasculature in CM victims. Sequestration of infected RBCs to the brain endothelium is an essential initial event and is facilitated by the binding of the *Pf*EMP1 surface protein to various endothelial adhesion molecules which in turn are upregulated and this may lead to impaired perfusion and cytotoxic brain edema as explained in 2.3.3.1.

However, in some fatal CM cases little or no sequestration of infected RBCs were detected giving rise to the increasing debate over this theory (Dunst *et al*., 2017). CM caused by *P. vivax* resulted in endothelial activation and brain swelling without any sequestration of infected RBCs as it lacks the *Pf*EMP1 adhesion protein. It also fails to explain how individuals with high parasitemia are immune to CM, especially in Africa (Storm and Craig, 2014). All these questions could be answered by the involvement of additional factors in CM pathogenesis.

The cytokine theory stems from the fact that there is an imbalance of pro- and anti-inflammatory cytokine release during CM which results in cerebral inflammation and

pathology. Increase in systemic cytokine levels in serum of fatal CM patients serves as a direct link to disease severity (Dunst *et al*., 2017). Endothelial and astrocyte activation along with increased accumulation of leukocytes are the major cause of the overproduction of cytokines and chemokines as described in 2.3.3.2 leading to severe inflammation and vasogenic edema.

Questions have been raised regarding this theory when some studies failed to show a correlation between TNFα concentration and disease severity. The role of cerebral accumulation of immune cells is also debatable as there are few reports of it in post-mortem studies in human CM (Storm and Craig, 2014). Discrepancies in clinical observations make it difficult to determine the primary events of CM pathogenesis. The two theories are dependent on each other and establish the fact that CM is linked to multiple phenomena and a lot remains to be understood about its pathogenesis.

2.3.5 DIAGNOSIS

Early and correct diagnosis of CM is of utmost necessity for a better outcome of the patient. Any comatose patient with high fever and chills in an endemic area or a history of being in an endemic area two months prior to the symptoms is generally considered to be affected by CM (Plewes *et al*., 2018). This definition is vague since cerebral dysfunctions could be caused by a myriad of other factors and diseases and hence can lead to mis-diagnosis of CM from other CNS related disorders and also from non-cerebral malaria. The first step to confirm malaria infection is by microscopic examination of stained blood smears collected from symptomatic patients or by rapid diagnostic tests. Presence of *P. falciparum* or in some cases, *P. vivax*, increases the chance of development of CM (Luzolo and Ngoyi, 2019).

Fundoscopic examination, by either direct or indirect retinoscopy, is a highly promising tool in correct diagnosis of CM. The characteristic retinal findings include retinal whitening, blood vessel colour changes and retinal haemorrhages (Swamy *et al*., 2018). Patients with clinically

defined CM who lacked malarial retinopathy were shown to have other causes of death on autopsy; thus, fundoscopy could help in avoiding mis-diagnosis of CM (Postels and Birbeck, 2013). Several novel imaging techniques like computed tomography (CT) and magnetic resonance imaging (MRI) have provided insight into CM pathology and are useful in follow up studies of survivors. They provide *in vivo* information about cerebral blood flow and damage to cerebral tissues which is otherwise impossible to attain (Sahu *et al*., 2015). A MRI study in African children affected with CM detected that 84% of the children who died had severe brain swelling; thus, rendering brain swelling and edema a strong fatal factor of CM and MRI an highly useful tool to detect it (Seydel *et al*., 2015).

However, the access to advance brain imaging techniques and fundoscopy are unfeasible in resource-limited, developing, rural regions with high malaria prevalence. Lack of information and knowledge prevents the implementation of useful tools to diagnose CM in its early stage (Luzolo and Ngoyi, 2019). In addition to these, a few biomarkers like Ang2/Ang1 ratio, histidine rich protein-2 (HRP2) and metabolic acidosis are explored but a single reliable potential biomarker for detecting CM development is still missing (Storm and Craig, 2014).

2.3.6 TREATMENT

Once a successful diagnosis of CM is made, treatment should begin immediately. The main course of treatment starts with anti-malarials, supportive care and anticipating and treating complications arising in the patient. The first line of treatment includes intravenous administration of artesunate or artemisinin-based combination therapies (ACT) approved by WHO (Postels and Birbeck, 2013). ACT administration should be continued orally for complete eradication of parasite load. However, ACTs act only against the parasites and are not helpful in treating the neurological complications which are often fatal.

Patients are generally administered in an intensive care unit and other life-saving interventions are necessary to increase survival. CM in adults might affect multiple organs like lungs, kidneys and liver and are constantly monitored (Postels and Birbeck, 2013). In comatose patients, intubation and mechanical ventilation might be vital for respiration (Plewes *et al*., 2018) . Seizures and convulsions are typical in CM patients, especially in children, due to hypoglycaemia. Administration of anti-convulsant drugs along with intravenous dextrose and fluids can help in these situations (Luzolo and Ngoyi, 2019). Anti-pyretic drugs are helpful in decreasing the high fever.

Adjunctive therapies have emerged in the last few decades which are simultaneously administered with anti-malarial treatment to reduce the complications of the disease (Varo *et al*., 2018). The aim is to target multiple pathways of CM development through multiple interventions and they are investigated through randomized controlled trials (RCTs) (Higgins *et al*., 2011). Some of them include modulating the immune response by corticosteroids to decrease brain swelling and inflammation, anti-TNF therapy to inhibit TNFα functioning, decreasing procoagulant effects by anti-coagulant drugs, blood transfusion to treat anaemia, treatment with osmotic diuretics to release intra-cranial pressure, restricting iron availability with iron chelators, treating hypoglycaemia and acidosis, decreasing nitric oxide levels and many more (Varo *et al*., 2018) (Higgins *et al*., 2011) (Golenser *et al*., 2006). While these interventions might be useful in some cases, the search for a successful adjunctive therapy have been unsuccessful so far and still goes on.

2.4 *In vivo* NEURO-IMAGING

Methods that are able to image *in vivo* the entire brain of experimental animals are of high relevance in preclinical neuroscience, in particular for analysing spatiotemporal patterns in disease progression. Non-invasive, *in vivo* imaging provides a direct insight into the unique

clinical features of the pathology of a neuronal disease. It helps to track the structural, functional and molecular changes occurring in the brain pathology in real time and has become an useful diagnostic tool (Misgeld and Kerschensteiner, 2006). This is a huge advantage over conventional post-mortem studies of neurological diseases. In the past decade, increased sensitivity and resolution of *in vivo* imaging techniques have advanced the understanding of brain dynamics to the level of a single cell (Hickson, 2009). Modern imaging techniques like computed tomography (CT) scans and magnetic resonance imaging (MRI) are used for anatomical imaging to evaluate structural abnormalities, location and the extent of the disease while radionuclide imaging techniques like single photon emission computed tomography (SPECT) and positron emission tomography (PET) can be used to assess the regional changes in biochemical properties of tissues and organs (Stout and Zaidi, 2008).

In order to evade the limitations of post-mortem studies in CM and to gain more insight about the disease pathology, tremendous efforts are being made to provide clinical imaging devices in malaria endemic regions. In this study, MRI and SPECT imaging techniques have been used to image the brains of malaria-infected mice to understand the disease pathology.

2.4.1 MAGNETIC RESONANCE IMAGING

The MRI is a powerful diagnostic tool crucial for monitoring and understanding the mechanisms involved in disease progression. It allows non-invasive imaging of organs and tissues in real time with non-ionising radiation and provides impressive soft tissue contrasts and both 2D and 3D data (Carr and Grey, 2002). Apart from structural and morphological parameters, MRI has the capability to provide functional information like diffusion, perfusion, flow, temperature and magnetic susceptibility (Moser *et al.*, 2009). Hence, the clinical applications of MRI are increasing and encompass the whole human body especially neurological, psychiatric, cardiac, abdominal, vascular and musculoskeletal complications.

MRI was developed after the discovery of nuclear magnetic resonance (NMR) in 1952 (Carr and Grey, 2002). It is based on the principle that the human body is predominantly composed of water and in presence of an external magnetic field when exposed to radio frequency (RF) pulses, the hydrogen (H^1) atoms in the water moiety absorb RF energy and align with the magnetic field. When the RF pulse is removed, the H^1 nuclei reaches equilibrium and releases back energy at radio frequencies which can be detected as a signal. It essentially maps the water and the fat content in a living organism due to their abundance of H^1 atoms. Normal and abnormal tissues release energies at different rates contributing to the diagnosis of diseased conditions (Carr and Grey, 2002) (Seth *et al*., 2017). T_1 and T_2 are the relaxation times that the H^1 nuclei take for the longitudinal and transverse decay of magnetization. T_1 images highlight fat while T_2 images highlight water (Fisher and Siegelman, 2002). Typically, a MRI consists of three main components: a main magnet providing high magnetic field, a gradient system to localize signals and the RF system to measure signals (Moser *et al*., 2009). MRI is gaining ground as a safer, non-invasive alternative imaging technique to CT, X-ray or SPECT scans which have minimal levels of ionising radiation.

Angiography is the imaging technique used to visualize the blood vessels and measure the blood flow in a specific organ. In MR angiography (MRA), the powerful magnet and the radio waves are utilised to visualize the blood vessels non-invasively and identify abnormalities in them. Since, MR imaging is highly sensitive to motion, non-contrast, flow-sensitive imaging techniques were first developed exploiting the motion of blood flow to generate high contrast images of blood vessels and are still widely in use for MRA. To overcome the limitations of flow related artifacts, new techniques with incorporation of a contrast agent were developed later and are known as contrast-enhanced techniques. However, injecting a contrast agent can sometimes lead to an allergic reaction (Ivancevic *et al*., 2009) (Okanovic *et al*., 2018). In the

present study, a non-contrast MRA technique known as time of flight (TOF) MRA was used in a small animal 9.4T MRI scanner (Figure 7A).

TOF-MRA is based on gradient echo method in which the static tissue is being hit by fast, consecutive series of slice-selective RF pulses at a resolve time shorter than tissue T1 and loses most of its signal because of T1 saturation. Flowing blood, because of not being hit by these RF pulses, enters the tissue slice fully magnetized and as a result of being unsaturated, these spins give very strong signals as compared to their stationary background (Ivancevic *et al*., 2009). TOF-MRA can be used for both 2D and 3D acquisitions. In 2D TOF, multiple, thin slices are imaged sequentially and perpendicular to the blood vessels and then reconstructed by maximum intensity projection (MIP) to obtain a 3D image of the blood vessels. In 3D TOF, multiple slabs are acquired simultaneously and the slabs are then divided into thin sections. 3D TOF takes longer to image while 2D TOF is faster (Okanovic *et al*., 2018). In the present study, non-contrast 2D TOF was used for MRA.

MRI has been identified as a promising tool in visualization of CM pathology *in vivo*. However, its use has mainly been restricted to animal models due to inaccessibility of advanced imaging techniques in malaria prone areas. In the few clinical studies where MRI was performed, increased intracranial pressure and brainstem herniation was associated with fatality in CM (Mohanty *et al*., 2014). However, the amount of data available is fractional to the number of cases reported and systemic, serial imaging from the early stages of CM is still missing.

2.4.2 SINGLE PHOTON EMISSION COMPUTED TOMOGRAPHY

SPECT is a nuclear medicine technique used for imaging the biodistribution of radiolabelled compounds in the body (McArthur *et al*., 2011). Brain SPECT is useful for measuring regional cerebral blood flow and receptor imaging of the brain (Warwick, 2004). The brain is metabolically more active, consuming more oxygen and glucose than the rest of the body;

therefore, regional cerebral blood flow (rCBF) is higher. Functional changes detectable with SPECT may appear before structural abnormalities occur (McArthur *et al*., 2011). SPECT can provide only limited information on anatomical relationships. When possible, it is combined with anatomical imaging techniques like CT and SPECT/CT has since been advantageous in locating structural and functional changes in the brain simultaneously (Bybel *et al*., 2008).

In SPECT imaging, a gamma camera captures the gamma radiation emitted from a radionuclide and gives a 3D image of its distribution and uptake in the brain (McArthur *et al*., 2011). To measure the regional cerebral blood flow in the present study, the highly lipophilic radiopharmaceutical ^{99m}Technetium-hexamethylpropylene-amine oxime (^{99m}Tc-HMPAO) was injected intravenously in a freely moving, unanaesthetised animal and was imaged with a Nano SPECT/CT^{TM} scanner for imaging small animals (Figure 7B). ^{99m}Tc-HMPAO can very rapidly cross the blood brain barrier and presumably in the astrocytes, ^{99m}Tc-HMPAO interacts with glutathione and is rapidly oxidised to a hydrophilic compound. This compound is unable to cross the BBB and gets trapped in the brain. The distribution of ^{99m}Tc-HMPAO depends on neural activity. The half -life of ^{99m}Tc is 6 hours which provides enough time for multiple scanning sessions. ^{99m}Tc-HMPAO-SPECT is a very well-validated approach frequently used in clinical routine for imaging pathological alterations in cerebral perfusion. Regions with increased cerebral activity has increased blood perfusion with a higher concentration of the radionuclide while regions with less activity has decreased perfusion and weaker signal of gamma radiation (Warwick, 2004) (Bybel *et al*., 2008).

Spatial resolution of SPECT is determined by the collimators used. ^{99m}Tc emits gamma photon with energy 140keV which can be detected by NaI-scintillator crystals. Collimators help to narrow down or align the gamma photons emitted before they can reach the crystal. For 2D projection image, parallel hole collimator may be used restricting the gamma rays coming at

oblique angles from reaching the detector. For magnified images, pinhole collimators are used. To increase sensitivity, current SPECT scanners have multiple pinhole collimators for a given field. Magnification sensitivity depends on the pinhole detector and pinhole object distances; the resolution of the images depends on pinhole diameters and detector resolutions. However, sensitivity decreases with decreasing pinhole diameter (Oelschlegel and Goldschmidt, 2020).

SPECT/CT have been used extensively in investigating dementia, Parkinson's disease, brain tumours, however, its application in the field of CM remains limited. Only two independent studies have so far performed SPECT/CT imaging in CM affected patients concluding SPECT has the potential to be a powerful diagnostic tool for malaria studies (Kampfl *et al*., 1997) (Moreno-Caballero *et al*., 2016). SPECT has lower time resolution but the advantage is that the tracer could be injected to an unanaesthetised, freely moving animal unlike in MRI. Hence, both the *in vivo* neuroimaging imaging techniques were used for this study.

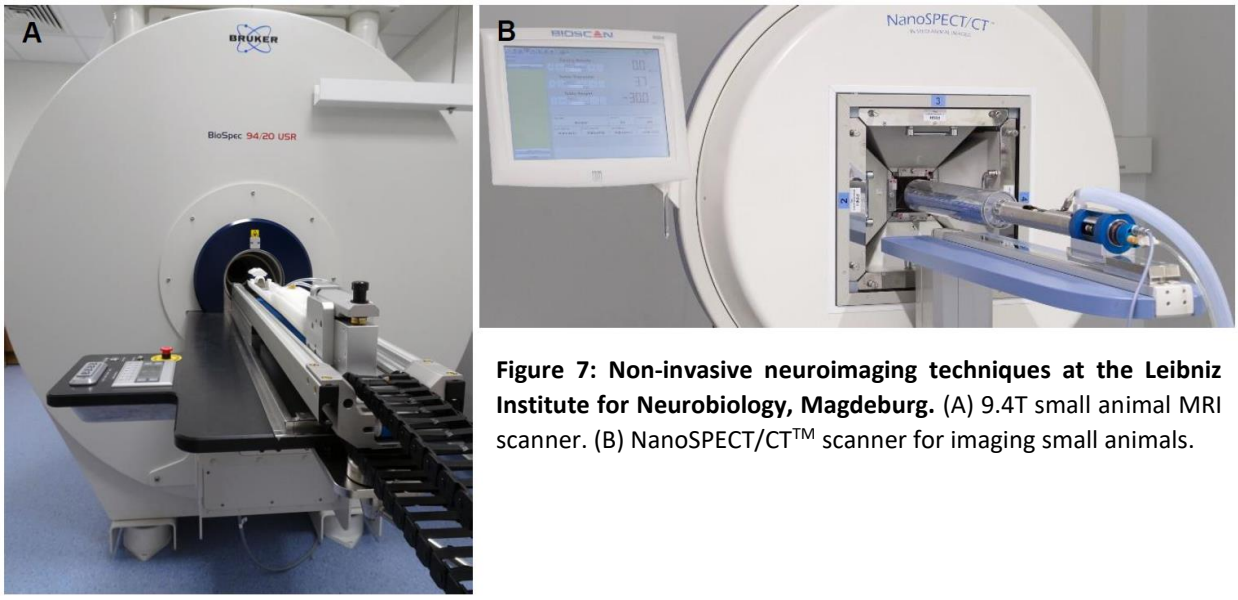

Figure 7: Non-invasive neuroimaging techniques at the Leibniz Institute for Neurobiology, Magdeburg. (A) 9.4T small animal MRI scanner. (B) NanoSPECT/CT^{TM} scanner for imaging small animals.

3. AIMS OF THIS STUDY

Though several decades of research has been carried out on cerebral malaria, the exact mechanism of the rapid progression of the disease and the consequent sudden death remains inconclusive. The link between the two theories of CM pathogenesis, sequestration of infected red blood cells to the brain endothelium and excessive inflammation caused by cytokines and chemokines, and their contribution to edema development during CM is largely unknown.

To investigate the cause of edema development and to monitor the brain pathology during ECM, it was aimed to:

1. Detect intracerebral iRBC sequestration at an early stage of the disease: SPECT/CT *in vivo* imaging was used to detect the distribution of radiolabelled iRBCs.
2. Visualize the changes in cerebral blood flow and venous efflux from an early phase of ECM: SPECT/CT imaging and MR angiography were performed respectively.
3. Monitor the changes in brain pathology from an early stage by studying:
    a. the migration of neuroblasts in the rostral migratory stream (RMS): immunofluorescent stainings were performed.
    b. the activation of cells forming the blood brain barrier and accumulation of immune cells in the brain: immunohistochemical stainings were carried out.
    c. the expression of pro-inflammatory cytokines and chemokines in different regions of the brain: quantitative reverse transcription-PCR was performed.
4. Introduce an early anti-malarial treatment and track the recovery in brain pathology: pyrimethamine, an anti-malarial drug, was administered.

4. MATERIALS AND METHODS

4.1 MATERIALS

4.1.1 ANIMALS

Age and sex matched C57BL/6J mice were used for the experiments and were obtained from Janvier (Le Genest Saint Isle, France). All animals were kept in isolation in the animal facility of the University hospital of the Otto-von-Guericke University, Magdeburg, Germany under pathogen-free conditions, in groups of 4, in standardized cages with 12 hours of light-dark cycle and food and water were provided *ad libitum*. For the SPECT and MRI experiments, 8-12 weeks old (body weight ~20-25g), male mice were used for their bigger size so that they could tolerate better the surgical procedures and repeated anaesthesia. Animal care and experiments were performed in compliance to the European animal protection law and were approved by the local authorities (Landesverwaltungsamt Halle, Germany, Licence number: 42502-2-1260 UniMD).

4.1.2 PARASITES

Plasmodium berghei ANKA (*Pb*A) was used for the murine malarial infection. Sporozoites were obtained from the salivary gland homogenate of 21 days infected female *Anopheles* mosquito from the research facility of Prof. Dr. Kai Matuschewski in the Max Planck Institute of Infection Biology, Berlin.

4.1.3 ANIMAL INFECTION AND EXPERIMENTS

Reagent	Company
Isoflurane (Forene ®)	Abbott, Germany
0.9% NaCl Sodium Chloride	Carl Roth, Germany

4% Paraformaldehyde (PFA)	Carl Roth, Germany
Ethanol 96%	Fischer, Germany
Heparin 5000U/ml	Biochrom AG, Germany
Alsevers solution	Sigma Aldrich, United Kingdom
Glycerol	Calbiochem, Germany
Pyrimethamine	Sigma Aldrich, Germany
Dimethyl sulfoxide (DMSO)	Sigma Aldrich, United Kingdom
Hydrochloric acid (HCl)	Carl Roth, Germany
Dulbecco's Phosphate-Buffered Saline (DPBS)	Gibco by Life Technologies, United Kingdom
Evans blue solution	Sigma Aldrich, United States of America
Immersion Oil	Leica Microsystems, Germany
Methanol	J. T. Baker, Netherlands

4.1.4 IMMUNOHISTOCHEMISTRY

Reagent	**Company**
2-methylbutane (isopentane)	Carl Roth, Germany
Sucrose	Sigma Aldrich, Germany
Sodium borohydride	Sigma Aldrich, Germany
Methanol	J. T. Baker, Netherlands
Hydrogen peroxide (H_2O_2)	Carl Roth, Germany
Bovine serum albumin (BSA)	Carl Roth, Germany
Triton X-100	Sigma Aldrich, Germany
Mayer's Hematoxylin solution	Sigma Aldrich, United States of America
Eosin	Merck, Germany
Vectastain® *Elite* avidin-biotin-peroxidase (ABC) kit	Vector Laboratories, United States of America
Diaminobenzidine (DAB)	Sigma Aldrich, United States of America
Imidazole	Sigma Aldrich, Germany
Tris	Carl Roth, Germany
Isopropanol	Carl Roth, Germany

Roticlear	Carl Roth, Germany
Merckoglas	Merck, Germany
Bromodeoxyuridine (BrdU)	eBioscience, United States of America
Hydrochloric acid (HCl)	Carl Roth, Germany
Dulbecco's Phosphate-Buffered Saline (DPBS)	Gibco by Life Technologies, United Kingdom
MOWIOL	Fluka, Germany

Primary Antibody	**Host**	**Dilution**	**Company**
Anti-glial fibrillary acidic protein (GFAP) (#z0334)	Rabbit	1:10000	Dako Denmark AS, Denmark
Anti-ionized calcium-binding adapter molecule 1 (Iba1) (#019-19741)	Rabbit	1:2000	Wako Chemicals GmbH, Germany
Anti-cleaved caspase 3 (Casp3) (#9661L)	Rabbit	1:500	Cell Signalling Technology, Germany
Anti-cytoplasmic domain 31 (CD31) (#550274)	Rat	1:2000	BD Biosciences, Germany
Anti-CD8 (#14-0808-82)	Rat	1:1000	eBioscience, Affymetrix Inc., USA
Anti-doublecortin (DCX) (#sc-8066)	Goat	1:1000	Santa Cruz Biotechnology, USA
Anti-bromodeoxyuridine (BrdU) (#ab6326)	Rat	1:2000	Abcam, United Kingdom

Secondary Antibody	**Dilution**	**Company**
Biotin-conjugated anti-rabbit IgG (#111-065-144)	1:200	Dianova, Germany
Biotin-conjugated anti-rat IgG (#712-065-153)	1:200	Dianova, Germany
Alexa-488 labelled anti-goat IgG (#A11055)	1:200	Invitrogen by Thermo Fischer Scientific, USA
Cy3-labelled anti-rat IgG (#712-165-153)	1:200	Dianova, Germany

4.1.5 MOLECULAR BIOLOGY

Reagent	Company
QIAshredder kit	Qiagen, Germany
RNeasy Mini Kit	Qiagen, Germany
β-mercaptoethanol	Carl Roth, Germany
Sterile distilled water	Berlin Chemie AG, Germany
Ethanol 96%	Fischer, Germany
Oligo-dT	Invitrogen, Germany
deoxyriboNucleosite Triphosphate (dNTP)	Invitrogen, Germany
Dithiothreitol (DTT)	Invitrogen, Germany
Superscript II reverse transcriptase	Invitrogen, Germany
5X first strand buffer	Invitrogen, Germany
PCR buffer, 10X	Qiagen, Germany
HotStar Taq	Qiagen, Germany
Primers for PCR	Eurofins MWG Operon, Germany
Agarose	Carl Roth, Germany
Tris	Carl Roth, Germany
TaqMan Universal PCR master mix	Applied Biosystems, Germany
Primers for qRT-PCR	Applied Biosystems, Germany
Cytochrome B primer	Eurofins MWG Operon, Germany
Light cycler 480 SyBr Green I master mix	Roche, Germany

4.1.6 NEURO-IMAGING

Reagent	Company
^{99m}Technetium (^{99m}Tc)	Department of Nuclear Medicine, University hospital, Magdeburg, Germany
Hexamethylpropylene-amine oxime (HMPAO)	GE Healthcare, Germany
Tin chloride ($SnCl_2$)	Sigma, Germany
Isoflurane (Forene ®)	Abbott, Germany

Heparin 5000U/ml	Biochrom AG, Germany
Percoll	GE Healthcare, Germany
RPMI 1640 medium	PAA Laboratories GmbH, Austria
Foetal calf serum	PAA Laboratories GmbH, Austria
Dulbecco's Phosphate-Buffered Saline (DPBS)	Gibco by Life Technologies, United Kingdom

4.1.7 LABORATORY EQUIPMENT

Equipment	Company
Centrifuge (ROTANTA 460R)	Hettich, Germany
Centrifuge (Mikro 22R)	Hettich, Germany
Vortex	IKA, Germany
Pipette boy	Eppendorf, Germany
Pipette tips	Eppendorf, Germany
Light microscope	Olympus, Japan
Malaria ocular	Olympus, Japan
Microscope slides	Thermo Fischer Scientific, USA
Omnifix®-F Syringe	Braun, Germany
Canula	Braun, Germany
24-well cell culture plate	Greiner Bio-one, Germany
Falcon tubes (50ml, 15ml)	Eppendorf, Germany
Microcentrifuge tubes	Eppendorf, Germany
Weighing balance	Sartorius, Germany
Microtome (Leica CM 1950)	Leica, Germany
Shaker	Gesellschaft für Labortechnik mbH, Germany
Gelatine-coated slides	Thermo Fischer Scientific, USA
Coverslips	Thermo Fischer Scientific, USA
Staining jar	Carl Roth, Germany
Staining rack	Carl Roth, Germany

Brightfield and epifluorescence microscope (Zeiss Axioskop 2)	Zeiss, Germany
Digital camera (Leica DFC 500)	Leica, Germany
Sony Alpha 200K digital camera	Sony, Germany
Incubator	Memmert, Germany
Laminar flow hood	Heraeus, Germany
Nanodrop (ND-1000)	Thermo Fischer Scientific, USA
PCR machine	Peq Lab, Germany
Power PAC 200	Bio-Rad, USA
Light cycler 480	Roche, Germany
NanoSPECT/CT^{TM} scanner	Mediso, Germany
Syringe infusion pump	Harvard Apparatus, USA
9.4T small animal MRI scanner (BioSpec 94/20 USR)	Bruker, Germany

4.1.8 SOFTWARE

Software	Company
GraphPad Prism 5	GraphPad Software, USA
ImageJ 1.50i	National Institute of Health, USA
CorelDRAW Graphic Suite X8	Corel Corporation, Canada
Pyrat	Scionics Computer Innovation, Germany
Leica application suite (LAS), version 3.6.0, build 488	Leica Microsystems Limited, Switzerland
Light cycler PCR software SDS (version 5,1)	Applied Biosystems, Germany
Microsoft Office 2013	Microsoft Corporation, USA
Invivoscope 1.43	Mediso, Hungary
HiSPECT^{TM}	SCIVIS, Germany
OsiriX^{TM} DICOM viewer, 32-bit version 3.7 and 64-bit version 5.7.1	Pixmeo, Switzerland
MPI Tool^{TM}, version 6.36	Advanced Tomo Vision, Germany

MATLAB, version R2017b (9.3.0.713579) 64-bit	MathWorks, USA
Photoshop™, version CS6	Adobe, USA

4.2 METHODS

4.2.1 MALARIA INFECTION

In order to achieve malaria infection in mice, 20.000 live sporozoites obtained from the salivary glands of infected female *Anopheles* mosquito were injected intravenously (i.v.) into C57BL/6J mice. Infected mice were monitored daily for neurological symptoms like paralysis, ataxia and convulsions. When the mice exhibited all the clinical, neurological symptoms of ECM, they were anesthetized using 4.5-5.0% isoflurane in 2:1 O_2:N_2O volume ratio. With the help of a heparin flushed syringe, blood was collected through cardiac puncture from these mice. Blood stabilates were prepared by mixing one part of collected blood with two parts of Alsevers solution which contained 10% glycerol. This mixture was filled into cryovials and immediately frozen in liquid nitrogen and stored at -80°C for later use (Table 4.1.3).

Every time mice were to be infected for experiments, these cryovials were thawed on ice for 15 minutes followed by a quick spin in the centrifuge. Each mouse was injected intraperitoneally (i.p.) with 100µl of this blood mixture containing around $1x10^6$ *Pb*A-infected red blood cells (iRBCs). The mice developed severe clinical, neurological symptoms of the disease around day 7 p.i.

Infected mice (n=10) were monitored and scored daily using the Rapid Murine Coma and Behaviour Scale (RMCBS) developed by Caroll *et al*., 2010 based on the appearance of clinical symptoms of ECM. The decrease in RMCBS score in the days post infection (p.i.) was plotted

as a line graph with standard deviation in GraphPad Prism 5. Mice were divided into different groups based on their RMCBS score.

4.2.2 ANTI-MALARIAL TREATMENT

To study the recovery of brain pathology through *in vitro* experiments, an anti-malarial drug was introduced. The drug, pyrimethamine, has been in use against *P. falciparum* and *P. vivax* malaria for several decades and is the anti-malarial drug of choice for the experiments. 25mg of pyrimethamine was dissolved in 1ml of dimethyl sulfoxide (DMSO) with the help of one drop of 5N HCl solution. 50µl of this solution was dissolved with 950µl of phosphate buffered saline (PBS) to prepare a working concentration of 1.25mg/ml. At day 5 p.i., one group of infected mice received the drug i.v. through tail vein injection (100µl/mouse). The other group received PBS as control and has been referred to as untreated mice in the text (Table 4.1.3). The percentage of appearance of neurological symptoms in infected, treated and untreated mice in days p.i. were plotted and the statistical differences between groups were determined using Log-rank test in GraphPad Prism 5. P values <0.05 is * significant, P values <0.01 is ** significant and P values <0.001 is *** significant.

4.2.3 PARASITEMIA

To measure the percentage of infected erythrocytes in peripheral blood, a drop of blood was collected daily from all the groups of infected mice by making a tail incision. The drop of blood was put on top a glass microscope slide and was made into a thin blood smear with the help of another glass slide. After air drying these slides for a few minutes, they were fixed in 100% methanol for 5 minutes. Each slide was stained for one minute in Diff. Quik I solution (pinkish red) followed by staining for one minute again in Diff. Quik II solution (bluish purple). They were washed quickly under running water for 30 seconds and left for air drying (Table 4.1.3).

A drop of immersion oil was placed on these slides, covered with a coverslip and placed under 100X objective lens of a light microscope. A count of total red blood cells (in pinkish red) and infected red blood cells (parasites stained in purple) in a defined area were made and the percentage of infected erythrocytes was calculated. Three sets of calculations were made from three different experiments to plot a graph and the statistical differences between groups were determined using the two-tailed Student *t* test in GraphPad Prism 5. P values <0.05 is * significant, P values <0.01 is ** significant and P values <0.001 is *** significant.

4.2.4 EVANS BLUE STAINING

To check the integrity of blood brain barrier, 2% solution of Evans blue was prepared in PBS. 100µl of this solution was injected i.v. through tail vein injection into 2 animals from each group of mice used for the experiments at day 0, day 5 p.i. and day 7 p.i. After one hour of injection, the mice were anesthetized using 4.5-5.0% isoflurane in 2:1 O_2:N_2O volume ratio and perfused transcardially with 0.9% NaCl (Table 4.1.3). The perfused brains were removed from the animals and photographed with a Sony Alpha A200K digital camera.

4.2.5 IMMUNOHISTOCHEMISTRY

To visualize the changes in brain pathology upon infection, immunohistochemical studies were performed (n=3 for all groups of mice). All groups of mice were anesthetized with 4.5-5.0% isoflurane in 2:1 O_2:N_2O volume ratio on the respective days and transcardially perfused with 0.9% NaCl followed by perfusion with 4% filtered solution of paraformaldehyde (PFA) in PBS. Their brains were collected and postfixed in 4% PFA solution for 48 hours at 4°C followed by cryoprotection for 72 hours in 30% filtered sucrose solution at 4°C. Thereafter, the brains were frozen for 3 minutes in -30°C isopentane which was cooled down by liquid nitrogen. 50µm thick sagittal sections were made from the entire frozen brains on the Leica

CM 1950 microtome set at -20°C. The sections were placed in cold 0.1M PBS solution in 24-well culture plates for further processing (Table 4.1.4, 4.1.7).

4.2.5.1 GFAP, Iba1, CD31, CD8 and cleaved Caspase 3 staining and brightfield microscopy

Sagittal sections of the mouse brain were used for staining. At first, the reactive aldehyde groups were blocked by placing the sections in 1ml of 1% sodium borohydride solution in PBS and incubating them on a shaker for 20 minutes at room temperature. Thereafter, they were washed in 0.1M PBS for 10 minutes twice on a shaker. The next step was to block endogenous peroxidases by putting the sections in 1ml of 1:1 mixture of methanol and PBS with 1 part of 30% H_2O_2 and shaking for 20 minutes at room temperature; followed by twice 10 minutes of washing with PBS. Blocking solution was prepared by mixing 5% bovine serum albumin (BSA) and 0.3% Triton in PBS. 1ml of this mixture was put over each section and incubated on a shaker for 45 minutes at room temperature to block unspecific antibody reactions followed by washing with PBS twice. Primary antibody solutions were prepared by mixing the respective antibody at the correct dilution with 0.1% BSA and 0.3% Triton solution made in PBS. Separate sections were stained for activation of astrocytes by glial fibrillary acidic protein (GFAP), microglia by ionized calcium-binding adapter molecule 1 (Iba1), endothelial cells by cytoplasmic domain 31 (CD31), accumulation of leukocytes by CD8 and apoptosis by cleaved Caspase 3 antibodies (dilution of each antibody is mentioned in Table 4.1.4). 500µl of primary antibody solution was added over respective sections and incubated overnight at 4°C on a shaker.

Next day, the first step involved washing the sections twice for 10 minutes in PBS. 500µl of 1:200 dilution of respective secondary antibody solution in PBS (Table 4.1.4) was added to each section and incubated on a shaker for 2 hours at room temperature; followed by washing twice for 10 minutes in PBS. For biotin visualization, 2 drops of each solution A and solution

B of the Vectastain Elite Kit were mixed with 50ml PBS and incubated for 30 minutes at room temperature. 1% BSA mixed with 0.3% Triton solution in PBS was added to this mixture and 1ml of this solution was then added over each section and incubated again for 2 hours in the dark at room temperature on a shaker. After this, washing with PBS for 10 minutes was performed once followed by washing with 0.05M Tris(hydroxymethyl)aminomethane-HCl buffer (TRIS) for 10 minutes. To initiate the chromogen reaction, 5mg diaminobenzidine (DAB) was mixed in 10ml TRIS with 100µl of 1M imidazole solution and 5µl of 30 % hydrogen peroxide. 1ml of this DAB solution was added over each section and incubated for 10 minutes with shaking. A single 10 minutes washing step in TRIS and twice washing in PBS followed. The brown-stained sections were mounted on gelatine coated glass microscope slides with the help of a brush and tap water and left to dry overnight at room temperature.

Next day, the slides were first rinsed twice for 5 minutes each in a 2:1 mixture of isopropanol and ethanol. This was followed by rinsing the slides in Roticlear thrice for 5 minutes each. The slides were then wiped dry with the help of a tissue and covered with the mounting solution, Merckoglas and glass cover slips and left overnight for drying at room temperature.

For IHC analysis, every single sagittal brain section was photographed with the help of a digital camera mounted on a combined brightfield and epifluorescence microscope. Images of different cerebral regions including olfactory bulb (OB), sub-ventricular zone (SVZ), rostral migratory stream (RMS), hippocampus, mid brain and pons, were acquired using a 20X objective lens under constant brightfield illumination for GFAP, Iba1, CD31, CD8 and cleaved Caspase 3 staining and their exposure times were 10 milliseconds (ms), 8ms, 7ms, 8ms and 7ms respectively. The respective images acquired were used for cell counting in 4.2.5.4. Magnified images were captured under 40X objective lens for all the staining.

4.2.5.2 H&E staining and brightfield microscopy

In order to visualize haemorrhagic lesions, three 50µm thick sagittal sections cut from PFA-fixed frozen brains were mounted on a single gelatine coated glass microscopic slide with the help of a brush and tap water and was left for drying overnight at room temperature. Next day, all the slides were placed in a staining rack and dipped in a staining jar filled with Haematoxylin solution for 5 minutes. It was followed by a quick dip in a jar filled with distilled water and then placed under running tap water for 10 minutes for washing. Then, the staining rack with the slides was dipped in a jar filled with Eosin solution for 10 minutes. Washing was carried under running tap water for 10 minutes. Dehydration was carried out by placing the slides first in 80% ethanol solution for 5 minutes and then twice in 100% ethanol for 5 minutes each. This was followed by placing the slides twice in Roticlear for 5 minutes each. Finally, the slides were dried with the help of a tissue and coated with Merckoglas and coverslips and left overnight for drying at room temperature (Table 4.1.4).

Images of different cerebral regions were acquired with the help of the brightfield microscope mentioned above. They were acquired using a 20X objective lens under constant brightfield illumination with an exposure time of 5ms.

4.2.5.3 BrdU and DCX immunofluorescence staining and epifluorescence microscopy

Bromodeoxyuridine (BrdU) staining was performed according to literature (Pan *et al.*, 2013). BrdU solution was administered i.p. in each mouse from individual groups (50µg/g body weight) 48 hours prior to sacrificing and perfusing them. Perfusion and freezing of brains were carried out as mentioned above. Doublecortin (DCX) staining was performed first to stain neuronal precursor cells and immature neurons. The first day of staining was carried out exactly as mentioned in 4.2.5.1 with primary antibody solution of DCX in the right dilution and

incubated overnight similarly. The next day, after washing in PBS twice, 500µl of 1:200 dilution of the respective secondary immunofluorescent antibody, Alexa-488, in PBS was added and incubated in dark for 2 hours at room temperature with shaking. This was followed by washing twice for 10 mins in PBS and once with distilled water for 5 minutes in dark.

The procedure for BrdU staining was started thereafter on the same day and all the incubation and washing steps had been carried out in the dark. The sections were placed in 2N HCl solution and incubated at 37°C for 30 minutes with intermittent shaking. Then, they were washed twice for 5 minutes each in 0.1M borate buffer to neutralize the acid. Three times thorough washing was done by putting the sections in PBS with shaking for 10 minutes each. The sections were blocked by a solution of 5% BSA and 0.3% Triton for 45 minutes at room temperature with shaking. After washing once with PBS, primary antibody solution against BrdU was added and incubated at 4°C overnight in dark with shaking. Next day, the sections were washed twice in PBS for 10 minutes each. 500µl of 1:200 dilution of the respective secondary immunofluorescent antibody, Cy3, in PBS was added and incubated in dark for 2 hours at room temperature with shaking. Sections were washed twice in PBS for 10 minutes each and mounted on gelatine coated glass microscope slides. They were wiped with tissue and covered with MOWIOL and coverslips and dried overnight at 4°C.

For acquiring the images in dark, the brightfield and epifluorescence microscope mentioned above was used again. Cy3 conjugated BrdU antibodies were excited at 550nm and Alexa-488 conjugated DCX antibodies were excited at 493nm. Emission wavelength of Cy3 is 570nm and that of Alexa-488 is 519nm and appropriate filters, specific to different wavelengths, were used in the microscope to capture the images using 5X objective in dark with exposure time of 590ms and 650ms, respectively. Magnified images were captured under 40X objective lens.

4.2.5.4 Cell counting and analysis

For counting the number or area of stained cells in each image, Image J software was employed. The 20X images from GFAP, Iba1, CD31 and CD8 and 5X images from BrdU and DCX staining were used for counting. In the software, the RGB images were converted to 16-bit grey scale images and threshold values were adjusted for each individual stain to highlight the structures to be counted. To reduce background noise in the images, background subtraction with rolling ball was carried out and particles were analysed. With the exception of CD8 staining, cell number for all other stainings were quantified by automated counting where the surface area covered by each cell type in the entire image was measured. For CD8 staining, the total number of $CD8^+$ cells in the whole image was counted manually with the Cell Counter plugin in Image J. For statistical analyses, three similar mediolateral sections each from three different animals per group of mice were stained and examined. The bar graphs were prepared and statistical differences between groups were determined using the two-tailed Student *t* test in GraphPad Prism 5. P values <0.05 is * significant, P values <0.01 is ** significant and P values <0.001 is *** significant.

4.2.6 QUANTITATIVE REVERSE TRANSCRIPTION-PCR (qRT-PCR)

To quantify the mRNA expression of cytokines and chemokines and parasite-specific mRNA, qRT-PCR method was used. Reverse transcription is the process of producing a complementary DNA (cDNA) from an RNA template with the viral enzyme, reverse transcriptase. This is coupled with polymerase chain reaction (PCR) to amplify specific DNA fragments which is monitored by fluorescence and the whole process is called quantitative reverse transcription-PCR (qRT-PCR). It is used for quantifying gene expression (Freeman *et al*., 1999).

Brains from all the groups of mice were isolated after 4.5-5.0% isoflurane in 2:1 O_2:N_2O volume ratio anaesthesia and 0.9% NaCl perfusion (n=4 for all groups). The brains were cut into olfactory bulb, cortex and brain stem regions and were placed in RLT buffer (from the RNeasy kit) mixed with 1% ß-mercaptoethanol for lysing the cells and also inactivating RNAses. Each part of the brain was grounded and homogenised using the QIAshredder kit. Then, mRNA isolation was carried out according to the protocols in the RNeasy kit: ethanol was added for right binding conditions followed by passing the sample through a mini spin column where the RNA gets bound to the membrane, washing thoroughly and eluting out the RNA in 30µl distilled water. This process ensures RNA moieties bigger than 200 nucleotides are purified which helps in enrichment of mRNAs from other smaller RNAs. Concentration of mRNA was measured with the help of the Nanodrop machine with distilled water as blank. An equal amount of mRNA was used to prepare cDNA. The enzyme, SuperScript II reverse transcriptase along with oligo(dT) primers, dNTPs and first strand buffer were used to transcribe mRNA into cDNA. Quantitative RT-PCR for interferon-γ (IFN-γ), tumor necrosis factor (TNF), chemokine (C-X-C motif) ligand 3 (CXCL-3), CXCL-9, CXCL-10, CXCL-11, lymphotoxin-α (LTα), LTβ and hypoxanthine phosphoribosyltransferase (HPRT) was performed. The cDNA prepared from olfactory bulb, cortex and brainstem regions of day 0, day 5, day 7 p.i. untreated and pyrimethamine treated mice along with the respective primers and Taqman gene expression assay were used. To determine the parasite load in these three regions of the brain, the cDNA prepared was amplified and quantified with *P. berghei* ANKA-specific, CytochromeB, primers (Bahamontes-Rosa *et al.*, 2016) and primers for the house keeping gene, HPRT, using Light cycler 480 SyBr Green I master mix (Table 4.1.5, 4.1.7).

Amplification of all the cDNA produced was performed with a Light cycler 480 machine. Quantification was performed using the Light cycler software SDS (Table 4.1.8), according to the $\Delta\Delta C_T$ threshold cycle method with HPRT as the housekeeping gene (Livak and

Schmittgen, 2001). Data are depicted as the increase in the level of mRNA expression in infected mice over that in uninfected controls of the respective mouse group. The bar graphs were prepared and statistical differences between groups were determined using the two-tailed Student *t* test in GraphPad Prism 5. P values <0.05 is * significant, P values <0.01 is ** significant and P values <0.001 is *** significant.

4.2.7 SPECT/CT IMAGING

4.2.7.1 Cerebral perfusion imaging with ^{99m}Tc-HMPAO

Male C57BL/6J mice, 11-12 weeks old were used for this experiment. Half of the animals were infected with *Pb*A-infected RBCs and other half remained uninfected as controls (n=10 for each group). Next steps of the imaging experiment were performed similarly as described in Kolodziej *et al*., 2014. Around day 3 p.i., all the animals were catheterized in their jugular vein under 1.0-1.5% isoflurane in 2:1 O_2:N_2O volume ratio anaesthesia and were given two days to recover. On the morning of day 5 p.i. and day 7 p.i., ^{99m}Technetium (^{99m}Tc) was obtained from the department of nuclear medicine, University hospital of Magdeburg in the form of TcO_4^-. This compound was then mixed with hexamethylpropylene-amine oxime (HMPAO) in the presence of the reducing agent Sn(II)Cl_2, which was added from a freshly prepared solution, to form the ^{99m}Tc-HMPAO intravenous solution. Around 200MBq of TcO_4^- was mixed with 0.9% NaCl solution to make a volume of 180µl. To this 125µl of HMPAO and 25µl of 200µM $SnCl_2$ solution was added to make a final solution of 330µl. The whole solution was put in a syringe and the radioactivity was measured. The jugular vein catheter of the mouse was connected to a Teflon tube connected to the syringe and the syringe was then placed in a syringe infusion pump. The ^{99m}Tc-HMPAO solution was then slowly injected into the animal over a period of 10 minutes. The syringe was then washed out by injecting 0.9% NaCl for 2 minutes. Then the animal was anaesthetized with 3% isoflurane and transferred to the SPECT/CT scanner. The

amount of radioactivity wasted in the syringe and the Teflon tube was measured and the actual dose of ^{99m}Tc in the body of the animal was calculated. Generally, the dose was around 100MBq per animal (Table 4.1.6).

SPECT/CT imaging was performed with a four headed NanoSPECT/CT^{TM} scanner (Table 4.1.7). Animals were scanned under gas anaesthesia (1.0-1.5% isoflurane in 2:1 O_2:N_2O volume ratio). CT and SPECT were co-registered. CT scans were made at 45kVp, 1.77µA, with 180 projections, 500ms per projection and 96µm isotropic spatial resolution, reconstructed with the manufacturer´s software at isotropic voxel-sizes of 100µm. SPECT scans were made using nine-pinhole mouse brain apertures with 1.2mm pinhole diameters. 24 projections were acquired during a scan time of 2 hours. Axial FOV was 23.9mm. Photopeaks were set to the default values of the NanoSPECT/CT (140keV +/− 5%). SPECT images were reconstructed using the manufacturer´s software, HiSPECT^{TM}, at an isotropic voxel output size of 450µm.

Data analysis with different software tools was carried out as described in Kolodziej *et al.*, 2014. SPECT/CT images were precisely aligned manually to high resolution, reference MR-mouse images from Ma *et al*, 2005, 2008 using the MPI-Tool^{TM}. From the whole head SPECT data sets, the brain-SPECTs were cut out in ImageJ for individual animal using the whole-brain volume-of-interest (VOI) made from template provided by Ma *et al.*, 2005, 2008. Brain-SPECT data from all the animals were normalized using global mean normalization in ImageJ. For illustrations, average of all normalized SPECT-brains was calculated for each group of mice by adding all the individuals of the respective group and then dividing by their total count in ImageJ. Similarly, average group CT images were prepared for individual groups of mice in ImageJ. Differences between individual groups were calculated by subtracting the average of brain-SPECT data of the infected groups of day 5 p.i. and day 7 p.i. from the respective control, uninfected group of day 0 animals in ImageJ. Unpaired t-tests were performed using MATLAB

calculate significant differences in normalized tracer uptake between the groups and to generate maps of p-values above certain thresholds, that is, probability maps (PMaps). At the end, all average, subtracted and t-test files were converted to DICOM format using MATLAB. Final images were illustrated in OsiriX™ DICOM viewer with the SPECT files merged with reference MR-images and then saved as TIFF files. Specific sections were chosen for illustration and the figures were edited and arranged in Photoshop™ and in Microsoft Powerpoint (Table 4.1.8).

4.2.7.2 Imaging of ^{99m}Tc-labelled infected erythrocytes in brain

On the day of the experiment, blood was collected from day 7 infected C57BL/6J mice through cardiac puncture under 4.5-5% isoflurane anaesthesia. This infected blood was enriched as described in Trang *et al*., 2004. The blood was mixed with equal volumes of PBS and centrifuged at 200xg for 3 minutes. The pellet was washed thrice in PBS and then suspended in nine volumes of RPMI-1640 medium mixed with 3% foetal calf serum to prepare a 10% suspension of the infected erythrocytes. Isotonic Percoll solution was prepared by mixing 60ml of Percoll to 7ml of 10X concentrated PBS solution and to this 33ml of 1X PBS was added to make a 60% Percoll solution. Two times volume of 60% Percoll was pipetted down slowly and gently into the bottom of the 10% erythrocyte suspension followed by centrifugation at 1500Xg for 20 minutes with speed 0 brake. A thin ring, rich with infected RBCs, formed at the interface between the sample and the Percoll layers. The ring was collected with the help of a pipette into a fresh tube and washed three times with PBS and finally suspended in 500µl of PBS. This suspension is supposed to have 95% pure infected RBCs (Trang *et al*., 2004) (Table 4.1.6).

The enriched infected-RBCs were then mixed with ^{99m}Tc-HMPAO for labelling them. Then the same reactions with HMPAO and $SnCl_2$ were carried out as mentioned in 4.2.7.1 to radiolabel the infected-RBCs. The lipophilic compound, ^{99m}Tc-HMPAO, passes the

erythrocyte cell membrane and after passage, is oxidized to a water-soluble compound that remains inside the iRBCs. The solution of the labelled iRBCs was then injected with the help of a syringe infusion pump into day 5 p.i. and day 0 mice and allowed to rest for 1 hour so that the infected-RBCs can accumulate in the brain (n=8 for each group). Whole body and brain SPECT/CT imaging was performed using the same aperture as mentioned in 4.2.7.1.

For calculation of percentage and standardized ^{99m}Tc-uptake values (SUV), the whole body ^{99m}Tc-content was determined from the whole-body SPECT-images using the OsiriX^{TM} software. Percentage uptake values represent the ^{99m}Tc-content as percent of injected dose, SUVs, which is calculated by dividing whole-body ^{99m}Tc-content with the body weight. Due to the homogeneous population of mice with respect to body weight, no differences between calculations based on percentage as compared to SUV uptake values were noted. Data are given here as SUVs. For analysis of group differences in brain SUVs, the SPECT/CT were manually aligned to the reference MR images as mentioned before in 4.2.7.1. ^{99m}Tc-contents were converted to SUVs in the MPI-Tool^{TM}. This was followed by preparing average group data of the day 5 p.i. and day 0 mice. Average group differences were made by subtracting the SUVs of infected-RBC in the brain of day 0 mice from that of day 5 p.i. mice in the MPI-Tool^{TM}. Final illustrations were done in OsiriX^{TM} where the SPECT images were overlaid on merged reference MR images and average group CTs. Specific sections were chosen and the figures were edited in Photoshop^{TM} to delete regions with high uptake surrounding the brain and arranged finally in Microsoft Powerpoint.

4.2.8 MR IMAGING

Time-of-flight (TOF) magnetic resonance angiography (MRA) was performed to visualize changes in flow of the large draining veins. TOF-MRA was accompanied by T1-weighted and T2-weighted MRI for imaging brain anatomy and edema development during the disease

progression. C57BL/6J mice were infected with *Pb*A-infected RBCs and imaged on day 0, day 5 p.i. and day 7 p.i. in a 9.4T Bruker MRI scanner (n=10 for each group) (Table 4.1.7). A combination of a ^{1}H volume coil of 86mm in inner diameter for transmission and a ^{1}H 3x1 surface array coil for receiving the signal was used for imaging the brain. The MRI protocol included a MAPshim method for local shimming of the entire brain, a T1-weighted 2D FLASH sequence (TR/TE = 3ms/425ms, flip angle = 30°, 2 averages) and a T2-weighted 2D TurboRARE (TR/TE = 4200ms /18.5ms, 2 averages) with equal field of view (25.6 x 25.6mm) serving as anatomical reference for the equivalent MR Angiography. Thus, a non-contrast-enhanced 2D TOF with flow-compensation was acquired with optimized parameters (TR/TE: 3ms/12ms in 80 slices with a slice thickness of 0.3mm, a slice overlaps of 0.1mm and an in-plane-resolution of 0.08 x 0.08mm resulting a scan time of ~4 minutes). The flip angle was set to 70° and the saturation slice, with a thickness of 3mm, was positioned with a 1mm gap towards the caudal side of the brain to solely image the venous architecture. The complete MRI protocol led to a total scan time of around 45 minutes.

Anaesthesia of the animals was induced with 2.5-3.0% isoflurane in 1:1 O_2:N_2O volume ratio followed by a reduction to 1.0%-1.5% isoflurane while MR imaging was being performed. Vital parameters of the mice, such as body temperature and breathing rate, were always monitored and kept constant during scanning procedure.

For analysis, the MR T2 images and the angiography images were aligned first to the reference MR mentioned before in 4.2.7.2 and then to respective average group CTs obtained from the SPECT/CT perfusion experiment and was carried out in the MPI-Tool^{TM}. Average group angiography images were created similarly as mentioned in the 4.2.7.2 followed by calculating the differences between the groups by subtracting the average blood flow of day 5 p.i. and day 7 p.i. from that of day 0, uninfected control in the MPI-Tool^{TM}. The normal, average and

difference angiography files were then merged with their respective group average CT and MR T2 images in OsiriX^{TM} and final images were created in Microsoft Powerpoint (Table 4.1.8).

A region of interest (ROI) file was created in the superior sagittal sinus (SSS) region from day 0 TOF in OsiriX^{TM} to measure the blood flow in the SSS region across different animals. That ROI was imported in OsiriX^{TM} for each individual angiography data set and signal intensities in this ROI were added up in each individual and averaged to find the mean flow in each group. The data was then plotted in GraphPad Prism 5 to create the bar graphs and to calculate the significant differences between the groups. P values <0.05 is * significant, P values <0.01 is ** significant and P values <0.001 is *** significant.

For the T2 images showing edema, representative animals from each group were chosen and imported in OsiriX^{TM}. Sections showing edema in day 7 p.i. animal were selected and same sections were selected from day 5 p.i. and day 0 animals for illustration. Final images were arranged in Microsoft Powerpoint.

5. RESULTS

5.1 Severe neurological symptoms of ECM develop around day 7 p.i.

C57BL/6J mice were infected using iRBCs, as described in 4.2.1, and the development of clinical symptoms of ECM were monitored daily. As mentioned in literature (Caroll *et al.*, 2010), the neurological symptoms of ECM start developing and progressed rapidly between day 5 and day 10 p.i. Appearance of clinical symptoms was determined based on the 10 physical traits described in 2.3.2 and was scored daily, as described in 4.2.1. In the beginning, from day 0-4 p.i., all mice appeared healthy and normal (RMCBS score: 15-20). Between day 5-6 p.i., slight clinical symptoms like slow gait and ruffled fur developed (RMCBS score: 10-14). But these animals did not exhibit any neurological symptom of ECM and hence, day 5 p.i. has been considered as an early stage of ECM for this study. Around day 7-8 p.i., the mice became severely sick exhibiting all the clinical, neurological symptoms of ECM like paralysis, apathy, ataxia, seizures (Figure 8) with a RMCBS score of 3-9. The neurological symptoms developed rapidly around day 7 p.i. which were fatal to the animals and this has been rendered as the late stages of the disease for further experiments. However, mice showing severe symptoms and having a RMCBS score of 5 or less were euthanized for ethical reasons.

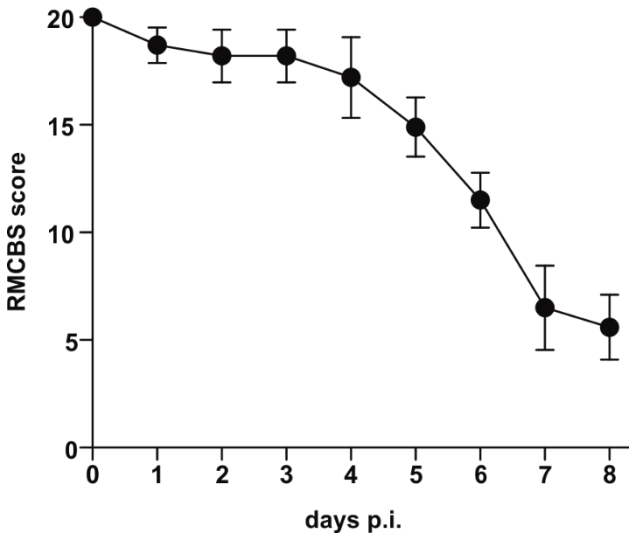

Figure 8: RMCBS score days post infection. Line graph depicts the decrease in Rapid Murine Coma and Behaviour Scale (RMCBS) score of malaria-infected mice depending on the development of the clinical, neurological symptoms of ECM (based on the scale developed by Caroll *et al.*, 2010).

5.2 Intracerebral iRBC sequestration is an early event in ECM development

As described in 2.3.3.1, sequestration of iRBCs to the brain endothelium might be a crucial factor for triggering the events leading to disease complications in human CM. Post-mortem studies have revealed iRBC sequestration in the microcirculation in patients who succumbed to this disease; however, it has remained unclear when and where in the vasculature iRBC sequestration starts. In addition, intracerebral sequestration of iRBCs in mice during ECM development has been controversially discussed and remains unclear. Therefore, accumulation of iRBCs at an early, neurologically asymptomatic stage was examined by injecting ^{99m}Tc-labelled iRBCs into mice at day 5 p.i. and at day 0, uninfected mice for control, followed by SPECT/CT imaging, as described in 4.2.7.

The dynamic measurements did not show any re-distribution of ^{99m}Tc in the day 5 infected and uninfected control mice. There was no difference between the earliest point of imaging (at 15 minutes) and the latest point of imaging (at 6 hours) post injection. However, uptake of the ^{99m}Tc-labelled iRBCs differed significantly between the control and the infected mice. Widespread uptake of ^{99m}Tc-labelled iRBCs was observed throughout the entire brains of day 5 infected mice whereas, it was significantly lower in the uninfected brains (Figure 9). There was a significant increase in the global, brain-wide sequestration of iRBCs in the infected group from an early stage of the disease with respect to that of the uninfected ones. The average brain uptake was 2.4 times higher in the infected ones in comparison to the uninfected ones.

The regions with highest iRBC accumulation peaked in areas corresponding to the large draining veins and sinuses of the mouse brain, especially the rostral rhinal vein, the superior sagittal sinus, the transverse sinus and the longitudinal hippocampal vein (Figure 10). Taken

together the data shows that intracerebral accumulation of iRBC is a global phenomenon and not restricted only to microcirculation and is present from an early stage of the disease.

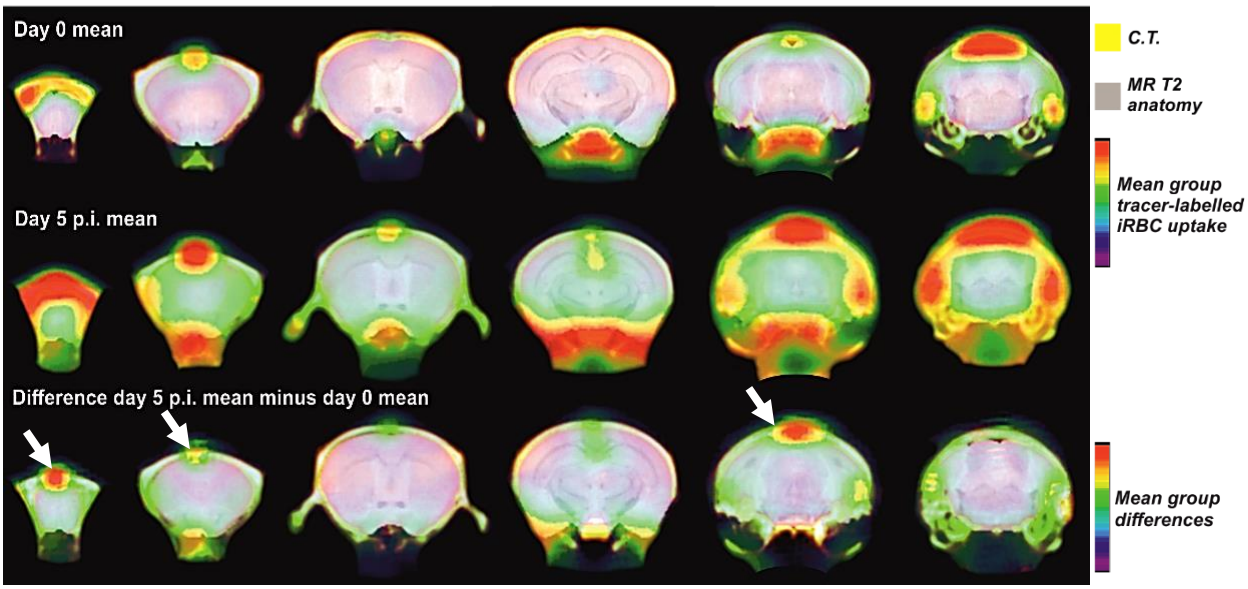

Figure 9: SPECT/CT imaging revealed widespread sequestration of iRBCs in the brain of malaria-infected mice at day 5 p.i. Rostral to caudal sections SPECT images of cerebral uptake of ^{99m}Tc-labelled iRBCs overlaid on CTs (in yellow) and anatomical reference MRs (in grey). Shown are images of mean standardized uptake values of ^{99m}Tc in control, uninfected mice (upper row), day 5 infected mice (middle row) and the difference between both groups (lower row). White arrows point to regions of highest increase in iRBC accumulation in day 5 infected mice as compared to uninfected ones.

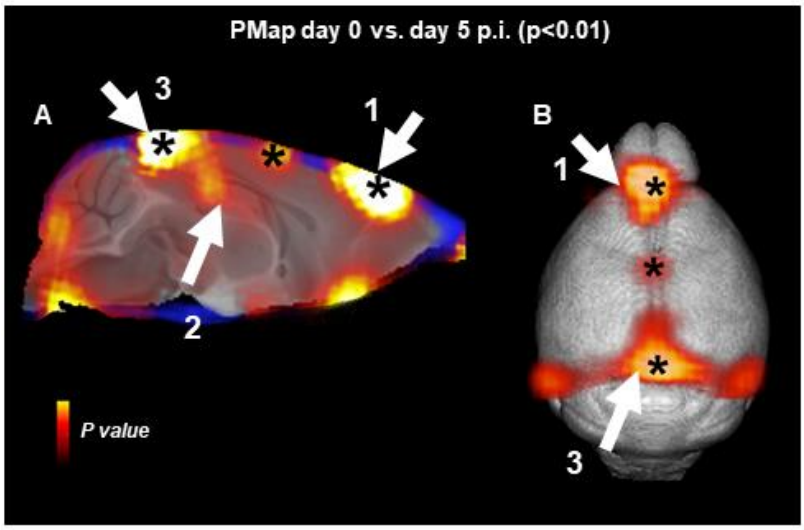

Figure 10: The highest accumulation of iRBCs was observed in and around the large draining veins and sinuses of the mouse brain. A sagittal section (A) and a top view on a volume-rendered 3D MR (B) overlaid with images of the difference in mean ^{99m}Tc-uptake between infected and uninfected mice. Arrows show peak differences overlying the junction of the rostral rhinal veins and the superior sagittal sinus (1), the longitudinal hippocampal vein (2) and the junction between the superior sagittal sinus and the transverse sinuses (3).

5.3 Severe reduction in venous efflux and edema formation progresses with ECM development

To visualize potential effects of iRBC sequestration on cerebral blood flow in the large draining veins during disease development, non-invasive 2D non-contrast time of flight MR

angiography (TOF MRA) was performed. Uninfected (day 0) mice, neurologically asymptomatic mice (day 5 p.i.) and severely sick mice (day 7 p.i.) animals were imaged as described in 4.2.8.

Vessel rarefication, meaning disappearance of blood vessels, previously described in literature in ECM by Hoffman *et al*., 2016, was observed in the TOF-MR angiographies of the brains of infected mice, particularly in the day 7 infected mice. The reduction in signal intensity of overall cerebral blood flow was already visible at the early stage of the disease at day 5 p.i. when compared to day 0 uninfected controls. There was a huge drop in signal intensity at the late stage of the disease at day 7 p.i. and in cases of mice close to death, the signal intensity was hardly detectable indicating a massive reduction in cerebral blood flow. In the present study, the vessel rarefication was analysed, for the first time, on a single vessel level. Marked reductions in flow were found in the rostral rhinal vein, the superior sagittal sinus and the longitudinal hippocampal (Figure 11). This corroborates the iRBC accumulation SPECT/CT data and suggests that there is obstruction of cerebral macro-circulation affecting larger veins rather than blockage of microcirculation only, as reported in literature till now. TOF-MRA method could prove to be a useful diagnostic tool for early detection of CM.

To quantify the reduction in venous efflux, TOF-MRA signal in the superior sagittal sinus region of the mice brain was measured. Significant decrease was observed in the signal intensity already at day 5 infected mice which worsened to a three-fold significant decrease at day 7 p.i. when compared to uninfected controls. The signal intensity was almost half of its value at day 7 p.i. when compared to day 5 p.i. (Figure 12).

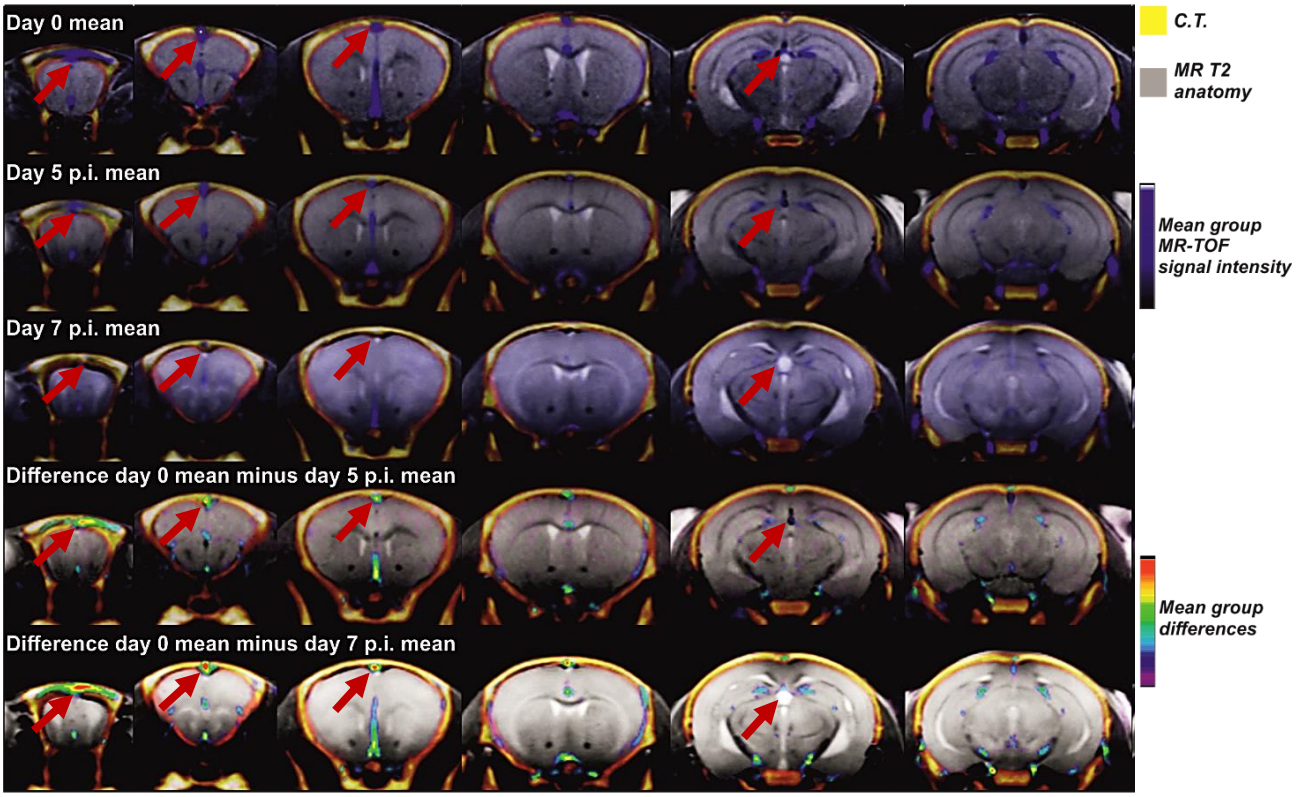

Figure 11: MR angiography revealed reduction in venous efflux observed already from early, neurologically asymptomatic stages of infection. Rostral to caudal sections of group means and group difference angiography images were overlaid on group mean CTs (in yellow) and anatomical MR reference (in grey). Red arrows point to the rostral rhinal vein (first column), the superior sagittal sinus (second and third column) and the longitudinal hippocampal vein (fifth column). TOF-MRA signal intensity decreased at day 5 p.i. and massively at day 7 p.i. indicating a huge reduction of cerebral venous efflux as compared to uninfected control mice.

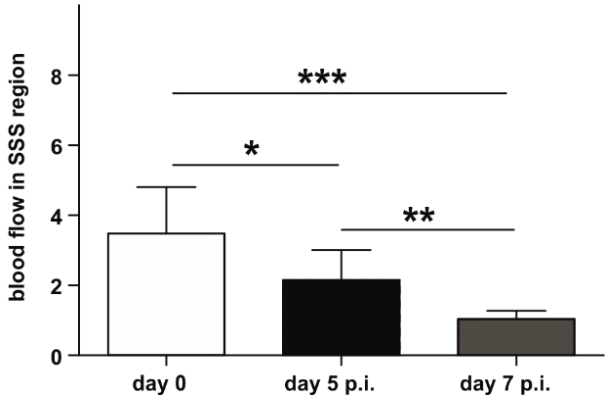

Figure 12: Marked reduction in blood flow was observed in the superior sagittal sinus (SSS) region. Quantification of signal intensity in the superior sagittal sinus region showed marked decrease of blood flow already at day 5 p.i. The intensity almost halved of its value at day 7 p.i. as compared to day 5 p.i. ($p<0.05$ is *, $p<0.01$ is ** and $p<0.001$ is ***).

Increased signal intensity in T2 weighted MR anatomy images of day 7 infected animals as compared to uninfected ones indicated signs of edema. Severe edema was observed in the brains of day 7 infected animals whereas, the same was not visible in the day 5 infected mice. In particular, animals that were severely sick at day 7 p.i. showed increased signal intensity

indicating severe edema wide-spread throughout the brain. The edema developed in a bilateral pattern. Development of edema around day 7 p.i. indicates that it is a late event in disease development. Regions of severe edema with high signal intensity were observed mainly around white matter fibre tracts (Figure 13).

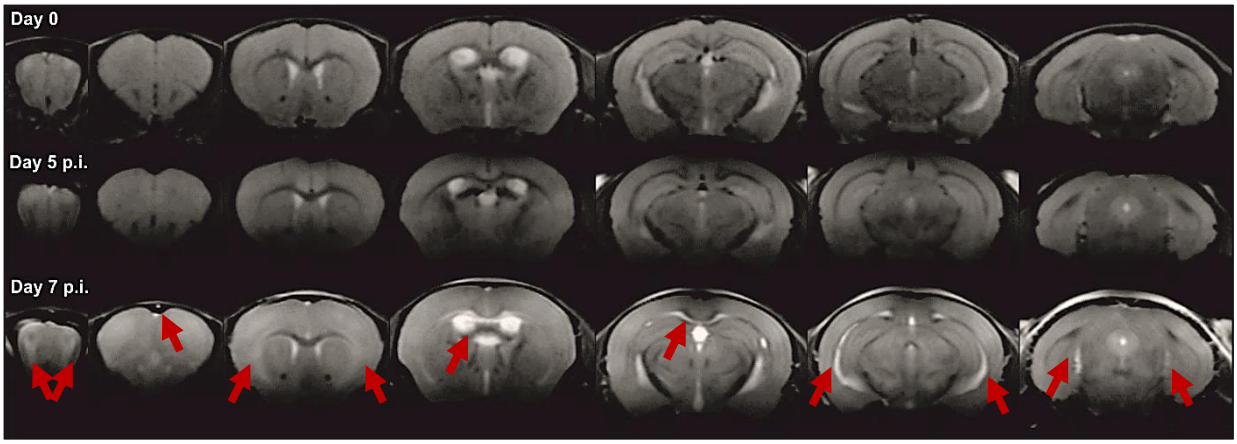

Figure 13: T2-weighted MR anatomy images showed development of severe edema at day 7 p.i. Red arrows point to regions of increased signal intensity observed only at day 7 p.i. indicating development of severe edema at a late time point in disease development, especially in the white matter fibre tracts.

5.4 Cerebral hypo-perfusion precedes the development of ECM neurological symptoms

To study where and when the brain perfusion deficits start and whether the spatial patterns of alterations in cerebral blood flow might be related to spatial patterns of iRBC sequestration and reductions in flow in large draining veins, the changes in the regional blood flow in the brain tissues were tracked from the early, neurologically asymptomatic stages of ECM. It was performed by injecting the radioactive lipophilic blood flow tracer, ^{99m}Tc-HMPAO, intravenously, followed by SPECT/CT imaging in uninfected mice (day 0), day 5 infected and day 7 infected mice as described in 4.2.7.

The SPECT data revealed minor but significant decreases in the global mean and normalized-^{99m}Tc uptake in the brains of day 5 infected mice as compared to uninfected controls. The reductions in cerebral blood flow were observed mostly in the territories of the large draining

veins and sinuses, in particular hypo-perfusions were observed in the regions of the olfactory bulb, the rostral rhinal vein and the superior sagittal sinus (Figure 14A). This hypo-perfusion became more pronounced and augmented at day 7 p.i., especially in the severely sick animals. At day 7 p.i., there were larger areas with reduced or no uptake of ^{99m}Tc indicating severe reduction in cerebral blood flow (Figure 14B). The hypo-perfusion was more pronounced in the regions corresponding to the bilateral white matter edema observed in T2 MR anatomy images in 5.3 and was also bilateral in nature individually as well as in group mean perfusion data. In correspondence to the vascular anatomy of the mouse brain, bilateral patterns of reduced blood flow indicate a reduced venous efflux rather than an arterial blockage. The large draining veins form a midline, collecting blood from both sides of the brains and hence, reductions in efflux in these midline draining veins affect cerebral blood flow on both sides in a similar pattern. Also, decrease in flow in large draining veins again suggests a hindrance to cerebral macro-circulation along with microcirculation of blood flow. The reductions in cerebral blood flow fit perfectly to the spatial patterns of iRBC accumulation and regions of cerebral venous efflux observed in 5.2 and 5.3 respectively.

Presence of few regions with higher tracer uptake were also detected, especially in the day 7 infected mice. This could be a result of the haemorrhagic lesions and BBB disturbances reported in cerebral malaria. Several studies, including the present one, have detected haemorrhages in severe cases of both human CM and ECM that could result in increased blood perfusion in some regions. However, such regions were few and the regions with hypo-perfusion were numerous and widely spread.

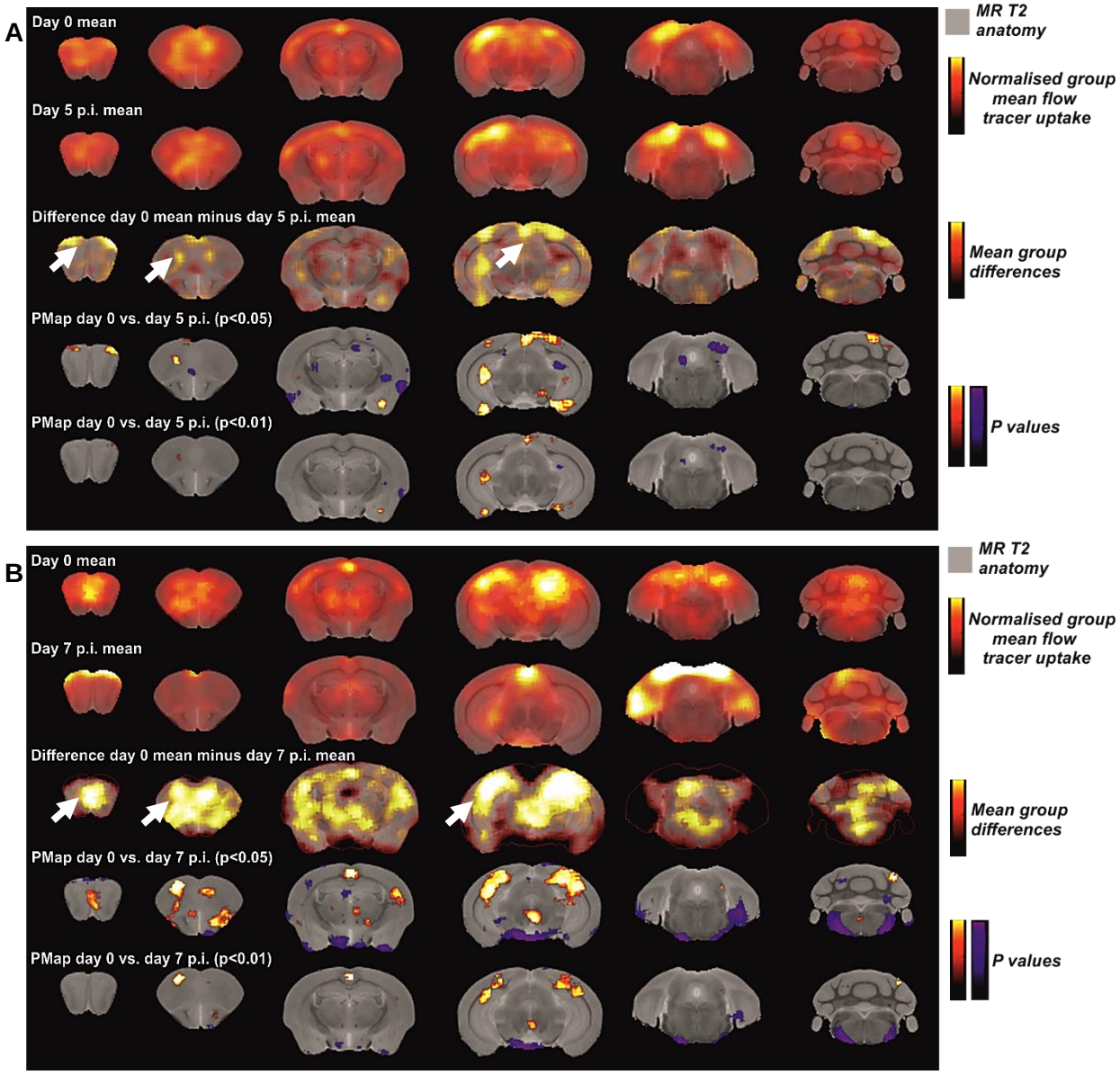

Figure 14: SPECT imaging detected widespread regions of cerebral hypo-perfusion, prior to development of ECM neurological symptoms. Rostral to caudal series of global, mean, normalized SPECT perfusion images were overlaid on anatomical MR reference (in grey). The upper image (A) shows perfusion patterns of day 5 infected mice group as compared to uninfected (day 0) controls and the lower one (B) shows comparison to day 7 infected group. The first row in both images show spatial pattern of average perfusion in uninfected mice. The second row shows mean perfusion of day 5 p.i. (in A) and of day 7 p.i. (in B). The third row depicts the difference in perfusion between the uninfected and the infected groups respectively. The last two rows show the significant changes in perfusion in infected mice as compared to uninfected controls. White arrows indicate at day 5 p.i. hypo-perfusion in the olfactory bulb (first column), rostral prefrontal cortex (second column), posterior cingulate cortex and adjacent visual cortex (fourth column). At day 7 p.i., marked decreases were observed also in the area of the corpus callosum (fourth column).

5.5 Anti-malarial treatment in the early stages prevents the spread of ECM

Since non-invasive neuroimaging experiments showed sequestration of iRBCs and minor but significant changes in the cerebral blood flow from day 5 p.i., the efficacy of anti-malarial

treatment, if provided immediately with the early detection of the disease, was determined. Day 5 infected mice were injected with pyrimethamine, an anti-malarial drug, once per day till day 7 p.i. The neurological symptoms of ECM, parasitemia in peripheral blood, blood-brain barrier integrity and parasite load in the brain of uninfected (day 0) mice, day 5 infected mice, day 7 infected untreated mice (injected with PBS for control) and day 7 infected pyrimethamine treated mice were monitored daily.

As mentioned in 5.1, at day 5 p.i., the animals did not show any neurological symptom of ECM. One half of the infected animals started receiving pyrimethamine while the rest of the infected animals received PBS as control from day 5 p.i., as mentioned in 4.2.2. Between day 6 and day 7 p.i., all the untreated (PBS injected), infected animals rapidly developed neurological symptoms of ECM like paralysis, apathy, ataxia, seizures and became severely sick and had to be euthanized. On the other hand, all the pyrimethamine treated mice appeared healthy, without any symptom of ECM and survived normally. Therefore, day 5 p.i. was an early stage of ECM, prior to development of neurological symptoms and anti-malarial treatment provided immediately after early detection, helped in survival of the infected mice (Figure 15A).

To determine the efficacy of the anti-malarial treatment in inhibiting the reproduction of the parasites in blood, the parasite load in the peripheral blood of all infected animals were monitored daily by Diff. Quik staining, as described in 4.2.3. Percentage of iRBCs started increasing slowly from around day 3 p.i. and was close to 2% around day 5 p.i. Comparatively, there was a huge increase in the percentage of infected erythrocytes in the untreated (PBS injected) animals from day 6 p.i., around 7% and it had doubled to approximately 14% on day 7 p.i. Meanwhile, in the pyrimethamine treated group, there was an immediate decrease of parasite load in the blood and on day 7 p.i., the parasite was close to elimination (Figure 15B). It supports the appearance of rapid neurological symptoms of ECM between day 6 and day 7

p.i. in the untreated, infected animals while the pyrimethamine treated ones survived normally, without symptoms. The anti-malarial drug was successful in inhibiting the reproduction of the parasites in blood.

Blood-brain barrier (BBB) damage is an important hallmark of human cerebral malaria, as discussed in detail in 2.3.3.4. To check the integrity of the BBB in mice, Evans blue dye was injected into all the infected animals and after one hour the animals were euthanized and their brains were checked for the uptake of the blue dye, as mentioned in 4.2.4. In normal, healthy brains, the dye would not be able to cross the BBB and the brain should appear white (Schmid *et al.*, 2017). A very light bluish tinge was observed in the olfactory bulb region of the day 5 infected mice indicating the beginning of the BBB damage in the course of ECM. If left untreated, the disease progressed and led to extensive breakdown of the BBB as observed with the completely blue brains of the animals at day 7 p.i. The blue dye could pass through the damaged BBB and was up taken completely in the brains of the untreated (PBS injected) mice at day 7 p.i. However, in the pyrimethamine treated animals, the brain appeared complete white indicating an intact BBB and therefore, no dye was up taken in their brains (Figure 15C). The minimal damage to the BBB visible at day 5 p.i. recovered upon anti-malarial treatment.

The accumulation of *Pb*A-iRBCs in the brains of the infected mice was further confirmed by quantifying the mRNA levels of the *Pb*A-specific CytochromeB (Bahamontes-Rosa *et al.*, 2016) in the different regions of the brain by quantitative RT-PCR, as described in 4.2.6. At day 5 p.i., there was little but significant rise in the mRNA levels of the parasite, especially in the olfactory bulb and the cortex regions as compared to the uninfected ones. This further corroborates the previous findings of the accumulation of iRBC in the SPECT/CT imaging experiment at day 5 p.i. as described in 5.2. At day 7 p.i., in the untreated group of mice there was a massive, wide-spread increase in the parasite load in all the regions of the brain: olfactory

bulb 2000 times, cortex 1000 times and brain stem 150 times approximately, in comparison to the uninfected mice. Subsequently, pyrimethamine treatment reduced the parasite burden in all the regions of the brain as observed by almost negligible levels of mRNA of the parasite (Figure 15D). The RT-PCR results supported the findings of the sequestration of iRBCs from day 5 p.i., an early stage of the disease and it worsened without treatment. However, anti-malarial treatment from day 5 p.i. helped in clearing and in reducing the number of accumulated iRBCs in the brain of infected mice.

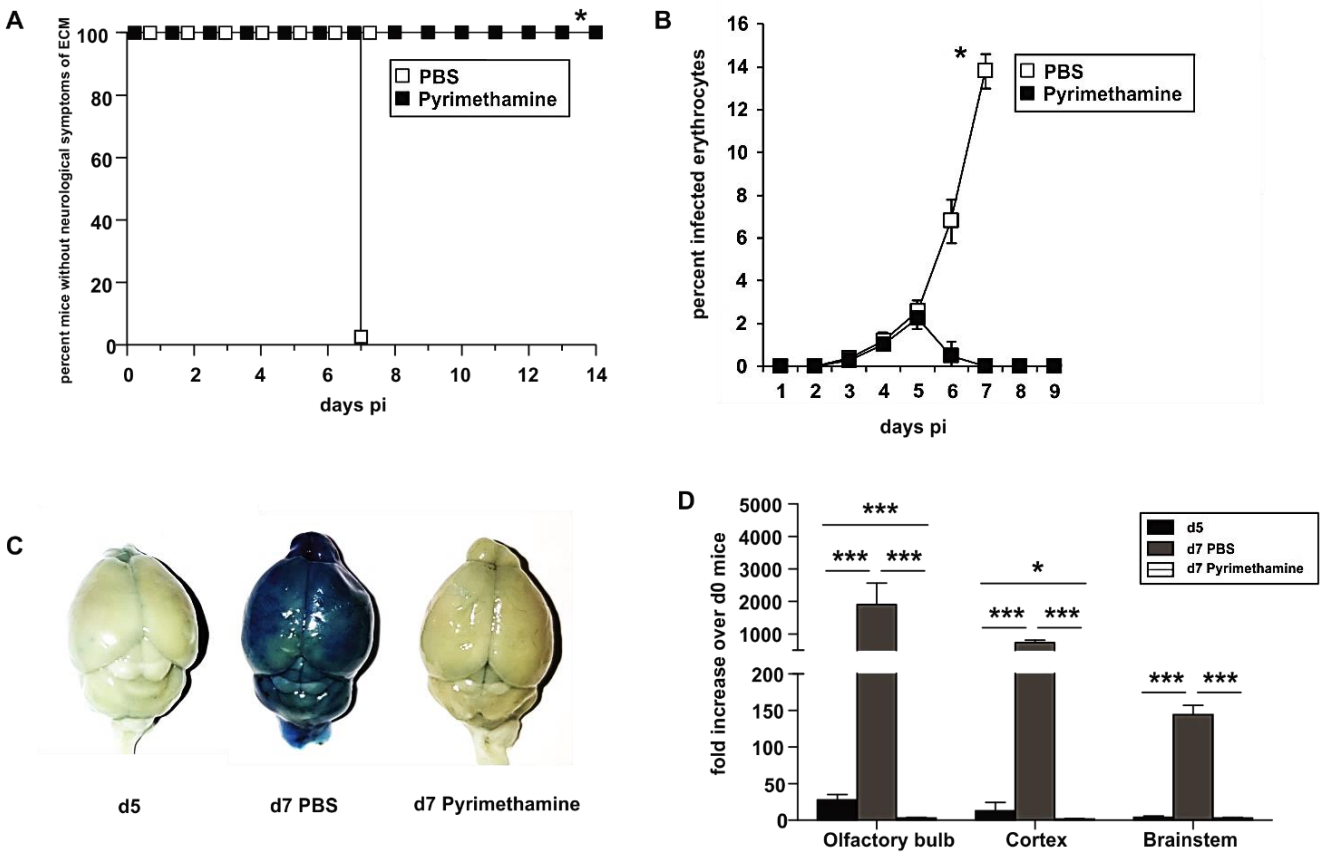

Figure 15: Anti-malarial treatment prevented the spread of the disease by reducing the parasite burden. (A) The neurological symptoms of ECM were monitored daily. Day 5 p.i. was a neurologically asymptomatic stage while all the untreated (PBS injected), infected mice rapidly developed severe symptoms of the disease in between day 6 and day 7 p.i. The pyrimethamine treated mice survived normally without any symptom. (B) The percentage of iRBCs in peripheral blood was quantified daily. Sudden increase in iRBCs was observed around day 6 and day 7 p.i. in the untreated mice whereas, pyrimethamine inhibited the growth of the parasites and reduced the number of iRBCs in the blood of the treated mice. (C) Blood-brain barrier (BBB) integrity was checked by Evans blue injection. Slight bluish tinge in the brain of day 5 (d5) infected mouse indicated beginning of BBB damage. Overall breakdown of BBB was displayed by the completely blue-stained brain of the untreated mouse (d7 PBS) whereas, a white brain of the pyrimethamine treated mouse (d7 Pyrimethamine) stipulated recovery of the minimal damages to BBB. (D) Intracerebral accumulation of iRBCs was measured by quantitative reverse transcription-PCR. Accumulation of iRBCs was already observed at day 5 p.i., similar to SPECT/CT imaging experiment and it increased massively at day 7 p.i. in the untreated mice. On pyrimethamine treatment, the parasite growth was reduced, thus, decreasing the accumulation of iRBCs in the brain of the infected mice ($p<0.05$ is *, $p<0.01$ is ** and $p<0.001$ is ***).

5.6 Progression of ECM results in the disruption of the rostral migratory stream from an early stage of the disease

Neurocognitive impairments have been reported in patients surviving CM, especially in children in Africa (Idro *et al*., 2005) but the reason behind it is largely unknown. In adult brains, neurogenesis takes place in the subventricular zone (SVZ) and the neuroblasts formed migrate to the olfactory bulb via the rostral migratory stream (RMS) differentiating into functional interneurons (Lim and Alvarez-Buylla, 2016). Hoffman *et al.*, 2016 had demonstrated that during ECM development, BBB disruption and edema formation initiated in the olfactory bulb and progressed through the SVZ into the brainstem. The study also reported activated microglia surrounding the RMS and severe misalignment of neuroblasts within the RMS. To assess the effect of iRBC sequestration and reduced venous efflux on the RMS and neurogenesis, BrdU, a synthetic analogue of thymidine, was injected into the mice and their brains were isolated 48 hours later. The quantity of BrdU incorporated and the expression of doublecortin (DCX), a marker of neuroblasts were analysed by immunofluorescence, as described in 4.2.5.

The migration and proliferation of neuroblasts were severely disrupted as visualized by massive reduction of BrdU staining and DCX labelled neuroblasts in the RMS of the untreated (PBS injected) mice at day 7 p.i. The number of neuroblasts already started significantly declining from an early stage of the infection, at day 5 p.i. and it progressed until day 7 p.i., when the RMS was completely disrupted, visible by the lack of any staining in the region (Figure 16A). This is in agreement with the SPECT/CT and TOF-MRA data where regions around the SVZ had progressive decrease in cerebral blood flow from day 5 p.i. Early anti-malarial treatment with pyrimethamine was able to prevent further damage to the RMS and fostered its repair as visible by significant increase in the numbers of BrdU and DCX staining at day 7 p.i. indicating proliferating and migrating neuroblasts respectively (Figure 16B).

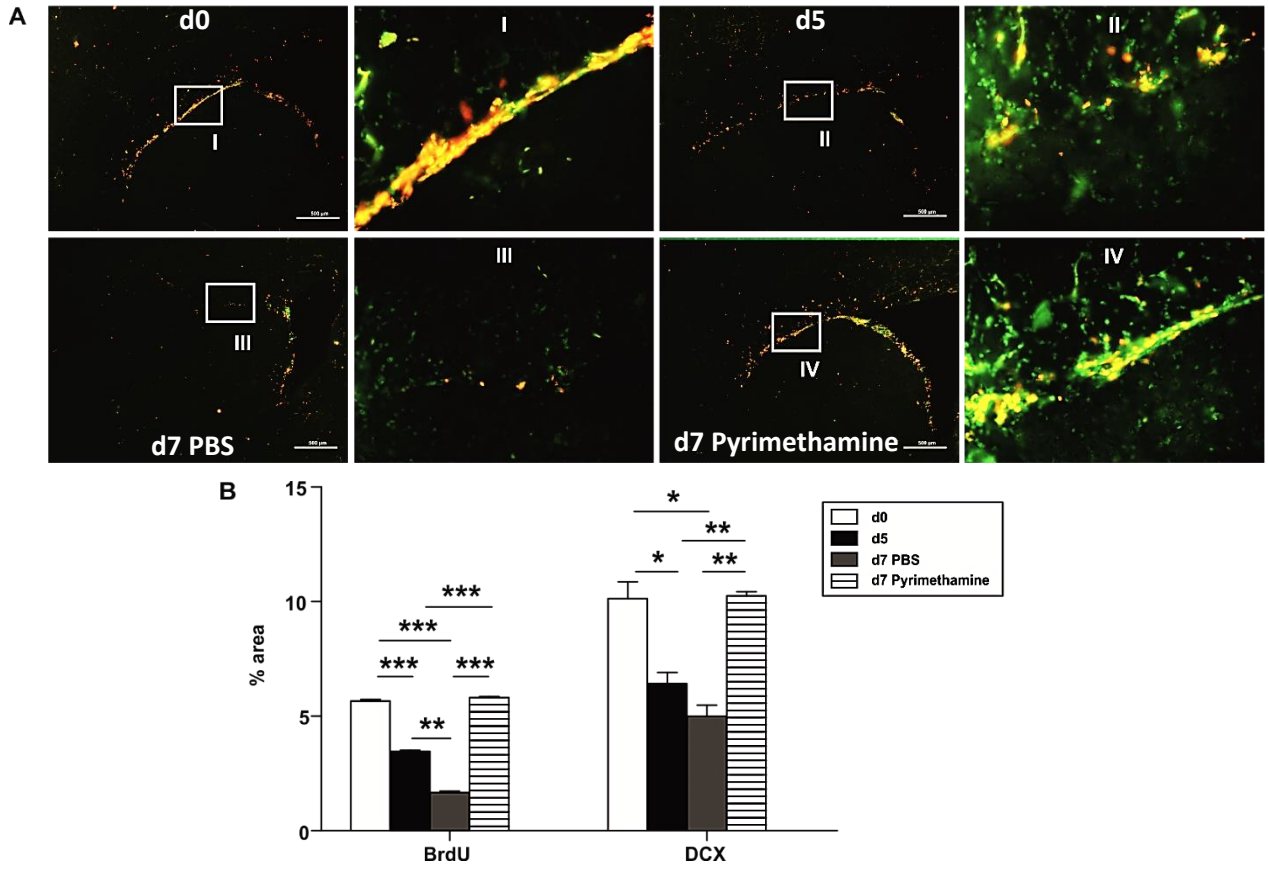

Figure 16: Immunofluorescence staining revealed disruption in migration and proliferation of neuroblasts in the rostral migratory stream beginning from an early stage of ECM. (A) Merged immunofluorescence staining (yellow) in the RMS region (BrdU in red and DCX in green) of the brain from different mice groups (5X magnification) and their magnified, close-up view (40X). In uninfected mice (d0), an intact RMS with both proliferating (BrdU) and migrating (DCX) neuroblasts was visible. At day 5 p.i. (d5), disruption was visible with the broken thread of the RMS which progressed till day 7 p.i. in the untreated mice (d7 PBS) where a complete lack of BrdU and DCX staining was observed indicating severe disturbances in proliferating and migrating neuroblasts. However, with early anti-malarial treatment (d7 Pyrimethamine), disruption of the RMS was prevented and was almost back to its normal, uninfected state. (B) Bar graphs show statistically significant differences in the number of proliferating and migrating neuroblasts in the RMS region ($p<0.05$ is *, $p<0.01$ is ** and $p<0.001$ is ***).

Immunohistochemical staining of the RMS region revealed acute inflammation as characterized by increased activation of astrocytes (Figure 17A), microglia (Figure 17B) and endothelial cells (Figure 17C), especially at day 7 p.i. This could have aided in further disruption of the RMS and neurogenesis. There was a decrease in the activation of these cells upon early anti-malarial treatment which helped in recovery of the RMS. Collectively, these data indicate that ECM progression leads to disruption of RMS that might lead to disturbances in neurogenesis and could be a reason for the neurocognitive impairments reported in human CM and could be resolved by providing anti-malarial treatment after early detection.

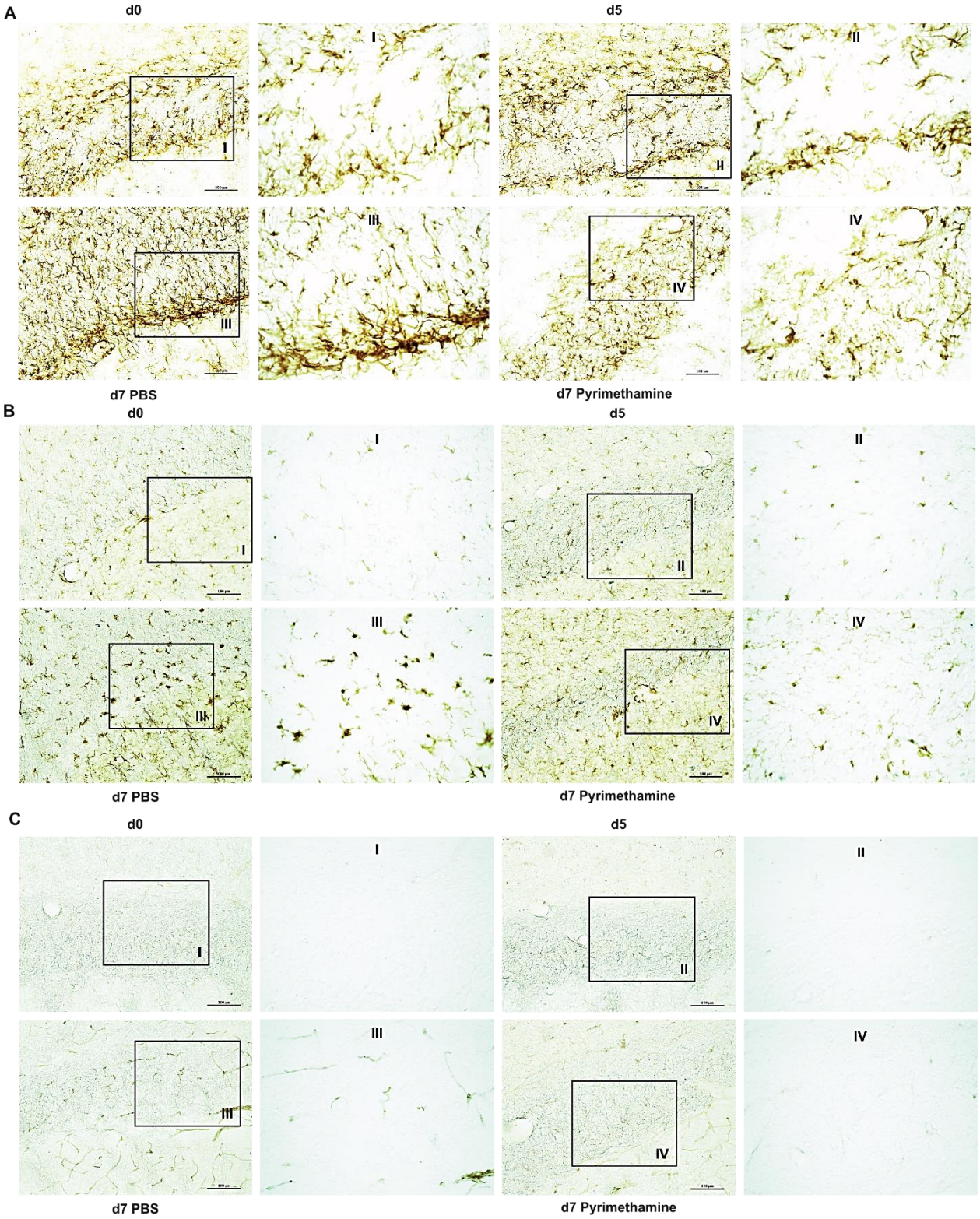

Figure 17: Histological analysis detected acute inflammation in the rostral migratory stream region in the later stages of ECM. Immunohistochemical staining was performed (20X magnification, close up 40X) which detected (A) elevated and denser glial fibrillary acidic protein (GFAP) staining already at day 5 p.i. (d5) as compared to uninfected brain (d0) and it increased hugely in the untreated mice (d7 PBS) indicating activation of astrocytes, (B) denser, de-ramified, activated microglia with increased ionized calcium-binding adapter molecule 1 (Iba1) staining in the brain of untreated mice at day 7 p.i. and (C) increased cytoplasmic domain 31 (CD31) staining indicating activation of endothelial cells in the untreated mice at day 7 p.i. Early anti-malarial treatment (d7 Pyrimethamine) reduced activation of these cells and helped in recovery of the RMS.

5.7 Acute inflammation develops throughout the brain in the later stages of ECM pathology

In literature, several studies support the theory of excessive inflammatory responses during CM development which leads to immune induced pathology and iRBC sequestration augments it further (Dunst *et al*., 2017). The timeline of sequestration of iRBC and the elevated immune responses during CM development remain inconclusive. To clarify whether the acute inflammation observed around the RMS region is localized or widespread, a detailed immunohistochemical analysis was performed in different regions of the mice brain to check the activation astrocytes, microglia and endothelial cells and the accumulation of leukocytes like $CD8^+$ T cells, as mentioned in 4.2.5. In addition, histological stains were performed to identify apoptotic cells and haemorrhagic lesions throughout the brain. Figure 18 shows an example of immunohistochemical staining of Iba1 for activation of microglia in five different regions of the mouse brain (rest immunohistochemical stainings are shown as supplementary figures S1, S2, S3, S4 and S5).

The area covered by brown-stained activated cells and the number of accumulated $CD8^+$ T cells were quantified in multiple animals and statistically analysed. At day 5 p.i, minor but significant activation of astrocytes was observed only in the olfactory bulb and activation of microglia only in the sub-ventricular zone. Contrarily, there was no activation of endothelial cells and accumulation of leukocytes in any region of the brain at day 5 p.i. The primary signs of severe brain pathology developed at day 7 p.i. in the untreated animals. Widespread astrogliosis was observed with the increase in expression of GFAP in activated astrocytes. The activation of astrocytes was significantly higher in the regions of the olfactory bulb, the sub-ventricular zone and the hippocampus as compared to the midbrain and the pons region (Figure

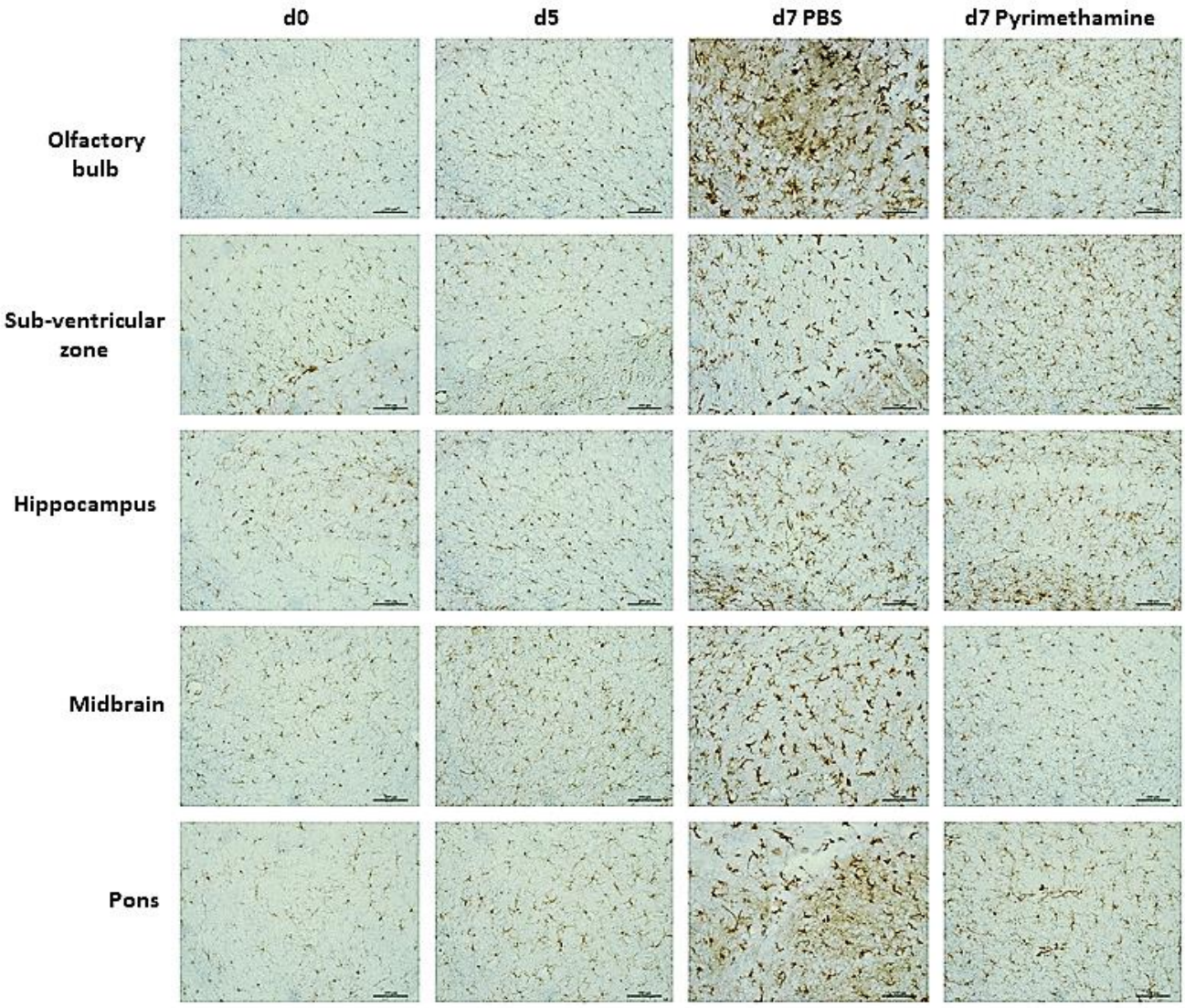

Figure 18: Immunohistochemical staining performed for activation of microglia in different regions of the brain. Example image shows immunohistochemical staining for ionized calcium-binding adapter molecule 1 (Iba1) in five different regions of the brain of uninfected (d0) mice, day 5 (d5) infected mice, untreated day 7 (d7 PBS) infected mice and pyrimethamine treated day 7 (d7 Pyrimethamine) infected mice (20X magnification). Similarly, other histological stainings were performed and images are shown as supplementary figures.

19A, S1). This coincides with the migratory route of the neuroblasts. Increased activation of microglia was also observed in all the regions of the brain in the untreated mice at day 7 p.i. whereas, the activation was higher in the olfactory bulb, the midbrain and the pons regions (Figure 19B, 18). CD31 staining intensity was stronger on activated endothelial cells in all regions of the brain, especially in the midbrain and the pons region in the untreated mice at day 7 p.i. (Figure 19C, S2). Activation of endothelial cells has been linked to increased pro-inflammatory response and vascular leakage (Dunst *et al.*, 2017). In concurrence with

literature, accumulation of $CD8^+$ T cells was detectable in all the regions of the brain in the untreated mice at day 7 p.i., mainly in the sub-ventricular zone and the midbrain regions (Figure 19D, S3). However, they remained in the microcirculation and did not enter in the brain tissues. $CD8^+$ T cells have been reported as a major mediator of ECM (Howland *et al*., 2015).

Additionally, cleaved caspase 3 staining for apoptotic cells were prominent in the pons region of the brainstem in the untreated mice at day 7 p.i. (Figure 19E, S4). Also, haemorrhagic lesions were observed with haematoxylin and eosin staining mostly in the midbrain region of the brainstem (Figure 19F, S5) in the untreated mice at day 7 p.i. This is in good agreement with the study which showed development of fatal brainstem pathology in case of ECM (Swanson *et al*., 2016). Taken together, severe brain pathology develops in ECM with increased activation of astrocytes, microglia and endothelial cells, accumulation of $CD8^+$ T cells and with the presence of apoptotic cells and haemorrhages in the brainstem region but mostly at the later, neurologically symptomatic stage of the disease.

To determine whether anti-malarial treatment after early detection will help in recovery of the brain pathology, pyrimethamine was injected from day 5 p.i. This treatment was able to significantly reduce the widespread activation and accumulation of cells throughout the brain. Hence, early anti-malarial treatment was successful in preventing the widespread acute inflammation which develops in the later stages of ECM (Table 1).

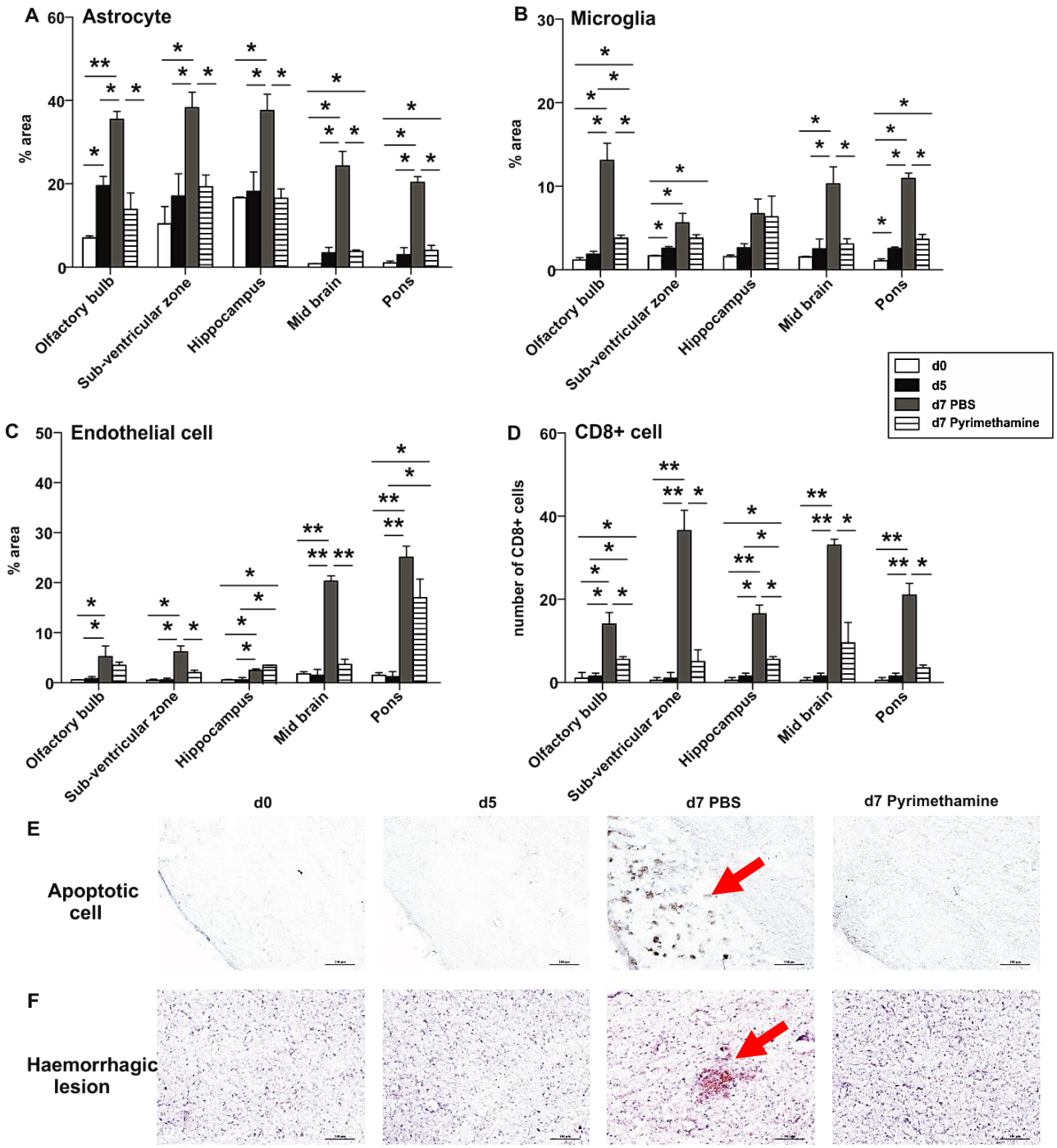

Figure 19: Acute intracerebral inflammation is widespread and a late event in ECM development. Bar graphs are depicting (A) activation of astrocytes through GFAP staining, (B) activation of microglia through Iba1 staining, (C) activation of endothelial cells through CD31 staining and (D) accumulation of $CD8^+$ leukocytes through CD8 specific staining ($p<0.05$ is *, $p<0.01$ is ** and $p<0.001$ is ***). Increased activation and accumulation of cells were observed in the untreated mice at day 7 p.i. (d7 PBS) indicating development of acute inflammation is a late event in ECM. Histological stainings show (E) apoptotic cells (red arrow) with cleaved caspase 3 staining and (F) haemorrhagic lesion (red arrow) with Haematoxylin and Eosin staining in the brainstem region of the untreated mice at day 7 p.i. (20X magnification). With early anti-malarial treatment (d7 Pyrimethamine), there was significant reduction in widespread activation, accumulation, apoptosis of cells and haemorrhages.

5.8 Increased expression of cytokines and chemokines in the later stages of ECM further augments the inflammation

Activated brain cells and accumulated leukocytes are mainly responsible for the excessive cytokine and chemokine responses in ECM (Ioannidis *et al*., 2014) (Hunt and Grau, 2003). To determine the contribution of pro-inflammatory cytokines and chemokines on the course of ECM progression, the expression of different cytokines and chemokines were measured by quantifying their mRNA levels in various parts of the brain by quantitative reverse transcription-PCR (qRT-PCR), as described in 4.2.6.

At day 5 p.i., slight expression of pro-inflammatory cytokines IFN-γ and TNF was observed. However, at day 7 p.i., their expression increased by massive folds throughout the brain of the untreated mice, the highest being in the olfactory bulb region (Figure 20). Both IFN-γ and TNF are responsible for inducing further cytokine and chemokine responses and recruitment of leukocytes to the brain endothelium, augmenting the detrimental inflammation process. Minor increase in the expression of lymphotoxin-α and β was observed in the brainstem regions at day 5 p.i. No further significant changes were observed in their expression level at day 7 p.i., indicating that IFN-γ and TNF play the major role as pro-inflammatory cytokines in the inflammation process.

Expression of chemokines like CXCL9, CXCL10 and CXCL11, responsible for recruitment of pathogen specific $CD8^+$ T cells, increased several folds at day 7 p.i. throughout the brain in the untreated mice, again the highest being in the olfactory bulb region followed by the brainstem region. CXCL3, responsible for recruitment of monocytes, increased slightly only in the olfactory bulb at day 7 p.i. in the untreated mice indicating $CD8^+$ T cells are the main leukocytes recruited to the infected brain (Figure 20).

Increase in cytokine and chemokine expression was observed only at day 7 p.i. making it a late event in ECM development when neurological symptoms are evident. With the introduction of early anti-malarial treatment, there was immediate decrease in the expression of all the cytokines and chemokines thus, preventing the pro-inflammatory responses and diminishing the inflammation related brain pathology (Table 2).

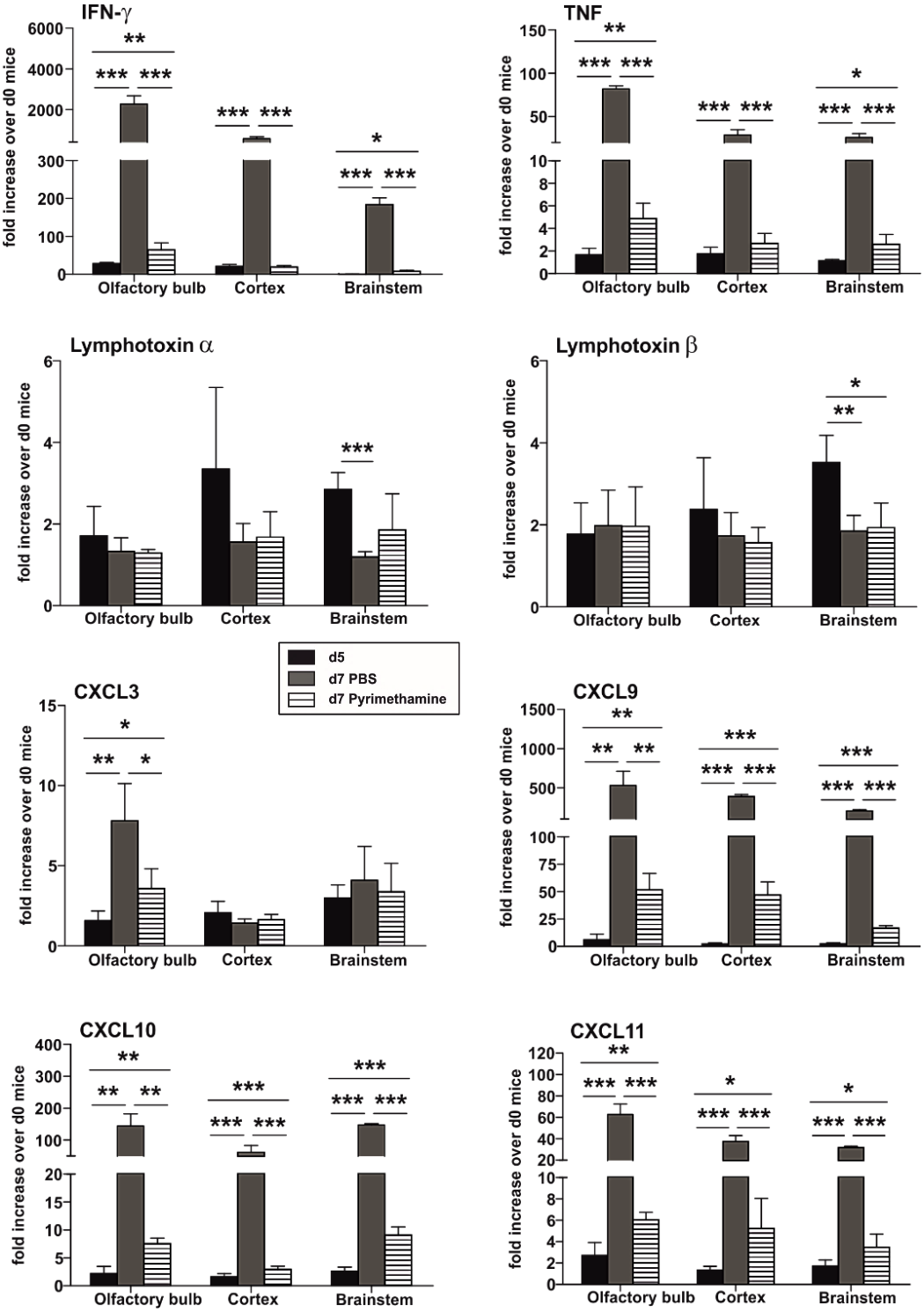

Figure 20: Pro-inflammatory cytokine and chemokine expression increases at a later stage of ECM aiding in the detrimental inflammatory brain pathology. Bar graphs show mRNA expression of cytokines and chemokines measured by qRT-PCR. Massive folds of increase in expression of pro-inflammatory cytokines IFN-γ and TNF and chemokines like CXCL9, CXCL10 and CXCL11 was observed throughout the brain only at day 7 p.i. in the untreated mice (d7 PBS). Anti-malarial treatment (d7 Pyrimethamine) helped in reducing their expression thus, preventing the spread of the inflammation ($p<0.05$ is *, $p<0.01$ is ** and $p<0.001$ is ***).

Cell	Olfactory bulb			Sub-ventricular zone			Hippocampus			Mid brain			Pons		
	d5 p.i.	d7 PBS	d7 Pyr.	d5 p.i.	d7 PBS	d7 Pyr.	d5 p.i.	d7 PBS	d7 Pyr.	d5 p.i.	d7 PBS	d7 Pyr.	d5 p.i.	d7 PBS	d7 Pyr.
Astrocyte	12.58	28.52	6.83	6.65	27.86	8.93	1.48	20.92	-0.10	2.58	23.48	2.93	2.01	19.39	3.00
Microglia	0.68	11.93	2.61	0.91	3.95	2.09	1.06	5.15	4.79	0.95	8.72	1.54	1.48	9.89	2.58
Endothelial cell	0.25	4.69	2.92	0.10	5.73	1.53	0.01	1.91	2.94	-0.28	18.52	1.86	-0.33	23.59	15.51
$CD8^+$ cell	0.5	13.5	4.5	0.5	36.0	4.5	1.0	16.0	5.0	1.0	32.5	9.0	1.0	20.5	3.0

Table 1: Summary of the results of the immunohistochemical studies. The table shows increased activation and accumulation of cells in the brain of day 5 infected mice, day 7 infected untreated (d7 PBS) mice followed by decrease of the same at day 7 infected pyrimethamine treated (d7 Pyrimethamine) mice as compared to uninfected control mice at day 0.

Cytokine/ Chemokine	Olfactory bulb			Cortex			Brainstem		
	d5 p.i.	d7 PBS	d7 Pyr.	d5 p.i.	d7 PBS	d7 Pyr.	d5 p.i.	d7 PBS	d7 Pyr.
IFN-γ	28.53	2271.79	64.43	21.22	564.90	19.08	1.04	184.17	7.96
TNF	1.68	82.05	4.90	1.76	28.88	2.68	1.12	26.08	2.61
Lymphotoxin-α	1.71	1.33	1.29	3.35	1.56	1.68	2.85	1.19	1.86
Lymphotoxin-β	1.78	1.98	1.97	2.38	1.73	1.57	3.52	1.85	1.93
CXCL-3	1.57	7.81	3.58	2.07	1.42	1.63	2.98	4.09	3.38
CXCL-9	5.96	529.20	51.57	2.19	387.74	47.01	2.38	204.65	16.89
CXCL-10	2.17	144.40	7.53	1.61	61.97	2.94	2.60	147.57	9.10
CXCL-11	2.70	62.79	6.06	1.35	37.60	5.26	1.72	31.74	3.49

Table 2: Summary of the results of the quantitative reverse transcription-PCR studies. The table shows fold increase or decrease in expression of pro-inflammatory cytokines and chemokines in the brain of day 5 infected mice, day 7 infected untreated (d7 PBS) mice and day 7 infected pyrimethamine treated (d7 Pyrimethamine) mice as compared to uninfected control mice at day 0.

5.9 Supplementary figures

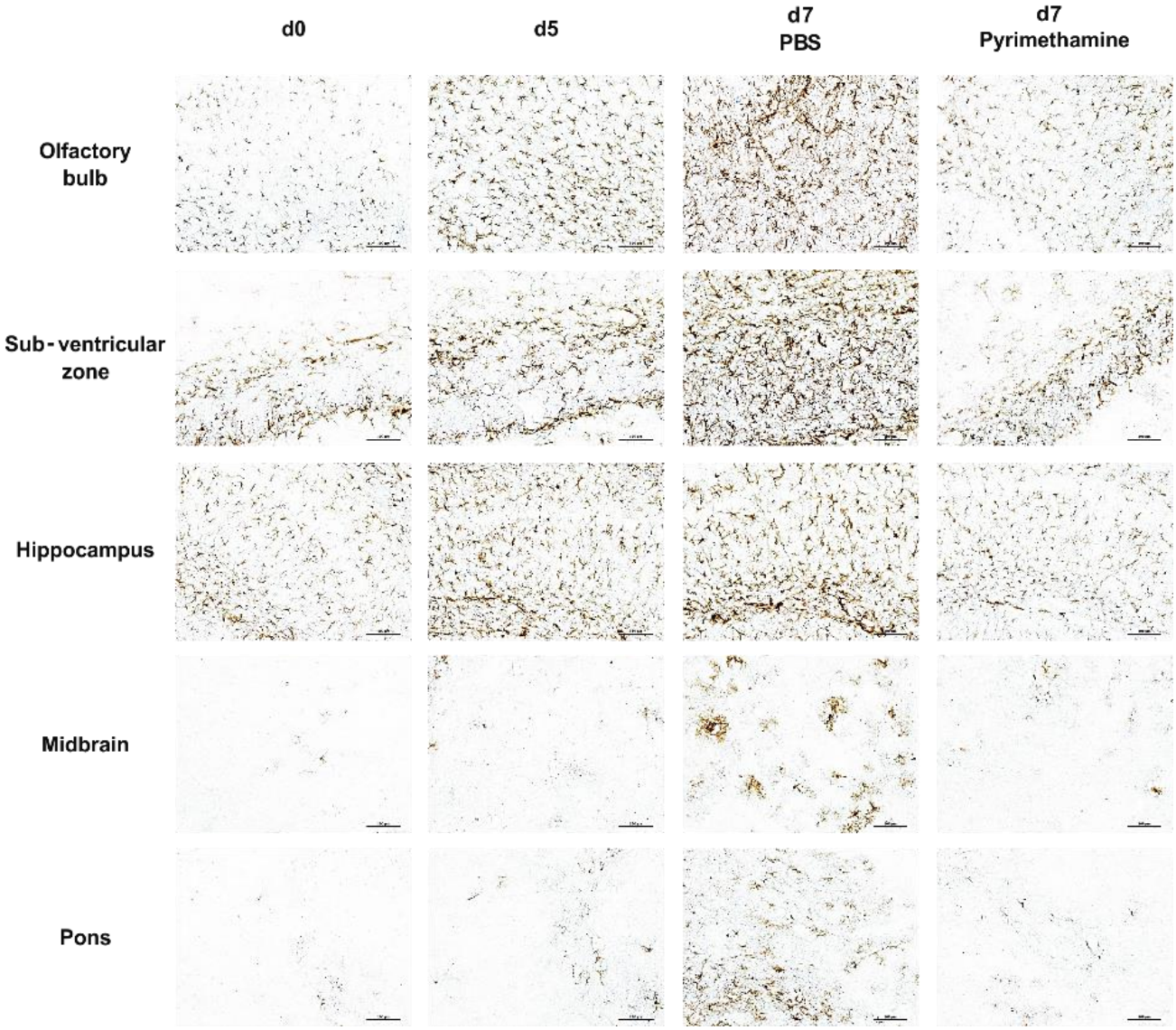

Figure S1: Immunohistochemical staining performed for activation of astrocytes in different regions of the brain. Image shows the staining for glial fibrillary acidic protein (GFAP) in different regions of the brain of uninfected (d0) mice, day 5 (d5) infected mice, untreated day 7 (d7 PBS) infected mice and pyrimethamine treated day 7 (d7 Pyrimethamine) infected mice (20X magnification).

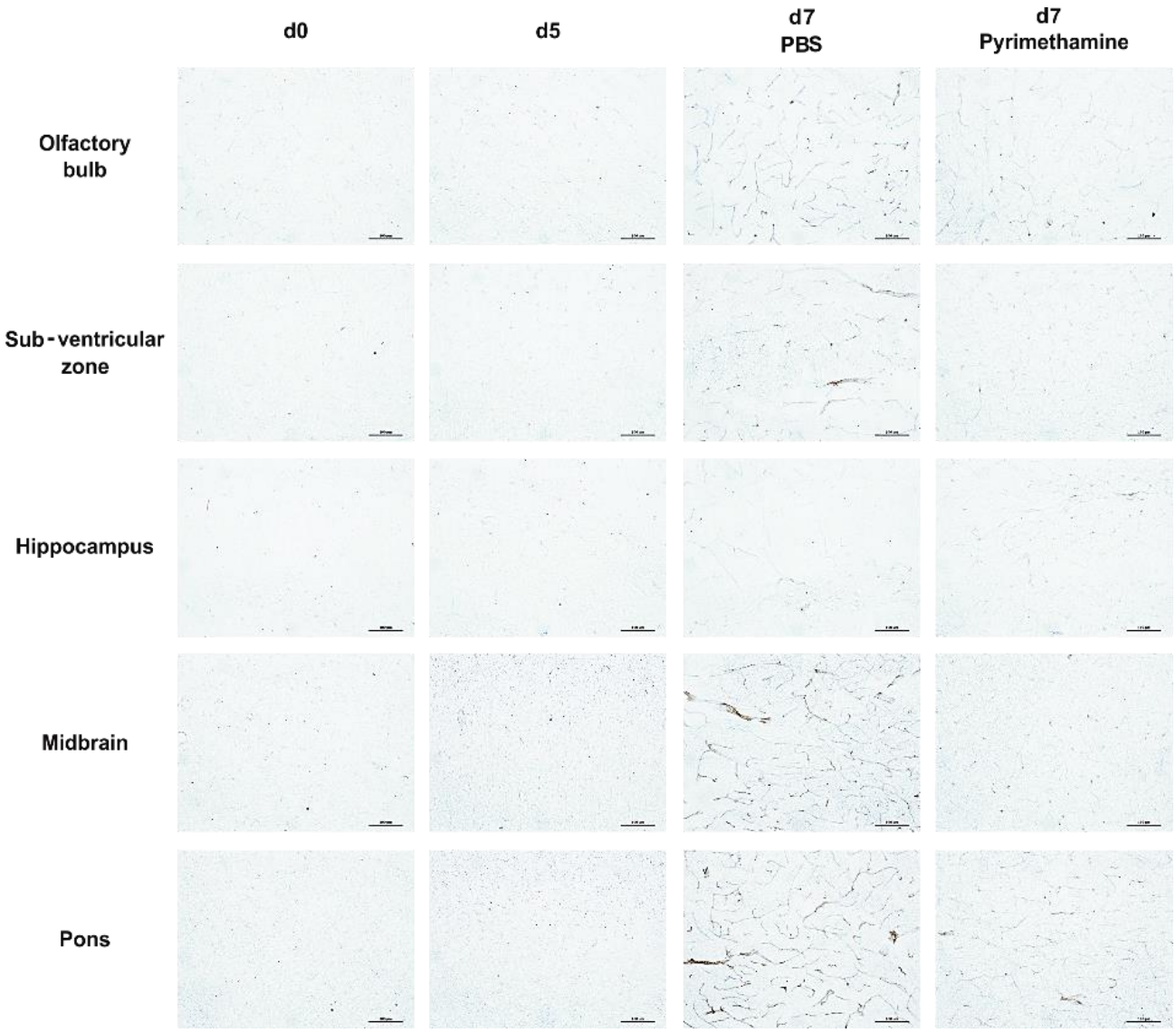

Figure S2: Immunohistochemical staining performed for activation of endothelial cells in different regions of the brain. Image shows the staining for cytoplasmic domain 31 (CD31) in different regions of the brain of uninfected (d0) mice, day 5 (d5) infected mice, untreated day 7 (d7 PBS) mice and pyrimethamine treated day 7 (d7 Pyrimethamine) mice (20X magnification).

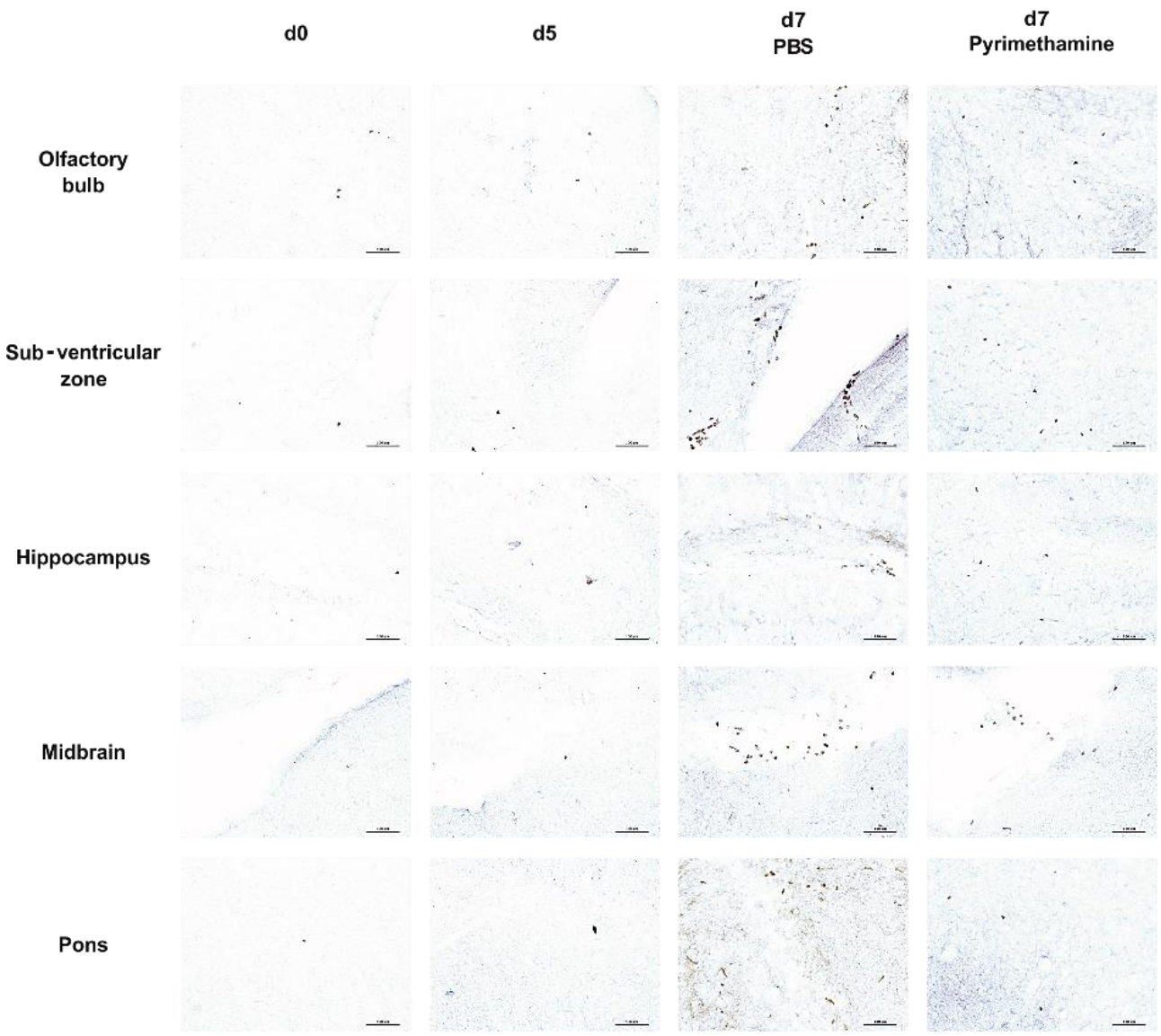

Figure S3: Immunohistochemical staining performed for accumulation of $CD8^+$ cells in different regions of the brain. Image shows the staining for cytoplasmic domain 8 (CD8) in different regions of the brain of uninfected (d0) mice, day 5 (d5) infected mice, untreated day 7 (d7 PBS) mice and pyrimethamine treated day 7 (d7 Pyrimethamine) mice (20X magnification).

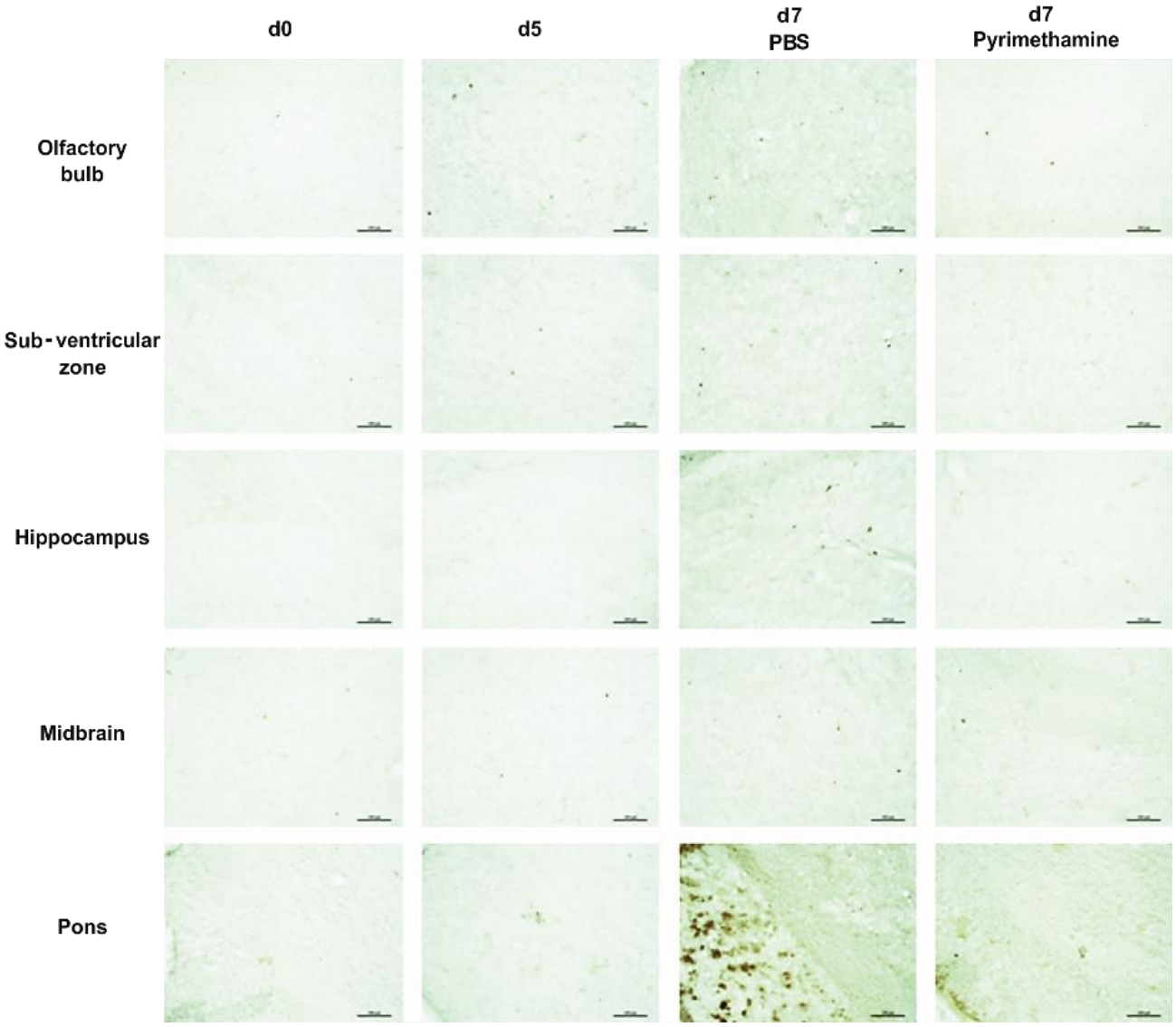

Figure S4: Immunohistochemical staining performed for detection of apoptotic cells in different regions of the brain. Image shows the staining for cleaved caspase 3 in different regions of the brain of uninfected (d0) mice, day 5 (d5) infected mice, untreated day 7 (d7 PBS) mice and pyrimethamine treated day 7 (d7 Pyrimethamine) mice (20X magnification).

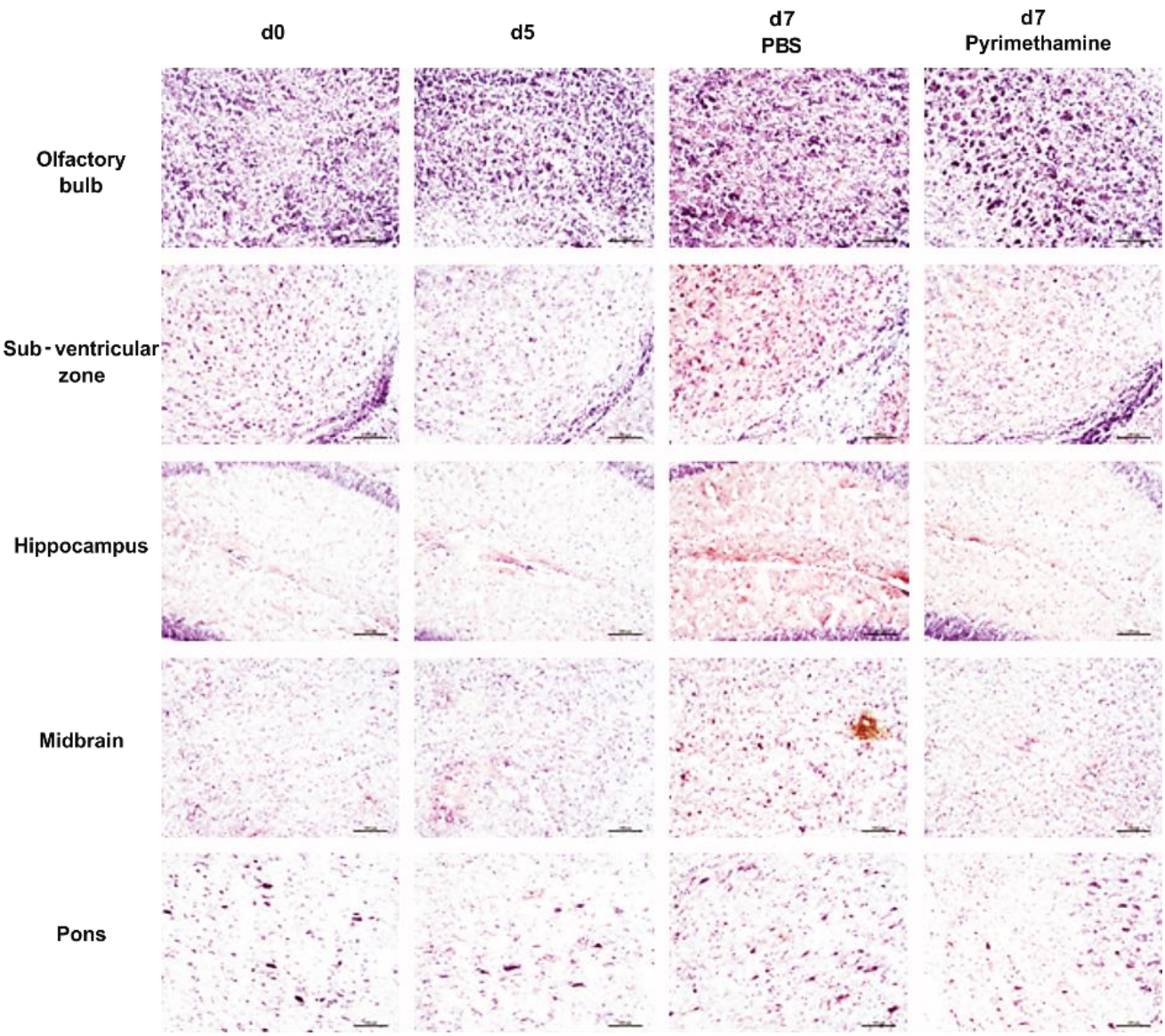

Figure S5: immunohistochemical staining performed for detection of haemorrhages in different regions of the brain. Image shows the staining for haematoxylin and eosin (H&E) in different regions of the brain of uninfected (d0) mice, day 5 (d5) infected mice, untreated day 7 (d7 PBS) mice and pyrimethamine treated day 7 (d7 Pyrimethamine) mice (20X magnification).

6. DISCUSSION

The present study provides, for the first time, a link between the two theories of CM pathogenesis: sequestration of iRBCs to the brain endothelium and the excessive inflammatory responses in the brain and their contribution to changes in cerebral blood flow and edema development. Intracerebral accumulation of iRBCs was found to be an important early event in ECM which led to reduction in cerebral venous efflux and impaired blood flow while it preceded the brain pathology and the excessive increase in cytokine and chemokine releases and resulted in edema development. The RMS was found to be severely disrupted, starting from an early phase of ECM, which could lead to disturbances in neurogenesis. Anti-malarial treatment, provided from an early stage of the disease, was successful in preventing further spread of the disease and helped in recovery of brain pathology.

6.1 Sequestration of iRBCs and cerebral blood flow

The three-dimensional *in vivo* distribution of iRBCs was imaged for the first time in the early stages of ECM. Day 5 p.i. was found to be an early stage in disease progression without any neurological symptom but with a considerate parasite load in the peripheral blood. Hence, the sequestration of iRBCs to the brain was checked at this early, neurologically asymptomatic stage of the disease. SPECT imaging detected significant increase in accumulation of ^{99m}Tc-labelled iRBCs throughout the brain of the day 5 infected mice as compared to the uninfected ones. Peak increases were in regions corresponding to the large draining veins and sinuses of the infected brains. In concurrence, there was a decline in venous efflux in the large draining veins in day 5 infected mice. There was further decrease in venous efflux to practically undetectable levels in the clinically sick mice at day 7 p.i. as observed in MR angiography. SPECT imaging performed to visualize the cerebral blood flow with the lipophilic blood flow

tracer, ^{99m}Tc-HMPAO, detected regions with minor but significant bilateral hypo-perfusion at day 5 p.i. which progressed to huge widespread regions of hypo-perfusion at day 7 p.i.

The cerebral venous circulation in rodents is slightly different from that of humans. The superior sagittal sinus drains into the rostral rhinal vein and this is one of the major venous efflux routes in mice (Mancini *et al*., 2015) (Dorr *et al*., 2007). All the changes in brain pathology related to iRBC sequestration and cerebral blood flow were observed, from the early stage of ECM, in close proximity to the regions draining into this venous efflux route. The highest intensity of the accumulated radiolabelled iRBCs was observed around the T-shaped junction of the rostral rhinal vein and the superior sagittal sinus. The decrease in cerebral venous efflux as detected by TOF-MRA was most prominent in the rostral rhinal vein, the superior sagittal sinus and the longitudinal hippocampal vein. At day 5 p.i., bilaterally impaired cerebral blood flow was observed in regions around the caudal olfactory bulb and rostral prefrontal cortex as well as in posterior cingulate and visual cortex, all of which drain into the rostral rhinal vein and the superior sagittal sinus (Mancini *et al*., 2015) (Xiong *et al*., 2017). At day 7 p.i. the intensity of the hypo-perfusion increased while spreading further throughout the brain. Taken together, it indicates a reduction in blood flow in the macro-circulation as well as in the microcirculation of the brain. These regions of the brain also showed development of severe, bilateral edema in the white matter at day 7 p.i. In literature, venous efflux impairments affecting the large draining veins and sinuses have been associated with venous thrombosis and mechanical obstructions, in both humans (Silvis *et al*., 2017) (Wilson, 2016) and rodents (Ueda *et al*., 2000) (Ungersböck *et al*., 1993) and this may be followed by BBB disruption, impaired perfusion, haemorrhages and edema. Though the present study does not reveal thrombosis in ECM, sinus thrombosis in human CM (Krishnan *et al*., 2004) (Pinzón *et al*., 2013) and transient occlusion in internal cerebral vein and vein of Galen (Seydel *et al*., 2015) have been rarely

reported; hence, it does not rule out the obstruction of venous efflux by iRBC sequestration as a major event in CM pathology.

The present study is the first of its kind to emphasize the effect of the sequestration of iRBCs on the widespread reduction in cerebral venous efflux in ECM. Significant intracerebral accumulation of iRBCs begins from an early stage of the disease, even before the onset of the neurological symptoms, BBB disruption, the increase in inflammatory responses and appearance of brain pathologies. This fact was corroborated by the increase in *Pb*A-specific mRNA levels from day 5 p.i., especially in the olfactory bulb region. It demonstrated that intracerebral iRBC sequestration is primarily responsible for reduction in venous efflux and the associated brain pathologies in ECM. This is in good concurrence with human CM where Kessler *et al*., 2017 had demonstrated higher parasite biomass as a strong indicator of the brain swelling. Furthermore, a post-mortem study in affected children identified a sub-group of patients with sequestration of iRBCs as the only pathological finding of the disease (Taylor *et al*., 2004).

In the present study, it was not possible to separate the effects of the iRBC sequestration on each and every blood vessel of the cerebral vascular system due to low spatial resolution. So far, studies have reported only about the disrupted microcirculation in CM pathology. However, the spatiotemporal overlap of the peaked intensities of radiolabelled iRBCs in SPECT imaging and reduction of the venous efflux in MRA-TOF in the rostral rhinal vein and the superior sagittal sinus regions, strongly suggest that iRBC sequestration mechanically obstructing the flow in large draining veins of the brain during disease progression as the primary event in ECM pathogenesis. The consequence of blocked blood vessels and reduced venous efflux could be severe resulting in the edema development observed in the later stages of the disease. This could explain the rise in intracranial pressure and brain swelling, associated

with edema, observed in human CM. An MRI study of affected children in Africa reported increased brain swelling in CM as a contributor to the fatality of CM cases (Seydel *et al*., 2015). Sequestration of iRBCs could serve as an early indicator of severe cases of CM.

The pathophysiology of CM is a complex phenomenon involving several phenotypes and causal pathways. The present study pinpoints to sequestration of iRBCs as an essential event for the onset of ECM manifestations. Both the iRBC sequestration and reduction in venous efflux were observed from an early stage of the disease and could potentially serve as early indicators of CM. Though few MR scans are being performed in the tropical and sub-tropical countries for the treatment of CM, it has never been used for early diagnosis. Early MR-TOF scans could be helpful in patients who are diagnosed with *P. falciparum* or *P. vivax* malaria to identify the initial signs of CM and immediately start an anti-malarial treatment.

6.2 Brain pathology and inflammation

Since first part of this study successfully established the relevance of sequestration of iRBCs in the progression of ECM, the contribution of intracerebral pro-inflammatory responses on the progression of ECM was analysed. This was accompanied by anti-malarial treatment to identify the pathogenic mechanism which can be targeted by an early intervention, how treatment can regulate these processes and thereby, the outcome of ECM. The treatment was successful in the survival of the animals without any neurological symptom and decreased the parasite load in peripheral blood. Leakage in the BBB was observed beginning slightly in the olfactory bulb region at day 5 p.i. which corroborates to the fact that the spread of ECM starts with the olfactory bulb-RMS axis (Hoffmann *et al*., 2016). Complete disruption of the BBB at the later, severe stages of ECM serves as a confirmation to the fact that the opening of the BBB is relevant for disease progression and CNS dysfunction (Nacer *et al*., 2012). This phenomenon had already been observed in previous studies which reported that extensive damage to the

BBB was associated with brain swelling and edema development in ECM (Rénia *et al*., 2012). Early anti-malarial treatment aided in complete recovery of the BBB.

A previous study (Hoffmann *et al*., 2016) had described microglial activation and misalignments of neuroblasts along the RMS in severe ECM. This study establishes that the disruption of the neuroblasts begins at an early stage of ECM and worsens with disease severity. Presence of brain pathology with activated astrocytes, microglia and endothelial cells in this region at a later stage of ECM coincides with the fact that the olfactory bulb-RMS axis is the pathway for immune and neuroblast trafficking in the brain (Hoffmann *et al*., 2016). The iRBC sequestration and reduced venous efflux in the rostral rhinal vein and the superior sagittal sinus overlaps with the RMS region and could most possibly be the cause of this disturbance. Disruption of the proliferation and migration of neuroblasts in the RMS could lead to impairments in neurogenesis which might provide a clue to the long-term neurocognitive impairments reported in surviving patients, especially in children (Idro *et al*., 2005). Noteworthy fact was that anti-malarial treatment from an early stage of ECM was successful in reducing the pathology of the RMS as neuroblast proliferation and migration recovered back to almost normal routine.

Astrocytes, microglia and endothelial cells form an integral part of the BBB and their activation and dysfunction are detrimental for the BBB (Nishanth and Schlüter, 2019). Heightened activation and altered morphology of astrocytes, microglia and endothelial cells have been reported as the important mediators of neuroinflammation during the course of ECM (Nishanth and Schlüter, 2019) (Rénia *et al*., 2012). This study presents a timeline for the alteration in activation of the brain cells and establishes this acute inflammation as a late event in ECM progression. Widespread activation was observed only at day 7 p.i. when the mice were severely sick, rendering it an effect potentially caused and aggravated by the early iRBC

sequestration and reduced global blood flow in the brain. Activation of astrocytes and microglia stimulates them to produce pro-inflammatory cytokines and chemokines which recruits leukocytes to the brain further aggravating the inflammation; whereas, activation of endothelial cells leads to their dysfunction and losing the BBB integrity (Nishanth and Schlüter, 2019). Leukocyte accumulation, in the form of $CD8^+$ cells, was also observed at day 7 p.i. Excessive accumulation of $CD8^+$ T cells has been identified as a driving factor of ECM lethality as they produced perforin and granzyme B and have been linked to reduction in expression of tight junction proteins between the endothelial cells opening up the BBB (Swanson *et al*., 2016) (Rénia *et al*., 2012). Presence of apoptotic cells and haemorrhagic lesions in the brainstem region in the later stages of the disease supports the evidence of neuronal death associated with brainstem pathology reported by Swanson *et al*., 2016.

In recent years, the evidences for the 'cytokine theory' of CM have grown as it could explain the syndromes associated with the severity of the disease. However, the present study shows that though there is a sudden, massive, global increase in expression of cytokines and chemokines but it is only very late into the disease progression. Heightened levels of pro-inflammatory cytokines, IFN-γ and TNF, and the chemokines, CXCL-9, CXCL-10 and CXCL-11, which attracts $CD8^+$ T cells to the brain, were observed only at day 7 p.i. when the mice were close to death. It helps in explaining the rapid progression of neurological symptoms between day 6 and day 7 p.i. and the disease severity observed around day 7 p.i. This storm of cytokines is responsible for recruiting pathogen specific $CD8^+$ T cells and induce brain pathology by activating astrocytes, microglia and endothelial cells (Nishanth and Schlüter, 2019); which in turn, releases more cytokines and chemokines, thus, leading to a continuous cycle of inflammatory responses and aiding in edema development. Moreover, the increase in cytokines and chemokines was observed all over the brain, especially in the olfactory bulb and brainstem regions and hence, was not localized only to the sites of iRBC sequestration. Though

previous studies have reported increase in pro-inflammatory cytokines, lymphotoxin-α and β, in ECM (Nishanth and Schlüter, 2019), in this study their expression levels did not change throughout the brain and might not be contributors of the inflammation. The chemoattractant for macrophages to the brain, CXCL-3, increased slightly only in the olfactory bulb at day 7 p.i., suggesting that recruitment of macrophages is not important role for ECM pathology.

Early anti-malarial treatment was successful in preventing the further spread of this inflammation by decreasing the activation of astrocytes, microglia and endothelial cells and accumulation of $CD8^+$ cells throughout the brain. Furthermore, it also reduced the expression of cytokines and chemokines and in the process, helped the recovery of global brain pathology.

Taken together, the present study could establish a timeline of the major events in ECM progression (Table 3). Widespread iRBC sequestration in the brain of the infected animal from an early, neurologically asymptomatic stage is the primary event in ECM development. It simultaneously results in global reduction in venous efflux and impaired perfusion in the brain, especially in the regions related to the large draining veins and sinuses. This leads to BBB disruption and disruption of RMS, further leading to disturbances in neuronal migration which also starts appearing from the early stage of the disease and worsens with disease progression. Excessive inflammation with widespread brain pathology caused by activated astrocytes, microglia, endothelial cells and increased pro-inflammatory cytokine and chemokine expression occurs at a later stage of the disease when the mice exhibit neurological symptoms of the disease and are severely sick. All these events lead to rapid progression of the disease and severe edema development, observed at this later stage, which is fatal for the infected animals. Early anti-malarial treatment was successful in recovering the brain pathology by rescuing the neuronal migration in the RMS, decreasing the activation of cells supporting the

BBB, reducing the accumulation of leukocytes, decreasing the expression of cytokines and chemokines and protecting the BBB from disruption (Figure 21).

Stage of infection	Appearance of brain pathology
day 5 p.i. (early, neurologically asymptomatic stage)	iRBC sequestration, impaired perfusion, reduced cerebral blood flow, presence of parasite mRNA, RMS disruption, slight BBB disruption
day 7 p.i. (late, severely sick stage)	activation of astrocytes, microglia and endothelial cells, accumulation of $CD8^+$ T cells, haemorrhage and apoptosis in the brain stem, excessive expression of *IFN-γ, TNF, CXCL9, CXCL10, CXCL11*, total disruption of the BBB, severe edema

Table 3: Timeline of appearance of brain pathologies. List of events which start appearing from the early, neurologically asymptomatic stages and the events which were observed only at the late, severely sick stage of disease progression.

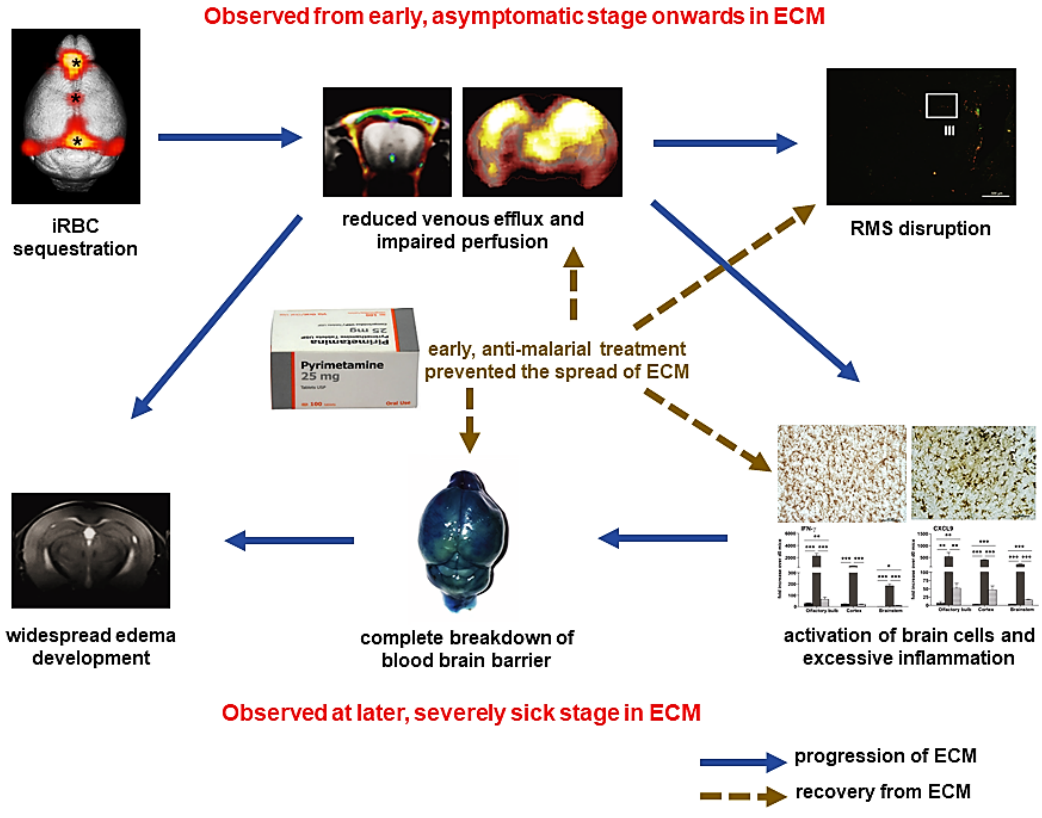

Figure 21: Summary of the present study. Representation of all the important events observed in this study, beginning from early iRBC sequestration to late edema development during ECM progression (in blue) and recovery after early treatment (in yellow).

BIBLIOGRAPHY

1. Bahamontes-Rosa, N. *et al*. (2016) “New molecular settings to support *in vivo* anti-malarial assays,” *Malar. J.*, vol. 15, no. 147.

2. Benns, H. J. et al. (2019) “Activity-Based Protein Profiling for the Study of Parasite Biology,” Curr. Top. Microbiol. Immunol., vol. 420, pp. 155–174.

3. Bhagavathula, A. S. *et al*. (2016) “Alternatives to currently used antimalarial drugs: in search of a magic bullet,” *Infect. Dis. Poverty*, vol. 5, no. 1, p. 103.

4. Bhanot, P. *et al*. (2005) “A Surface Phospholipase Is Involved in the Migration of Plasmodium Sporozoites through Cells,” *The J. of Biol. Chemis.*, vol. 280, no. 8, pp. 6752–6760.

5. Brian De Souza, J. *et al*. (2010) “Cerebral malaria: Why experimental murine models are required to understand the pathogenesis of disease,” *Parasitology*, vol. 137, no. 5, pp. 755–772.

6. Bybel, B. *et al*. (2008) “SPECT/CT Imaging : Clinical Utility of an emerging technology,” *Radiographics*, vol. 28, no. 4, pp. 1097–1113.

7. Carr, M. W. and Grey, M. L. (2002) “Magnetic Resonance Imaging,” *Am J. Nurs.*, vol. 102, no. 12, pp. 26–33.

8. Carroll, R. W. *et al.* (2010) “A rapid murine coma and behavior scale for quantitative assessment of murine cerebral malaria,” *PLoS One*, vol. 5, no. 10, p. e13124.

9. Carrolo, M. *et al.* (2003) “Hepatocyte growth factor and its receptor are required for malaria infection,” *Nat. Med.*, vol. 9, no. 11, pp. 1363–1369.

10. Clark, I. A. and Rockett, K. A. (1994) “The cytokine theory of human cerebral malaria,” *Parasitol. Today*, vol. 10, no. 10, pp. 410–412.

11. Combes, V. *et al*. (2010) “Microvesiculation and cell interactions at the brain-endothelial interface in cerebral malaria pathogenesis,” *Prog. Neurobiol.*, vol. 91, no. 2, pp. 140–151.

12. Cowman, A. F. *et al*. (2016) “Malaria: Biology and Disease,” *Cell*, vol. 167, no. 3, pp. 610–624.

13. Cox, F. E. (2010) “History of the discovery of the malaria parasites and their vectors,” *Parasites and Vectors*, vol. 3, no. 1, pp. 1–9.

14. Daneman, R. (2012) "The blood-brain barrier in health and disease," *Ann. Neurol.*, vol. 72, no. 5, pp. 648–672.

15. Dondorp, A. M. *et al*. (2000) "Abnormal Blood Flow and Red Blood Cell Deformability in Severe Malaria," *Parasitology Today*, vol. 16, no. 6., pp. 228–232.

16. Dorovini-Zis, K *et al*. (2011) "The Neuropathology of Fatal Cerebral Malaria in Malawian Children," *Am. J. Pathol.*, vol. 178, no. 5, pp. 2146–2158.

17. Dorr, A. *et al*. (2007) "Three-dimensional cerebral vasculature of the CBA mouse brain: A magnetic resonance imaging and micro computed tomography study," *Neuroimage*, vol. 35, no. 4, pp. 1409–1423.

18. Dunst, J. *et al*. (2017) "Cytokines and chemokines in cerebral malaria pathogenesis," *Front. Cell. Infect. Microbiol.*, vol. 7, p. 324.

19. Erber, W. N. (2000) "The laboratory diagnosis of malaria," *Aust. J. Med. Sci.*, vol. 21, no. 1, p. 56.

20. Fisher, A. R. and Siegelman, E. S. (2002) "Magnetic resonance imaging: Techniques," *Clin. Liver Dis.*, vol. 6, no. 1, pp. 53–72.

21. Fowkes, F. J. I. *et al*. (2016) "Immunity to malaria in an era of declining malaria transmission," *Parasitology*, vol. 7, no. 2016, pp. 1–15.

22. Freeman, W. M. *et al*. (1999) "Quantitative RT-PCR: Pitfalls and Potential," *BioTechniques*, vol. 26, no. 1, pp. 112–125.

23. Frimpong, A. *et al*. (2018) "Novel strategies for malaria vaccine design," *Front. Immunol.*, vol. 9, p. 2769.

24. Garg, S. *et al*. (2013) "Calcium-dependent permeabilization of erythrocytes by a perforin-like protein during egress of malaria parasites," *Nat. Commun.*, vol. 4, no. 1736.

25. Ghazanfari, N. *et al*. (2018) "Cerebral malaria in mouse and man," *Front. Immunol.*, vol. 9, p. 2016.

26. Golenser, J. *et al*. (2006) "Conventional and experimental treatment of cerebral malaria," *Int. J. Parasitol.*, vol. 36, no. 5, pp. 583–593.

27. Gomes, P. S. *et al*. (2016) "Immune escape strategies of malaria parasites," *Front. Microbiol.*, vol. 7, p. 1617.

28. Hamaoka, B. Y. and Ghosh, P. (2014) “Structure of the essential *Plasmodium* host cell traversal protein *SPECT1*,” *PLoS One*, vol. 9, no. 12, p. e114685.

29. Haque, A. *et al.* (2011) “*Granzyme B* expression by $CD8^+$ T cells is required for the development of Experimental Cerebral Malaria,” *J. Immunol.*, vol. 186, no. 11, pp. 6148–6156.

30. Hickson, J. (2009) “*In vivo* optical imaging: Preclinical applications and considerations,” *Urol. Oncol. Semin. Orig. Investig.*, vol. 27, no. 3, pp. 295–297.

31. Higgins, S. J. *et al*. (2011) “Immunopathogenesis of *falciparum* malaria: Implications for adjunctive therapy in the management of severe and cerebral malaria,” *Expert Rev. Anti. Infect. Ther.*, vol. 9, no. 9, pp. 803–819.

32. Hoffmann, A. *et al*. (2016) “Experimental Cerebral Malaria Spreads along the Rostral Migratory Stream,” *PLoS Pathog.*, vol. 12, no. 3, p. e1005470.

33. Howland, S. W. *et al*. (2015) “Pathogenic CD8+ T cells in experimental cerebral malaria,” *Semin. Immunopathol.*, vol. 37, no. 3, pp. 221–231.

34. Hunt, N. H. *et al.* (2006) “Immunopathogenesis of cerebral malaria,” *Int. J. Parasitol.*, vol. 36, no. 5, pp. 569–582.

35. Hunt, N. H. and Grau, G. E. (2003) “Cytokines: Accelerators and brakes in the pathogenesis of cerebral malaria,” *Trends Immunol.*, vol. 24, no. 9, pp. 491–499.

36. Hviid, L. and Jensen, A. T. R. (2015) "*Pf*EMP1 - a parasite protein family of key importance in *Plasmodium falciparum* malaria immunity and pathogenesis", *Adv. Parasitol.*, vol. 88, pp. 51–84.

37. Idro, R. *et al*. (2005) “Pathogenesis, clinical features, and neurological outcome of cerebral malaria,” *Lancet Neurol.*, vol. 4, no. 12, pp. 827–840.

38. Ioannidis, L. J. *et al*. (2014) “The role of chemokines in severe malaria: More than meets the eye,” *Parasitology*, vol. 141, no. 5, pp. 602–613.

39. Ivancevic, M. K. *et al*. (2009) “Technical Principles of MR Angiography Methods,” *Magn. Reson. Imaging Clin. N. Am.*, vol. 17, no. 1, pp. 1–11.

40. Kampfl, A. *et al*. (1997) “Impaired microcirculation and tissue oxygenation in human cerebral malaria: a single photon emission computed tomography and near-infrared spectroscopy study,” *Am. J. Trop. Med.*, vol. 56, no. 6, pp. 585–587.

41. Kariu, T. *et al*. (2006) “CelTOS, a novel malarial protein that mediates transmission to mosquito and vertebrate hosts,” *Mol. Microbio.*, vol. 59, no. 5, pp. 1369–1379.

42. Kessler, A. *et al*. (2017) "Linking EPCR-Binding PfEMP1 to Brain Swelling in Pediatric Cerebral Malaria," *Cell Host Microbe*, vol. 22, no. 5, pp. 601–614, e5.

43. Klotz1, C. and Frevert, U. (2008) “*Plasmodium yoelii* sporozoites modulate cytokine profile and induce apoptosis in murine Kupffer cells,” *Int. J. Parasitol.*, vol. 38, no. 14, pp. 1639–1650.

44. Kolodziej, A. *et al*. (2014) “SPECT-imaging of activity-dependent changes in regional cerebral blood flow induced by electrical and optogenetic self-stimulation in mice,” *Neuroimage*, vol. 103, pp. 171–180.

45. Krishnan, A. *et al*. (2004) “Cerebral venous and dural sinus thrombosis in severe *falciparum* malaria,” *J. Infect.*, vol. 48, no. 1, pp. 86–90.

46. Laurens, M. B. (2018) “The Promise of a Malaria Vaccine—Are We Closer?,” *Annu. Rev. Microbiol.*, vol. 72, no. 1, pp. 273–292.

47. Lee, K. S. *et al*. (2009) “Morphological features and differential counts of *Plasmodium knowlesi* parasites in naturally acquired human infections,” *Malar. J.*, vol. 8, no. 73.

48. Lim, D. A. and Alvarez-Buylla, A. (2016) “The adult ventricular–subventricular zone (V-SVZ) and olfactory bulb (OB) neurogenesis,” *Cold Spring Harb. Perspect. Biol.*, vol. 8, no. 5, pp. 1–33.

49. Livak, K. J. and Schmittgen, T. D. (2001) “Analysis of relative gene expression data using real-time quantitative PCR and the $2^{-\Delta\Delta CT}$ method,” *Methods*, vol. 25, no. 4, pp. 402–408.

50. Luzolo, A. L. and Ngoyi, D. M. (2019) “Cerebral malaria,” *Brain Res. Bull.*, vol. 145, pp. 53–58.

51. Ma, Y. *et al*. (2005) “A three-dimensional digital atlas database of the adult C57BL/6J mouse brain by magnetic resonance microscopy,” *Neuroscience*, vol. 135, no. 4, pp. 1203–1215.

52. Ma, Y. *et al.* (2008) “*In vivo* 3D digital atlas database of the adult C57BL/6J mouse brain by magnetic resonance microscopy,” *Front. Neuroanat.*, vol. 2, p. 1.

53. Mancini, M. *et al.* (2015) “Head and neck veins of the mouse. A magnetic resonance, micro computed tomography and high frequency color Doppler ultrasound study,” *PLoS One*, vol. 10, no. 6, p. e0129912.

54. Manning, L. *et al*. (2012) "A histopathologic study of fatal paediatric cerebral malaria caused by mixed *Plasmodium falciparum*/*Plasmodium vivax* infections," *Malaria J.*, vol. 11, no. 107.

55. Manson-Bahr, P. (1938) "The Jubilee of Sir Patrick Manson (1878-1938) a tribute to his Work on the Malaria Problem," *Post-Grad. Med. J.*, pp. 345–357.

56. Marks, M. *et al*. (2014) "Managing malaria in the intensive care unit," *Br. J. Anaesth.*, vol. 113, no. 6, pp. 910–921.

57. Marsh, K. and Kinyanjui, S. (2006) "Immune effector mechanisms in malaria," *Parasite Immunol.*, vol. 28, no. 1–2, pp. 51–60.

58. McArthur, C. *et al*. (2011) "Applications of cerebral SPECT," *Clin. Radiol.*, vol. 66, no. 7, pp. 651–661.

59. Medana, I. M. *et al*. (2001) "Central nervous system in cerebral malaria: 'Innocent bystander' or active participant in the induction of immunopathology?," *Immunol. Cell Biol.*, vol. 79, no. 2, pp. 101–120.

60. Medana, I. M. and Turner, G. D. H. (2007) "*Plasmodium falciparum* and the Blood-Brain Barrier—Contacts and Consequences ," *J. Infect. Dis.*, vol. 195, no. 7, pp. 921–923.

61. Ménard, R. *et al*. (2013) "The first steps in malarial infection and immunity," *Nat. Rev. Microbiol.*, vol. 11, no. 10, pp. 701–712.

62. Milner, D. A. (2018) "Malaria pathogenesis," *Cold Spring Harb. Perspect. Med.*, vol. 8, no. 1, pp. 1–11.

63. Misgeld, T. and Kerschensteiner, M. (2006) "*In vivo* imaging of the diseased nervous system," *Nat. Rev. Neurosci.*, vol. 7, no. 6, pp. 449–463.

64. Mohanty, S. *et al.* (2014) "Magnetic resonance imaging during life: The key to unlock cerebral malaria pathogenesis?," *Malar. J.*, vol. 13, no. 1, pp. 1–8.

65. Moreno-Caballero, M. *et al.* (2016) "Contribution of brain perfusion SPECT in the diagnosis of a case of cerebral malaria," *Rev. Esp. Med. Nucl. Imagen Mol.*, vol. 35, no. 4, pp. 253–256.

66. Moser, E. *et al*. (2009) "Magnetic resonance imaging methodology," *Eur. J. Nucl. Med. Mol. Imaging*, vol. 36, no. Suppl. 1, pp. 30–41.

67. Mota, M. M. *et al.* (2001) "Migration of *Plasmodium* Sporozoites through cells before infection," *Science*, vol. 291, no. 5501, pp. 141–144.

68. Mukkala, A. N. *et al*. (2018) "An Update on Malaria Rapid Diagnostic Tests," *Curr. Infect. Dis. Rep.*, vol. 20, no. 12, pp. 1–8.

69. Müller, H. M. *et al*. (1993) "Thrombospondin related anonymous protein (TRAP) of *Plasmodium falciparum* binds specifically to sulfated glycoconjugates and to HepG2 hepatoma cells suggesting a role for this molecule in sporozoite invasion of hepatocytes.," *EMBO J.*, vol. 12, no. 7, pp. 2881–2889.

70. Nacer, A. *et al*. (2012) "Neuroimmunological Blood Brain Barrier opening in Experimental Cerebral Malaria," *PLoS Pathog.*, vol. 8, no. 10, p. e1002982.

71. Nishanth, G. and Schlüter, D. (2019) "Blood–Brain Barrier in Cerebral Malaria: Pathogenesis and Therapeutic Intervention," *Trends Parasitol.*, vol. 35, no. 7, pp. 516–528.

72. Nitcheu, J. *et al.* (2003) "Perforin-dependent Brain-infiltrating Cytotoxic $CD8^+$ T Lymphocytes mediate Experimental Cerebral Malaria Pathogenesis," *J. Immunol.*, vol. 170, no. 4, pp. 2221–2228.

73. Oelschlegel, A. M. and Goldschmidt, J. (2020) "Functional Neuroimaging in Rodents using Cerebral Blood Flow SPECT," *Front. Phys.*, vol. 8, p. 152.

74. Ohnishi, K. (2009) "Cerebral malaria," *Brain and Nerve*, vol. 61, no. 2, pp. 122–128.

75. Okanovic, M. *et al*. (2018) "Time-of-flight MR-angiography with a helical trajectory and slice-super-resolution reconstruction," *Magn. Reson. Med.*, vol. 80, no. 5, pp. 1812–1823.

76. Pain, A *et al*. (2001) "Platelet-mediated clumping of *Plasmodium falciparum*-infected erythrocytes is a common adhesive phenotype and is associated with severe malaria," *PNAS*, vol. 98, no. 4, pp. 1805–1810.

77. Pan, Y. W. *et al*. (2013) "Assessment of adult neurogenesis in mice," *Curr. Protoc. Toxicol.*, chapter 12, unit 12.20.

78. Payne, D. (1988) "Use and limitations of light microscopy for diagnosing malaria at the primary health care level," *Bull. World Health Organ.*, vol. 66, no. 5, pp. 621–626.

79. Pham, N. M. *et al*. (2018) "Malaria and the 'last' parasite: How can technology help?," *Malar. J.*, vol. 17, no. 1, pp. 1–16.

80. Pinzón, M. A. *et al*. (2013) "*Plasmodium vivax* cerebral malaria complicated with venous sinus thrombosis in Colombia," *Asian Pac. J. Trop. Med.*, vol. 6, no. 5, pp. 413–415.

81. Plewes, K. *et al*. (2018) “Pathophysiology, clinical presentation, and treatment of coma and acute kidney injury complicating *falciparum* malaria,” *Curr. Opin. Infect. Dis.*, vol. 31, no. 1, pp. 69–77.

82. Plewes, K. *et al*. (2019) “Malaria: What’s New in the Management of Malaria?,” *Infect. Dis. Clin. North Am.*, vol. 33, no. 1, pp. 39–60.

83. Postels, D. G. and Birbeck, G. L. (2013) "Cerebral malaria", *Handb. Clin. Neurol.*, vol. 114, no. 3, pp. 91–102.

84. Randall, G. and Seidel, J. S. (1985) “Malaria,” *Pediatr. Clin. North Am.*, vol. 32, no. 4, pp. 893–916.

85. Rénia, L. *et al*. (2012) “Cerebral malaria: Mysteries at the blood-brain barrier," *Virulence*, vol. 3, no. 2, pp. 193–201.

86. Renslo, A. R. and McKerrow, J. H. (2006) “Drug discovery and development for neglected parasitic diseases,” *Nat. Chem. Biol.*, vol. 2, no. 12, pp. 701–710.

87. Risco-Castillo, V. *et al.* (2015) “Malaria sporozoites traverse host cells within transient vacuoles,” *Cell Host Microbe*, vol. 18, no. 5, pp. 593–603.

88. Rodrigues, J. A. *et al.* (2015) “Parasite Glycobiology: A Bittersweet Symphony,” *PLoS Pathog.*, vol. 11, no. 11, p. e1005169.

89. Sahu, P. K. *et al*. (2015) “Pathogenesis of cerebral malaria: New diagnostic tools, biomarkers, and therapeutic approaches,” *Front. Cell. Infect. Microbiol.*, vol. 5, p. 75.

90. Schiess, N. *et al*. (2020) “Pathophysiology and neurologic sequelae of cerebral malaria,” *Malaria J.*, vol. 19, no. 266.

91. Schmid, U. *et al*. (2017) “The deubiquitinating enzyme cylindromatosis dampens $CD8^+$ T cell responses and is a critical factor for experimental cerebral malaria and blood-brain barrier damage,” *Front. Immunol.*, vol. 8, p. 27.

92. Seth, A. *et al*. (2017) “Current perspective on *in vivo* molecular imaging of immune cells,” *Molecules*, vol. 22, no. 6, p. 881.

93. Seydel, K. B. *et al*. (2015) “Brain Swelling and Death in Children with Cerebral Malaria.” *N. Engl. J. Med.*, vol. 372, no. 12, pp. 1126–1137.

94. Silvis, S. M. *et al*. (2017) “Cerebral venous thrombosis,” *Nat. Rev. Neurol.*, vol. 13, no. 9, pp. 555–565.

95. Simpson, A. G. B. *et al.* (2002) “The Discovery of *Giardia*,” *Proc. Natl. Acad. Sci.*, vol. 19, no. 4, pp. 147–153.

96. Singh, B. and Daneshvar, C. (2013) “Human infections and detection of *Plasmodium knowlesi*,” *Clin. Microbiol. Rev.*, vol. 26, no. 2, pp. 165–184.

97. Sinnis, P. and Zavala, F. (2012) “The skin: Where malaria infection and the host immune response begin,” *Semin. Immunopathol.*, vol. 34, no. 6, pp. 787–792.

98. Stanley, J. (1997) “Malaria,” *Emerg Med Clin North Am.*, vol. 15, no. 1, pp. 113–155.

99. Storm, J. and Craig, A. G. (2014) “Pathogenesis of cerebral malaria- inflammation and cytoadherence,” *Front. Cell. Infect. Microbiol.*, vol. 4, p.100.

100. Stout, D. B. and Zaidi, H. (2008) “Preclinical Multimodality Imaging in Vivo,” *PET Clin.*, vol. 3, no. 3, pp. 251–273.

101. Strangward, P. *et al.* (2017) "A quantitative brain map of experimental cerebral malaria pathology," *PLoS Pathog*, vol. 13, no. 3. p. e1006267.

102. Sultan, A. A. *et al.* (1997) “TRAP is necessary for gliding motility and infectivity of *Plasmodium* sporozoites,” *Cell*, vol. 90, no. 3, pp. 511–522.

103. Swamy, L. *et al*. (2018) “Funduscopy in cerebral malaria diagnosis: An international survey of practice patterns,” *Am. J. Trop. Med. Hyg.*, vol. 98, no. 2, pp. 516–519.

104. Swanson, P. A. *et al*. (2016) “$CD8^+$ T Cells Induce Fatal Brainstem Pathology during Cerebral Malaria via Luminal Antigen-Specific Engagement of Brain Vasculature,” *PLoS Pathog.*, vol. 12, no. 12, pp. 1–34.

105. Tavares, J. *et al.* (2013) “Role of host cell traversal by the malaria sporozoite during liver infection,” *J. Exp. Med.*, vol. 210, no. 5, pp. 905-15.

106. Taylor, T. E. *et al*. (2004) “Differentiating the pathologies of cerebral malaria by postmortem parasite counts,” *Nat. Med.*, vol. 10, no. 2, pp. 143–145.

107. Taylor, T. E. and Molyneux, M. E. (2015) “The pathogenesis of pediatric cerebral malaria: Eye exams, autopsies, and neuroimaging,” *Ann. N. Y. Acad. Sci.*, vol. 1342, no. 1, pp. 44–52.

108. Thu, A. M. et al. (2017) “Combating multidrug-resistant *Plasmodium falciparum* malaria,” *FEBS J.*, vol. 284, no. 16, pp. 2569–2578.

109. Torre, S. *et al*. (2018) "Genetic analysis of cerebral malaria in the mouse model infected with *Plasmodium berghei*," *Mamm. Genome*, vol. 29, no. 7–8, pp. 488–506.

110. Trang, D. T. X. *et al*. (2004) "One-step concentration of malarial parasite-infected red blood cells and removal of contaminating white blood cells," *Malar. J.*, vol. 3, no. 7.

111. Ueda, K. *et al*. (2000) "Impact of anatomical difference of the cerebral venous system on microcirculation in a gerbil superior sagittal sinus occlusion model," *Acta Neurochir. (Wien).*, vol. 142, no. 1, pp. 75–82.

112. Ungersböck, K. *et al*. (1993) "Cerebral blood flow alterations in a rat model of cerebral sinus thrombosis," *Stroke*, vol. 24, no. 4, pp. 563–56.

113. Varo, R. *et al.* (2018) "Adjunctive therapy for severe malaria: A review and critical appraisal," *Malar. J.*, vol. 17, no. 1, pp. 1–18.

114. Wah, S. T. *et al*. (2016) "Molecular basis of human cerebral malaria development," *Trop. Med. Health*, vol. 44, no. 1, p. 33.

115. Warwick, J. M. (2004) "Imaging of brain function using SPECT," *Metab. Brain Dis.*, vol. 19, no. 1–2, pp. 113–123.

116. Wassmer, S. C. and Grau, G. E. R. (2017) "Severe malaria: what's new on the pathogenesis front?," *Int. J. Parasitol.*, vol. 47, no. 2–3, pp. 145–152.

117. White, N. J. (1996) "The treatment of malaria," *N. Engl. J. Med.*, vol. 335, no. 11, pp. 800–806.

118. White, N. J. *et al*. (2013) "Lethal Malaria: Marchiafava and Bignami were Right," *J. Infect Dis.*, vol. 208, no. 2, pp. 192–198.

119. Wilson, M. H. (2016) "Monro-Kellie 2.0: The dynamic vascular and venous pathophysiological components of intracranial pressure," *J. Cereb. Blood Flow Metab.*, vol. 36, no. 8, pp. 1338–1350.

120. Wongsrichanalai, C. *et al*. (2007) "A review of malaria diagnostic tools: Microscopy and rapid diagnostic test (RDT)," *Am. J. Trop. Med. Hyg.*, vol. 77, no. Suppl. 6, pp. 119–127.

121. World Health Organization (2015) "Guidelines for the treatment of malaria," vol. 3rd edition.

122. World Health Organization and Global Malaria Programme (2017) "A Framework for Malaria Elimination,".

123. World Health Organization (2020) “World Malaria Report 2020”.

124. Xiong, B. *et al.* (2017) “Precise cerebral vascular atlas in stereotaxic coordinates of whole mouse brain,” *Front. Neuroanat.*, vol. 11, p. 128.

125. Yam, X. Y. and Preiser, P. R. (2017) “Host immune evasion strategies of malaria blood stage parasite,” *Mol. Biosyst.*, vol. 13, no. 12, pp. 2498–2508.

DECLARATION OF HONOUR

I hereby declare that I prepared this thesis without the impermissible help of third parties and that none other than the aids indicated have been used; all sources of information are clearly marked, including my own publications.

In particular I have not consciously:

- fabricated data or rejected undesirable results,
- misused statistical methods with the aim of drawing other conclusions than those warranted by the available data,
- plagiarized external data or publications,
- presented the results of other researchers in a distorted way.

I am aware that violations of copyright may lead to injunction and damage claims by the author and also to prosecution by the law enforcement authorities.

I hereby agree that the thesis may be electronically reviewed with the aim of identifying plagiarism.

This work has not yet been submitted as a doctoral thesis in the same or a similar form in Germany, nor in any other country. It has not yet been published as a whole.

Magdeburg, 25.06.2021

Rituparna Bhattacharjee